DESIGN AND ANALYSIS OF OPTIMAL MULTI-LAYER WALLS FOR TIME-VARYING THERMAL EXCITATION

by

Danielle E.M. Bond

B.S. in Engineering, Swarthmore College, 2006

Submitted to the Graduate Faculty of

the Swanson School of Engineering in partial fulfillment

of the requirements for the degree of

Doctor of Philosophy

University of Pittsburgh

2014

UNIVERSITY OF PITTSBURGH

SWANSON SCHOOL OF ENGINEERING

This dissertation was presented

by

Danielle E.M. Bond

It was defended on

June 11, 2014

and approved by

Daniel G. Cole, Ph.D., Associate Professor,

Department of Mechanical Engineering and Materials Science

Zhi-Hong Mao, Ph.D., Associate Professor,

Department of Electrical Engineering

Dissertation Co-Advisor: Mark Kimber, Ph.D., Assistant Professor,

Department of Mechanical Engineering and Materials Science

Dissertation Director: William W. Clark, Ph.D., Professor,

Department of Mechanical Engineering and Materials Science

DESIGN AND ANALYSIS OF OPTIMAL MULTI-LAYER WALLS FOR TIME-VARYING THERMAL EXCITATION

Danielle E.M. Bond, Ph.D.

University of Pittsburgh, 2014

U.S. buildings are a significant source of energy consumption (about 50%) and carbon emissions (about 40%), and providing conditioning to building interiors is a major portion of that expenditure. Improving building envelope performance can reduce the amount of energy used for heating and cooling, since external walls provide an important barrier between occupied building spaces and variable ambient conditions. In general, multi-layer exterior walls tend to perform better than single-layer walls, even for the same overall R-value and thermal capacitance. This work addresses practical choices in multi-layer wall design to minimize internal temperature swings that result from outside, or ambient, temperature fluctuations. An electrical analogy is used to model one-dimensional heat conduction using RC circuits. A frequency response analysis is conducted based on a period of one day. For a fixed wall thickness, four features are optimized: materials, proportion of materials, number of layers, and material distribution. Key design features include pairing insulating and thermally massive materials, distributing layers evenly, and positioning the insulating layers at the inner- and outer-most layers of the wall (i.e., near the indoor and outdoor environments). Methods for determining the optimal proportion of each material and number of layers are also presented. Combined, these easily implemented features can reduce interior temperature fluctuations by several orders of magnitude compared to ambient temperature variations. This helps maintain

steady indoor temperatures, which is more comfortable for building occupants, and supports energy management strategies, like reducing peak heating and cooling loads.

TABLE OF CONTENTS

LIST OF TABLES

LIST OF FIGURES

PREFACE

Thank you to the Department of Mechanical Engineering and Materials Science, the Mascaro Center for Sustainable Innovation, and the Office of the Provost at the University of Pittsburgh for supporting my efforts to complete this work. Thanks to the members of my committee, and especially my advisors, for their patience, guidance, and insight. It has been a privilege to collaborate on this interdisciplinary research and to work with engaging minds from different disciplines, including many talented students.

I am eternally grateful to my parents for everything they do for their children and for making it possible for me to reach this day. To my siblings, thank you for continuing to inspire me in your professional pursuits and passion for life. And to my husband, thank you, because of you, I am better in every way.

1.0 INTRODUCTION AND BACKGROUND

Building insulation is a fundamental component in managing building energy consumption. Data reported by the U.S. government's "Better Buildings Challenge" in 2013 [1] shows that U.S. commercial and industrial buildings spend about $400 billion per year on energy and account for about half of the total energy consumption in the U.S. The cost and percentage is more than industry and transportation and an increase from five years ago in 2009 [1, 2]. This energy use also leads to about 40% of total U.S. carbon emissions [2]. Within U.S. residential and commercial buildings, heating and cooling represent 42% and 29%, respectively, of the total energy consumed [2]. Improving the insulating performance of building envelopes is one element of an integrated approach towards improving overall energy efficiency and reducing energy consumption in buildings. Reducing building energy consumption helps reduce building operating costs as well as emissions and other related impacts.

Ongoing research has focused on investigating insulation and the design of external walls towards the goal of mitigating energy used for heating and cooling in buildings. Many studies focus on specific buildings, climates, and economic conditions. Optimizing insulation thickness for a given climate and economy is one approach that numerous authors have examined. Other studies have considered the position of insulation within a multi-layer wall, demonstrating how some arrangements perform better than others under steady periodic conditions, even with the same amount of building material. Integrated building models can be used to evaluate wall

performance based on instantaneous and peak transmission loads and annual energy demands, but the characteristics of a standalone wall (i.e., independent of a complete building simulation model) are typically evaluated using three primary metrics: R-value, decrement factor, and time lag.

R-value is a measure of thermal resistance that captures the ability of a specified thickness of insulating material to resist conductive (and convective) heat transfer. (Practically, convective heat transfer is restricted as a result of the small, discontinuous air gaps in insulation that restrict air flow and convection currents.) Its inverse is thermal conductance [3]. Thermal conductivity (k), whose inverse is thermal resistivity, is a material property with units of W/m·K [3]. R-value is defined by thickness (L) and thermal conductivity, both assumed to be constant values. US units for R-value are h·ft²·°F/Btu. Another definition for R-value with equivalent units is the ratio of the temperature difference across the material slab and the steady state heat flux (heat transfer per unit area per unit time) through the material. Equation (1.1) shows both formulas with SI units.

$$R = \frac{L}{k} = \frac{\Delta T}{q''_A} = \frac{[m]}{[W/m \cdot K]} = \left[\frac{m^2 \cdot K}{W}\right] \tag{1.1}$$

Since R-value ratings are based on fixed, or steady state, conditions and measure the heat flux required to maintain a specified temperature difference, the definition is considered a characterization of the static performance of an insulating material. To evaluate performance in response to a periodic input, rather than fixed boundary conditions or heat flux, the decrement factor and time lag are used.

The decrement factor is an indication of the thermal penetration, and is defined as the ratio of inside to outside temperature fluctuations. The time lag indicates how long exterior temperature changes take to affect interior conditions. In the current work, to avoid ambiguity and consistently define positions within a wall, “inside” and “outside” refer to the indoor and outdoor environments, while “middle” refers to those layers sandwiched between the inside and outside surfaces of the wall.

In frequency response analysis, the decrement factor is equivalent to the magnitude ratio of the system transfer function evaluated at the frequency of the source signal. In other words, "…the time it takes for heat wave to propagate from the outer surface to the inner surface is named ‘time lag’ and the decreasing ratio of its amplitude during this process is named ‘decrement factor’" [4]. In this work, the wall temperature at the outside surface is denoted as $T_{s,amb}$ (or $T_{s,out}$), while the wall temperature at the inside surface of the wall is denoted $T_{s,rm}$ (or $T_{s,in}$),. The inside room and surface temperature will oscillate as a result of the outside temperature fluctuation. The outside temperature is modeled as a sinusoidal input with a fixed (typically 24 hour) period. The wall acts as a filter to reduce the amplitude of the transmitted signal and to shift the signal in time, as in Figure 1.1 (a). Given the definition of the decrement factor (*df*), it can simply be expressed as the magnitude ratio (*M*) as shown in Equation (1.2).

$$df = \frac{Amplitude\ of\ T_{s,rm}}{Amplitude\ of\ T_{s,amb}} = \frac{A_{rm}}{A_{amb}} = \left|G\left(j\omega\right)\right| = M \tag{1.2}$$

If the period of interest is 24 hours, then the magnitude ratio is evaluated at $\omega = \omega_{day}$. Similarly, time lag can be converted from the system phase lag. The phase angle ($\phi(\omega) = \angle G(j\omega)$) can

likewise be evaluated at $\omega = \omega_{day}$ (or other frequencies of interest) in order to find the time lag (t_{lag}) in hours according to Equation (1.3).

$$t_{lag} = \angle G\left(j\omega_{day}\right) \cdot \frac{24\ hr}{2\pi} \tag{1.3}$$

A block diagram in Figure 1.1 (b) shows the system frequency response function $G(j\omega)$ with an ambient sinusoidal input and the output as a modified amplitude and peak time shifted by ϕ.

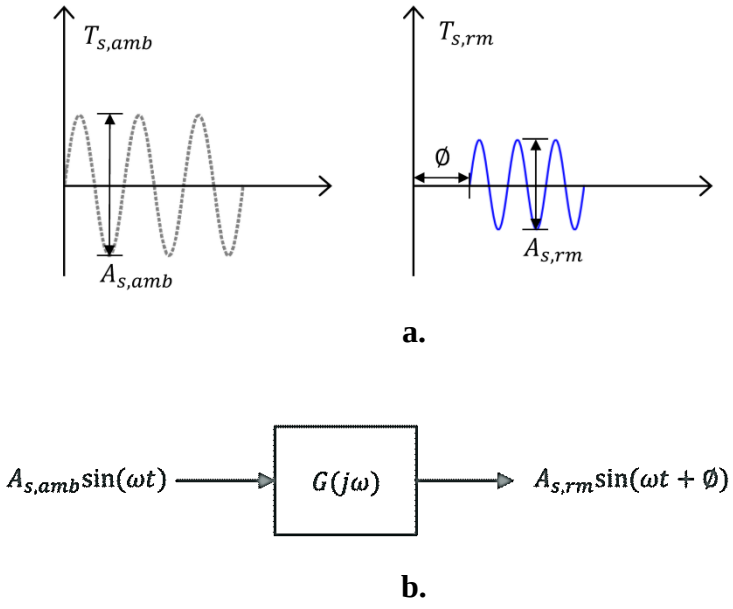

Figure 1.1. (a) Ambient temperature (left) and inside wall temperature after filtering (right), (b) Frequency response representation of wall.

Determining how best to assemble multi-layer walls to reduce decrement factor and increase time lag can enhance the energy efficiency and reduce the overall energy footprint for multiple types of buildings [5-8]. Specifically, reducing decrement factor has the effect of decreasing daily peak transmission loads which may increase energy savings in two ways. First, decreasing the peak transmission load will decrease the overall energy required to maintain an interior setpoint temperature. Second, reduced peak loads reduce the size requirements of the building heating, ventilation, and air conditioning (HVAC) equipment, thereby cutting down on "over-sized" equipment designs and enabling the HVAC equipment to run at more efficient operating loads (along their performance curves). Multi-layer wall design also increases time lag, which has the effect of shifting peak loads. Shifting peak loads can provide beneficial or 'free' conditioning (and thereby energy savings) during appropriate weather conditions, such as swing seasons or desert-type climates with large diurnal temperature variations. Load shifting can also enable HVAC equipment to handle peak loads when operating conditions are more favorable or when time-based incentives reduce the cost of energy purchased from utility companies. Coffman, et al. [9] also suggest that a desired time lag may be achieved using less mass with a multi-layer wall configuration, thereby reducing the overall footprint for building envelope construction. For all these reasons, the study of multi-layer insulation continues to be a rich area of research.

2.0 LITERATURE REVIEW

2.1 EFFECT OF INSULATION POSITION AND NUMBER OF LAYERS

The order of layers in a multi-layer wall does not affect the wall thermal response when subjected to constant thermal conditions, but it is important when sinusoidal (and other non-constant) conditions are considered [4]. Several studies evaluate the effect of insulation position within an external wall. Many studies compare performance when insulation is placed near the inside or outside wall surface. Others experiment with various multi-layer configurations. Some studies consider both insulation optimization and investigation of the actual configuration (i.e., order and number of layers).

For example, Al-Sanea and Zedan [10] compare two wall configurations using single layers of insulation and thermal mass. The decrement factor is analyzed for the two wall configurations and for different response time periods, including an initial transient or instantaneous response and a steady periodic response. Between the two configurations, insulation towards the inside yields a lower instantaneous load, but insulation towards the outside has a much longer time lag (almost 10 times). The results are somewhat conflicting, since insulation on the inside is better for reducing the load while insulation at the outside is better for increasing time lag, both features of effective insulating walls. In a follow up study [11], the two configurations are studied while varying the amount and position of thermal mass under steady

periodic conditions. The total wall resistance is maintained by varying the mass and insulation layer thicknesses. Results show that increasing the amount of thermal mass in the wall leads to lower transmission loads during swing seasons when temperatures are not extreme. They find that for any set amount of thermal mass, positioning the mass towards the inside surface and positioning the insulation near the outside surface yields better overall thermal performance.

Kossecka and Kosny [12] evaluate six wall configurations using a simplified building model and a one story residential model building simulated with six different U.S. climates. The thermal performance of the walls is evaluated in terms of annual building heating and cooling demands and total annual energy demands as calculated by the building modeling program. Each wall has internal layers of concrete and insulation with either one or two layers of each such that all of the walls have the same total resistance and capacitance values. The study agrees with previous findings that walls with concrete layers at the inside and insulation layers at the outside show the best building energy savings. In terms of dynamic performance criteria, part of the study indicates that a concrete/insulation/concrete configuration has a lower decrement factor than a configuration of insulation/concrete/insulation, which has a longer time lag. The authors describe an even distribution of insulation on either side of the mass, but they do not consider other wall configurations with unevenly distributed layers. Furthermore, because these results seem to conflict, the need for clear and unambiguous guidelines for assembling multi-layer walls remains.

Sonderegger [13] uses a matrix method and Fourier transforms to analyze steady sinusoidal heat transfer through building walls and then applied to a single room building. Walls and roofs are limited to one or two layers. The study focuses on comparing the effect of insulation at the inside or outside of "the main wall mass." It is found that insulation at the

outside reduces the temperature variation inside resulting from both outside temperature variations and internal heat gains. Insulation at the inside position means the room temperature responds faster to changes at the outside or inside and to thermostat settings.

Two other studies consider different mass/insulation configurations. Bojic and Loveday [14] find an alternating insulation/mass/insulation configuration is better under intermittent heating conditions and an alternating mass/insulation/mass configuration is better under intermittent cooling conditions. In a separate study from Bojic [15], six wall configurations are analyzed within a full building model of two high-rise residences comprised of various flats facing different directions on each floor. Results show that thicker insulation reduces the cooling load and insulation at the inside position yields the lowest annual cooling load. Cooling demand results are varied, however. It is lower for insulation at the outside position for some flats and at the inside positions for other flats. The authors suggest this is due to the different orientation of the flats within the building. The mixed results suggest that whole building simulation may not be the best tool for analyzing thermal dynamic wall performance.

In a slightly different study, Aste [16] analyzes six representative wall configurations as a Southern facing wall within a whole building analysis. All of the walls have the same R-value but different values of thermal capacity and mass per unit area. The wall system with the lowest energy demand is a two layer wall with insulation towards the outside. The highest energy demand results from a light weight wall configuration with no significant thermal mass layers. The lack of thermal mass in this poorly performing assembly illustrates its importance.

Ciampi, et al. [4] recognize the conclusions drawn from numerous studies that consider a two layer wall and show better insulating performance when the insulating, or the more

thermally resistant layer, is placed towards the outside of the wall, and the more thermally capacitive layer is located toward the inner surface of the wall.

Unlike other studies that consider different combinations and configurations of insulation and thermal mass layers in a wall, Asan and Sancaktar [17] evaluate the thermal performance of various building materials independently. They develop a numerical solution to the one dimensional heat equation and investigate the effects of wall thickness and material properties on time lag and decrement factor. Results demonstrate common conclusions, such as the time lag increases and decrement factor decreases with increasing heat capacity; time lag increases and decrement factor decreases with increasing thickness; and, low thermal conductivity and high heat capacity yield longer time lags. In a subsequent study, Asan [18] evaluates heat conduction in 26 building materials. The time lag and decrement factor for each building material are calculated for 8 variations of a single layer wall thickness. For all the materials, the decrement factor decreases with increased wall thickness, and for small thicknesses (roughly less than 0.050m) the decrement factor is nearly constant. The decrement factor tends to zero for wall thickness greater than 1m, and all materials exhibit zero time lag for wall thickness less than 1cm. In the second part of the study, two multi-layer walls are analyzed: one with three layers and no insulation and one with five layers including insulation. For the same thickness wall, the wall with insulation has a longer time lag and lower decrement factor. In these two works, Asan analyzes a large set of walls and provides generalized conclusions relating material properties to thermal performance but suggests that future work will aim to optimize insulation thickness and position to achieve larger time lags and smaller decrement factors.

In another study, Asan [19] evaluates six wall configurations for time lag and decrement factor based on a Crank Nicolson numerical solution to the one-dimensional heat equation with

periodic convection boundary conditions. Fewer than six configurations are actually studied due to overlap between the different configuration ‘families’. Two different thermal mass and insulation materials are selected each, so that a total of four thermal mass-insulation combinations are studied. The minimum decrement factor is achieved with half the insulation at the inner and outer walls, while the maximum time lag is achieved with two layers of insulation located within the wall, equidistant from the inner and outer surfaces. While practical guidelines for renovating building walls for improved insulating performance are provided from the results, the number of layers studied was limited and different weighting configurations were not considered.

Another such study that addresses insulation thickness and position is Al-Sanea and Zedan [20]. They evaluate the number and distribution of insulation layers in a wall with fixed amounts of insulation and thermal mass. The wall thickness is fixed and the total amount of insulation is optimized for cost and energy performance. Different wall configurations are arranged and thermal performance evaluated. The study concludes that the best configurations for insulating performance have either two layers of insulation divided between the outside and middle layers or three layers of insulation split evenly among the outside, middle, and inside layers. The study only considers evenly distributing insulation layers, and the analysis is limited to using one, two, and three layers of insulation. The effects of increasing the number of insulation layers further is not explored nor is the concept of using unevenly distributed layers.

In a supporting study, Mavromatidis et al. [21] investigate the effects of wall composition and orientation on time lag and decrement factor. The authors conclude that their multi-layer insulation (MTI) has the best overall thermal performance and increases time lag compared to insulation alone, citing similar results from Al-Sanea.

Tsilingiris [22] determines transient wall heat flux numerically based on a step input at one side to analyze the thermal time constant of a wall. Ten wall configurations are studied. Results show that this time constant is specific to the room side and ambient side, called forward and reverse. The ratio of the forward and reverse time constants is also examined, but the two are identical for a symmetric wall. A quasi-dynamic analysis shows how the time constant changes as the position of an insulation layer moves with respect to the thermal mass of the wall. This demonstrates the effect of layer positioning on dynamic performance criteria like time lag.

In another study from Al-Sanea, et al. [6], the authors introduce two variables called ‘‘thermal-mass energy-savings potential’’ and ‘‘critical thermal-mass thickness’’ as part of an optimization method for finding the best thermal mass thickness given a prescribed energy savings percentage. The thermal response of a wall with fixed overall resistance is considered for steady periodic conditions while varying the thickness and location of thermal mass layers. The analysis is limited to two wall configurations, one with insulation at the inside layer position and one with insulation at the outside layer position, and the climatic data of Riyadh, Saudi Arabia. Insulation thickness is reduced as thermal mass thickness is increased to maintain a fixed overall thermal resistance. This resistance is described by a nominal R-value. A definition for a dynamic R-value is also introduced. The dynamic R-value changes with amount and location of the thermal mass layer and represents actual variations in transmission loads. Results show that increasing the amount of thermal mass in the wall leads to lower transmission loads during swing seasons when temperatures are not extreme. Generally, more thermal mass also yields lower peak loads, a lower decrement factor, and a larger time lag. For any set amount of thermal mass, positioning the mass towards the inside of the wall and positioning insulation at the outside yields better overall thermal performance, as other studies have shown.

In their most recent work, Al-Sanea, et al. [23] use a previously developed model to study the effects of (1) solid versus hollow concrete blocks and (2) values of surface absorptivity on the two concepts: “thermal-mass energy-savings potential” and “critical thermal mass thickness”. These two parameters are used to obtain a critical thermal mass thickness for a prescribed energy savings percentage. A daily averaged dynamic thermal resistance is defined as the ratio of the integral over 24-hours of the absolute value of the temperature difference across the wall to the integral over 24-hours of the absolute value of the instantaneous transmission load. This term is determined for each month’s representative day with respect to climate/weather input. The yearly averaged value is calculated as a weighted average, and the authors describe this parameter as an "effective resistance" for comparing wall performance. Two west-facing walls consist of cement plaster at the outer layers with one layer of thermal mass and one layer of insulation (molded polystyrene is used). One wall has insulation towards the outside and the other has insulation towards the inside. Results suggest that heavy wall construction with high thermal mass and low surface absorptivity is best in locations where large daily temperature variations occur, and the thermal mass is best towards the inside compared to the outside position, based on the assumption of steady periodic conditions.

In a recent review of building insulation work, Kaynakli [24] reports that most studies determine optimum insulation thickness from heating and cooling loads, material and energy costs, and other economic factors for a given climate. Most studies also evaluate insulation thickness using static conditions. A few, however, consider the dynamic performance of multi-layer walls. The studies described here indicate that multi-layer walls yield better overall thermal performance than single or double layer walls [12, 20, 21]. Some studies [12, 20] find insulation towards the inside and outside to be best. Several find that insulation towards the outside (with

thermal mass towards the inside) provides better thermal performance than insulation towards the inside [6, 10-12, 16, 25], and most agree that, generally, more thermal mass yields lower peak loads, a lower decrement factor, and a larger time lag [11, 16, 17]. Other studies cited in Aste [16] that consider insulation position and use different analyses and performance criteria, such as cooling loads, time lag, and decrement factor, also find that insulation at the outside layer yields better thermal performance.

While the studies mentioned above provide some meaningful results about assembling insulation and thermal mass layers in a wall, a limited number of configurations are evaluated and the study of multi-layer insulation walls is limited. The effect of increasing layer divisions and re-positioning insulation layers within an assembly is not fully characterized.

2.2 OPTIMIZING WALL CONFIGURATIONS

2.2.1 Optimizing Insulation Thickness

In addition to the studies described previously, certain studies have focused on optimizing the quantity of insulation used in a given wall based on specific climatic and economic conditions. Mishra [7] uses a life cycle cost analysis to determine the optimum insulation thickness, energy savings, and payback periods where two different insulating materials and three different thermally massive materials are considered. Optimum thickness depends on heating Degree-Days and total wall thermal resistance as well as different fuels. The analysis yields a range for optimum insulation thickness. This analysis is limited to specific materials and a restricted

number of wall layers and configurations, and the results are very specific to the given application in terms of climate and economy.

Ozel [26] studies exterior solar absorptivity for its effect on optimum insulation thickness, as well as annual heating and cooling transmission loads, annual average time lag and decrement factor, and energy savings. An implicit finite difference numerical method is developed to calculate heating and cooling transmission loads, which are then used in an economic based model to determine the optimum insulation thickness of a south-facing wall. Steady periodic conditions are considered for a climate in Turkey. Results indicate solar absorptivity does substantially affect time lag, decrement factor, and optimum insulation thickness, but has more pronounced effect on transmission loads and (subsequently) energy savings and payback period. Additionally, solar absorptivity affects cooling loads more than heating loads. Optimization results suggest an insulation thickness of 0.048m and solar absorptivity of 0.6 to maximize energy savings and minimize payback period for this particular application. Again, these results are fairly specific to the case studied and not easily transferable or generalized.

In another study, Ozel [27] calculates optimum insulation thickness using a lifetime cost analysis based on the cooling transmission load, time lag, and decrement factor as calculated by an implicit finite difference method using steady periodic conditions for different wall orientations and climate data for summer in Turkey. The economic model uses insulation cost and the present value of energy consumption costs over the lifetime of the building. Results show that north facing walls require the least amount of insulation while east and west require the thickest due to the high cooling loads. With some variability possible between climates, these results indicate that wall configurations can be optimized for different wall orientations in terms

of balancing insulation cost and energy performance. However, such results are specific to the type of insulation and economic conditions evaluated. In both Ozel studies, only insulation thickness is optimized while its relative position in the wall, its placement in relation to thermally massive layers, and the overall number of layers is not studied.

2.2.2 Other Optimization Parameters and Solution Methods

Whereas other studies rely on specific case study data or methods, some studies have focused on optimizing non-economic or case-based building insulation and wall design parameters. For instance, Mikhailov [28] uses a penalty function method to optimize multi-layer thermal insulation by determining insulation layer thickness with minimum mass subject to temperature constraints**.** N-layers of various materials and thickness are considered and thermal contact between layers is assumed to be ideal. The use of a penalty function transforms the problem from finding a minimum with constraints to solving multiple minimization problems without constraints. Minimizing mass may be advantageous for certain applications but not in terms of optimizing time lag and decrement factor. This study does not help illustrate the effect that the configuration of insulation and thermal mass layers contributes to optimizing time lag and decrement factor.

Focusing on energy, Ginestet, et al. [29] aim to optimize envelope design to limit heating load demands. A transmission matrix or quadrupole thermal modeling method is used with an optimization algorithm in the study of multi-layer building walls. A reflective Newton algorithm is used to realize an optimal building wall configuration. A least square criterion is used to minimize the error between desired indoor temperatures and the expected model response where outdoor dry bulb temperature, solar radiation, and heating flux are considered quasi periodic

signal inputs. Specifically, the authors seek to determine building parameters for a wall with insulation at the outside, brick, and plaster at the inside with a fixed thickness in order to minimize the difference between estimated and desired indoor temperatures. However, the materials and layer configuration seem to be pre-determined, so the optimization results are not clear. The wall configuration, at least, and potential realizations are overly restricted.

Jiang, et al. [30] present an analytical optimization method for evaluating the specific heat of internal envelopes for the purpose of controlling indoor air temperature. The problem is developed in terms of a simplified, passive solar room. With seemingly many limiting assumptions, the problem is reduced to what appears as simply heat exchange between two parallel plates with internal forced convection. It is not clear what exactly the internal envelope is meant to represent or how it is oriented in relation to the exterior envelope. The optimization problem is constructed as a problem of minimizing enthalpy in determining the internal envelope specific heat that yields the greatest improvement to indoor thermal comfort, subject to a constraint. The optimal solution appears to show the behavior of a phase change material (PCM), which can be considered a subset of variable property materials, in general, as opposed to constant property building materials considered in other studies. In particular, results show the specific heat of the internal envelope varying with the change in temperature of the internal envelope. The optimal specific heat is shown approaching the form of a dirac delta impulse function, which represents “the equivalent specific heat form of phase change material" [30]. While phase change materials may be used to limit internal temperature swings in theory, the viability of their application is still a challenge that has prevented even limited implementation. Furthermore, the results do not inform the assembly of multi-layer walls for improving decrement factor and time lag.

In Sambou, et al. [31], the authors review methods that have been studied to help reduce overheating that results from large amounts of insulation, such as 'free cooling', building orientation and natural ventilation, and thermal mass, or thermal inertia. Using genetic algorithms with results presented in a Pareto front, the authors seek to maximize both thermal resistance and capacitance. Each wall consists of N layers of homogeneous and isotropic material with fixed thickness. The optimization considers four parameters for each layer: thickness, thermal conductivity, density, and specific heat, each of which is constrained by a minimum and maximum value. The study limits the number of layers (N) to three, citing that the Pareto optimal front of solutions is identical for N greater than or equal to three. The first study considers fictitious materials while the second and third consist of ASHRAE classified materials with thicknesses fixed in the former and to be determined in the latter. Results show, as other studies have, that thermal mass at the interior with insulation at the exterior is best among the configurations considered. The authors a highlight a novel contribution, that is, the thickness of the optimal thermal mass is equivalent to 1/4th of the thermal wavelength. They describe the thermal wavelength as depending on the material and period of daily outside temperature oscillation. This work appears to be based on the assumption that more thermal inertia is necessarily better and leads to reduced building energy consumption, however, this is not always the case. For instance, Masoso shows [25] the potentially negative effect of increasing insulation on increasing annual energy consumption for a South African climate. Furthermore, the authors neglect common performance criteria, such as time lag and decrement factor, in focusing solely on maximizing the overall thermal resistance and capacitance of a multi-layer wall. The choice to maximize thermal resistance and capacitance also seems to neglect the original concern with overheating that was highlighted. The study is further limited to just two or three total layers.

A series of papers published in the 1980s from Duffin and Knowles [9, 32] focus on the thermal performance of adobe walls found in the American Southwest. The authors observe that the massive adobe walls work with large diurnal temperature variations to create a relatively cool indoor space during the day and warm conditions at night, even when temperatures drop in the desert. The authors suggest that this effect results from a phase lag close to 12 hours and refer to it as a “thermal flywheel effect” [9, 32]. An analogous RC ladder filter is used to represent one-dimensional conduction through a multi-layer wall, with common ground potential and sinusoidal input. The output is measured as the voltage across the final capacitor. The model includes skin resistance terms and room loads as optimization parameters. An analytical solution is proposed wherein the wall resistance and capacitance is assumed to vary exponentially across the thickness of the wall. In the first study, the goal is to choose resistor values given fixed capacitor values and phase lag while minimizing attenuation (or maximizing magnitude ratio). The attenuation factor, defined as the ratio of outside temperature amplitude to the inside temperature amplitude, is the inverse of the magnitude ratio.

In a subsequent work [32], the authors aim to minimize attenuation using two to three different layers of material. Based on an impedance matching analogy, the authors suggest that with wall capacitance higher towards the outside and decreasing towards the inside, less attenuation is achieved. These results are consistent with more recent studies that aim to increase attenuation and show the opposite configuration (placing insulation towards the outside and thermally massive material towards the inside) yields increased attenuation (decreased decrement factor). However, they are limited, because, for example, the procedure is based on assuming that resistance and capacitance layers vary exponentially across the wall, the phase lag is fixed, and the overall thermal resistance or capacitance of the wall is not fixed. So, the work does not

specifically address optimizing layer position and number for decrement factor and time lag with fixed overall thermal resistance and capacitance.

Citing the above work from Duffin and Knowles, Tsilingiris [33] develops and validates a numerical method for calculating transient and quasi-steady state heat transfer for two wall families with increasing amounts of thermal mass. The model considers both time varying solar insolation and ambient temperature with specific interior conditions prescribed. Two basic families are considered: both start as a lightweight construction with one layer of insulation between two layers of plaster. In the first, a layer of concrete is then added and progressively increased in thickness. Single and double layer brick walls with insulation and plaster are considered second. In total, six concrete and six brick wall configurations are studied. It is shown that increased heat capacity leads to lower peak and average heat flux values in both summer and winter conditions for climate data from Athens, considered the quasi-steady state input. It is also shown that transient responses are proportional to wall heat capacity. Finally, the brick walls seem to be better in winter and summer than the concrete walls. Like the other studies described, this work is limited by number of layers, materials, and configurations considered.

Ciampi, et al. [4], aim to optimize the order of resistive and capacitive layers in an external building wall to minimize the conditioning required in a room, while keeping the total wall resistance and capacitance fixed. The multi-layer wall is modeled as alternating layers of resistive and capacitive materials. To minimize conditioning, the indoor air temperature should be maintained even when subjected to external temperature variations. The external temperature variation is described by sinusoidal or impulse inputs. The indoor room air temperature is represented by Fourier components in terms of outside air temperature (shaded), sol-air temperature to account for solar radiation, and the thermal power (heating or cooling) supplied

by the HVAC system. This formula is adapted for different conditions so that optimizing the wall is transformed into minimizing some formulation of the temperature expression. A dimensionless parameter σ is defined that equals the product of the angular frequency (ω) and the RC time constant of the wall. Results are based on different ranges of values for σ and indicate that a configuration optimized for lower frequency (longer period) will not be optimal for higher frequency (shorter period). The authors conclude, generally, that "…the optimization should be carried out considering lower frequencies, because higher frequencies have a minor impact on the interiors" [4]. For a sinusoidal input and $\sigma < 18$, a symmetrically distributed three layer wall with capacitive layers sandwiched between resistive layers in an insulation / thermal mass / insulation configuration is best. As σ increases, the number of layers increases, and as σ becomes large (tends to infinity), the configuration approaches a homogeneous slab. Finally, the optimal configuration from an impulse input matches that of the sinusoidal input for small σ (three layers configured symmetrically in an R-C-R configuration). The authors also present a method for determining which common building materials achieve the thermal response of the optimized R-C-R wall configuration, but it is limited to one type of insulation and two types of thermally massive concrete material. Furthermore, while the number of layers ranges from one to some value *n*, it is not clear how the optimization procedure determines the optimal number of layers, because the procedure is developed for discrete cases (*n=1*, *n=2*, *n=3*, and *n=4*). A generalized procedure is not clearly outlined, and results are not expressed in terms of number of wall layers, so the effect of number of layers is not demonstrated. The accuracy of representing each layer as one lumped resistance or one lumped capacitance is also not addressed, which highlights a limitation in the model, that it is not necessarily a close physical representation of the actual wall system.

2.3 INTELLECTUAL MERIT AND BROADER IMPACTS

Given the notable body of literature evaluating building envelope design for energy performance, it is surprising that more universal guidelines do not already exist for wall assembly. Many studies have focused on specific building, location, and climate applications. Certainly, it is important to consider such specifics for intelligent and effective whole building design. However, the physics describing heat transfer and system response suggest that certain features of building design, such as wall configuration design guidelines, may benefit from a more generalized analysis. This work facilitates a generalized analysis by using analogous thermal-electrical modeling for one-dimensional heat conduction. It is shown Appendix B that that a steady periodic input with a 24 hour frequency is the dominant driving frequency for an exterior building wall, which supports the use of the frequency response analysis for analyzing the thermal performance of different wall configurations. The primary result that appears from the literature is the improvement in insulating performance and energy reduction from placing insulation towards the outside and thermal mass towards the inside of a wall. Because a limited number of configurations have been studied, it is not clear that this is the optimal configuration, only that it is better than placing insulation towards the inside with thermal mass towards the outside. The work here goes beyond this by studying the general response of multi-layer walls from a steady sinusoidal input, evaluating a larger number of wall configurations, searching for an optimal configuration, and finally, providing a rough estimate of the relative energy saving potential of an optimal configuration.

In Chapter 3, two RC network methods are presented for determining the frequency response of a multi-layer wall. Initial results in Chapter 4 provide general design guidelines about assembling multi-layer walls for improved insulating performance that go beyond results presented in the literature. The work shows that certain configurations yield superior insulating performance for a steady periodic input and the same overall thermal resistance and capacitance. An important result from this work is that an optimal configuration appears to exist. As a follow up to the initial results, a heuristic optimization study described in Chapter 5 explores the effects of increasing the number of layers in different wall configurations with fixed overall thermal resistance and capacitance and steady periodic input. Like other studies, this work illustrates the benefit of multi-layer wall configurations over single or double layer walls on improving decrement factor and increasing time lag. This approach also demonstrates that a specific number of layer divisions minimizes the magnitude ratio (decrement factor) for a given configuration family, confirming that an optimal configuration exists for some multi-layer walls. The literature is very limited in addressing the existence of optimal multi-layer configurations, and no formal optimization methods have been implemented to specifically minimize the magnitude ratio (decrement factor) for a steady periodic input. Therefore, the formal approach described in Chapter 5.3 of this work validates and supplements the findings from the heuristic studies in Chapters 5.1 and 5.2.

The analysis will first enable a designer to determine an optimal wall configuration given pre-selected building materials and wall thickness. This analysis may also be used for non-building applications, such as industrial processes where the minimization of periodic thermal loading is desired. For instance, material exposed to a periodic thermal fluctuation often fails sooner from loading fatigue than if insulated from temperature variations. To further address the

broader impacts of determining optimal wall configurations, Chapter 7 seeks to estimate the energy saving potential of an optimal configuration. Evaluating the energy savings of optimal configurations that minimize decrement factor and increase time lag will provide motivation for the development of new wall assembly and insulating material products, the latter being a focus for materials science research. Regarding new wall assemblies, it may be possible to utilize pre-fabricated building panel construction to implement multi-layer wall designs for different U.S. climate zones and desired insulation performance. The results of this work will also provide the motivation and basis for further development of adaptive wall structures, which has been largely dominated by research on vacuum insulation panels and phase change materials.

3.0 ANALYSIS TOOLS AND MODELING APPROACH

3.1 RC NETWORK REPRESENTATIONS (A HISTORICAL PERSPECTIVE)

RC network representations were particularly valuable to researchers before modern computing power made the implementation of numerical simulations feasible and relatively easy. However, limited computational resources meant that implementing RC network models could still be difficult, since a lumped parameter model typically requires a larger number of parameters or discretized nodes to achieve accurate modeling of a continuous medium. As a result, developing accurate reduced order models was of interest.

In his earlier work, Davies [34] presents a method for determining the values of a lumped parameter T-network RC model when limiting each multi-layer wall to four or fewer T-networks total. This work aims to determine values for the reduced order lumped parameter representation of thermal resistance and capacitance. For a sufficiently thin wall, the proposed method may be carried out analytically, without computational assistance. The reduced order model parameters are determined by minimizing the sum of the squares of the differences between the transmission matrix elements of the model and of the real wall. Davies concludes that most walls may be reasonably represented by three T-networks in a cascaded RC ladder model. This work is less relevant today than perhaps when it was first developed, given the increase in computational ability available for evaluating relatively high order models in a small, fraction of time and given

the automated model order reduction methods available from commercial software programs such as Matlab. Nonetheless, the work demonstrates the ability of the RC ladder representations to achieve accurate heat transfer modeling results, even with reduced order lumped parameter models. Thermal-electrical analogy methods have also been expanded for different applications.

For example, Hui and Tan [35] develop transmission line theory with numerical methods for modeling heat conduction (diffusion) in thin films with single and multiple layers for surface heating by a laser, which means that the "heat-penetration depth" is much smaller than the thickness of the material being studied. And Weber and Jóhannesson [36] develop two RC-network models (a 'simplified star-network' and a 'triangular network') to simulate thermally activated building components, which represent liquid filled pipes. In their justification for developing a new method, they describe drawbacks of numerical simulation methods, including small time steps that expend computation time and risk instability. The authors suggest RC-network, transfer function, and simplified analytical methods, or methods that combine the three aforementioned strategies, as viable and worthy alternatives to numerical simulation methods.

More recently, a thermal model based on an electrical analogy has been developed by Parnis [37] where circuit elements represent building construction properties and climate data. An "electric circuit simulator program" called SPICE is used to simulate the system in the time and frequency domain. To demonstrate the method, a house is modeled. The model uses *n*-length RC ladders to represent building layers. A method for developing lumped wall representations is presented, and the building time constant is discussed. In general, the focus of the Parnis thesis is on representing building layers to use in simplified building simulations, as opposed to optimizing those layers within a given envelope (wall, roof, floor) [37].

The convergence of an RC ladder representation to the 'exact' solution is described by Davies [38] and in more detail by Parnis [37]. As the number of T-networks (n) increases in an n-length RC ladder model, the transmission matrix (the product of cascading networks) approaches the “limiting analytic matrix” based on total layer resistance, capacitance, and period of excitation. To demonstrate convergence of the n-length RC ladder representation, Parnis [37] creates error functions to compare the elements of the total transmission matrix with the analytical elements for the same overall resistance and capacitance of a concrete layer and two temperature fluctuation periods (12 and 2 hours). Results indicate that more networks are needed as frequency increases (period decreases). Specifically, the error functions are reduced below 1% with a 9^{th} order model for the 12 hour period and a 27^{th} order model for the 2 hour period.

The transmission matrix method presented in this chapter also uses an RC ladder representation. This method is explored by Davies [38] and also Maillet, et al. [39], who present the term ‘quadrupole’ to describe the method which “relates four scalars or poles.” Carslaw and Jaeger [40, 41] are traditionally credited with introducing the transmission method for heat conduction.

These works demonstrate the enduring relevance of the RC network representations and the applicability to different types of heat transfer problems. The method has been used, as Davies originally investigated, to determine suitable reduced order representations of multi-layer walls, for integration within whole building models, and for simplified building models.

In this work, the basic T-section RC network representation is implemented and a refined model is developed that enables quick and easy analysis of the thermal response of a multi-layer wall. In these methods, the total thermal resistance and capacitance of the model is

taken to equal that of the real wall based on the thermophysical properties and thickness of the material. This serves to maintain physical relevance between the model system and actual wall.

3.2 ANALOGOUS ELECTRICAL REPRESENTATION OF THERMAL PROCESSES

In a thermal-electrical analogy, temperature is analogous to electrical potential, expressed as a voltage, and heat flux is analogous to current, or the rate of charge flow through a given surface. The electrical resistance term *R* represents thermal resistance and is equivalent to R-value (Equation (3.1)). The resistance of a layer to one-dimensional heat conduction depends on the thermal conductivity of the material and the overall thickness of the layer.

$$R = \frac{x}{k} = \frac{\Delta T}{\dot{Q}_A} = \left[\frac{m^2 \cdot K}{W}\right] \tag{3.1}$$

Similarly, the thermal storage capacity of a layer depends on the layer thickness and material properties. In particular, thermal capacitance is analogous to electrical capacitance and is defined as the product of material thickness (x), density (ρ), and specific heat (C_p) (Equation (3.2)).

$$C = x \cdot \rho \cdot C_p = \left[\frac{J}{m^2 \cdot K}\right] \tag{3.2}$$

Figure 3.1 shows a single T-shaped RC circuit representing one material layer with thermal capacitance C_1 and thermal resistance R_1.

3.3 “FOLDING” VOLTAGE DIVIDER METHOD

Throughout this study, each wall layer is modeled as an R-C-R T-network with the resistance divided evenly on each side of the capacitance, as shown in Figure 3.1. The centered temperature node represents an average temperature in the layer described by the R-C-R T-network. This analysis is in accordance with multiple studies [34, 42, 43] that determine the magnitude ratio (decrement factor) and phase lag (time lag) for heat conduction in external walls using an electrical analogy. The RC system is formed by connecting each layer in series with resistance added at each end to capture the convective heat transfer at both interior ($R_{h,rm}$) and exterior ($R_{h,amb}$) sides of the wall.

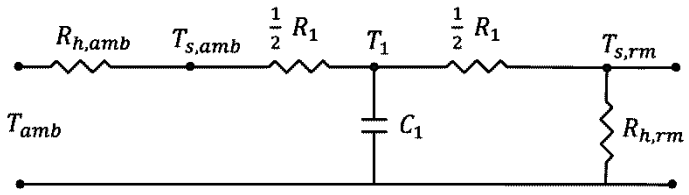

Figure 3.1. RC Network Model for a Single Layer Wall Represented by One Temperature Node

The wall system transfer function is determined for frequency analysis using a variation on traditional impedance methods and a voltage divider calculation, termed the “folding” method [44]. Figure 3.2 (a) shows the RC circuit model for a wall with N layers, where T_{amb} is the input and $T_{s,rm}$ is the system output. In this model, regardless of layer thickness or thermal properties, each layer of material is represented by a single R-C-R T-network where R_i is the layer’s thermal resistance and C_i is the layer’s thermal capacitance. The outside and inside surface heat transfer coefficients (h_{amb} and h_{rm}) may be approximated using the ASHRAE [45]

procedure for estimating surface conductance. A summer time wind speed of 7.5 mph and building material emissivity of 0.90 is used in the calculation to obtain h_{amb} = 16.74 W/m^{2}K and h_{rm} = 8.23 W/m^{2}K.. The resistance (R) and capacitance (C) of each layer is defined according to Equations (3.1) and (3.2). The impedance value for the resistance of layer "i" is shown in Equation (3.3), where the division by two is included to account for the fact that the thickness of each layer is divided into two. The corresponding impedance for the capacitance of layer "i" is shown in Equation (3.4).

$$Z_{R_i} = \frac{1}{2} R_i \tag{3.3}$$

$$Z_{C_i} = \frac{1}{sC_i} \tag{3.4}$$

The RC circuit in Figure 3.2 (a) can be simplified by recognizing that the transfer function of primary interest, $G(j\omega) = T_{s,rm}/T_{s,amb}$, can be expressed as the product of intermediate transfer functions, shown in Equation (3.5).

$$\frac{T_{s,rm}}{T_{s,amb}} = \frac{T_n}{T_{s,amb}} \cdot \frac{T_{n-1}}{T_n} \cdots \frac{T_1}{T_2} \cdot \frac{T_{s,rm}}{T_1} \tag{3.5}$$

To determine the intermediate transfer functions, the circuit is collapsed from right to left by combining individual impedances in series or in parallel. The transfer function relating each

layer is calculated as the circuit is reduced. The transfer function for the innermost layer, including convective resistance ($R_{h,rm}$), is calculated first. In Equation (3.6), T_1 represents the temperature in the first layer, measured as the voltage across the first capacitor C_1. The circuit can then be reduced as shown in Figure 3.2 (b) using an equivalent impedance Z_{eq_1} defined in Equation (3.7). The transfer function relating T_1 to T_2 is also calculated as a voltage divider and shown in Equation (3.8).

$$\frac{T_{s,rm}}{T_1} = \frac{R_{h,rm}}{R_{h,rm} + Z_{R_1}},\ Z_{R_1} = \frac{1}{2}R_1 \tag{3.6}$$

$$Z_{eq_1} = \left[\frac{1}{Z_{R_1} + R_{h,rm}} + \frac{1}{Z_{C_1}}\right]^{-1} \tag{3.7}$$

$$\frac{T_1}{T_2} = \frac{Z_{eq_1}}{Z_{eq_1} + Z_{R_1} + Z_{R_2}} \tag{3.8}$$

Defining a new nested impedance, Z_{eq_2}, the circuit can be further collapsed as shown in Figure 3.2 (c), where equivalent impedance Z_{eq_2} is calculated in a similar manner. The general expression for equivalent impedance for the i^{th} layer Z_{eq_i} is shown in Equation (3.9). Subsequent transfer functions relating T_2 to T_3, T_3 to T_4, and eventually T_{i-1} to T_i, are calculated according to Equation (3.10).

$$Z_{eq_i} = \left[\frac{1}{Z_{eq_{i-1}} + Z_{R_{i-1}} + Z_{R_i}} + \frac{1}{Z_{C_i}} \right]^{-1} \tag{3.9}$$

$$\frac{T_{i-1}}{T_i} = \frac{Z_{eq_{i-1}}}{Z_{eq_{i-1}} + \left(Z_{R_{i-1}} + Z_{R_i} \right)} \tag{3.10}$$

Then taking the product of each intermediate transfer function, as shown in Equation (3.5), gives the final relationship of interest $G(j\omega) = T_{s,rm}/T_{s,amb}$ or $G(j\omega) = T_{s,rm}/T_{amb}$ when the outside convection coefficient is included, which is easily evaluated for any value of ω. In this work, the magnitude ratio and phase at a period of 24 hours (ω_{day} = 7.27e-5 rad/s) are extracted from the frequency analysis for each wall assembly system. This procedure is used to develop transfer functions for each wall assembly considered, thereby enabling a quick and simple frequency analysis procedure.

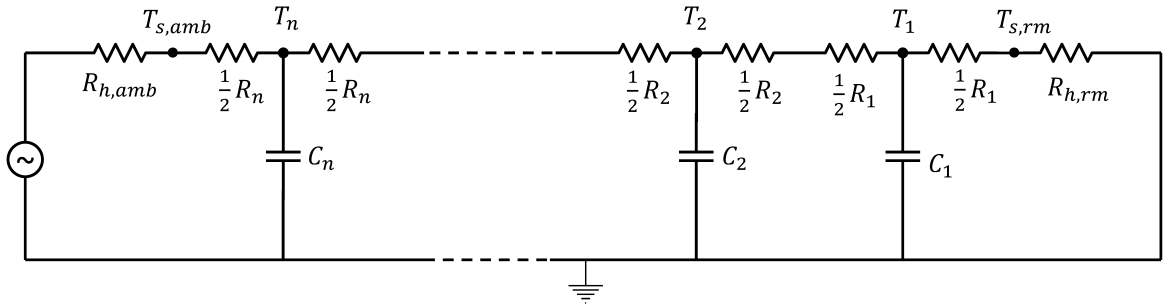

a.

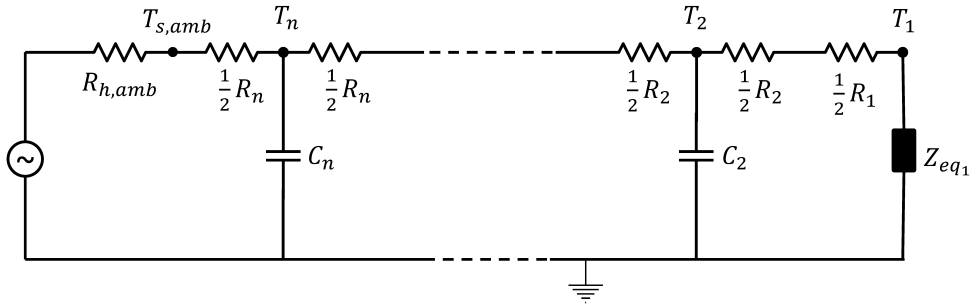

b.

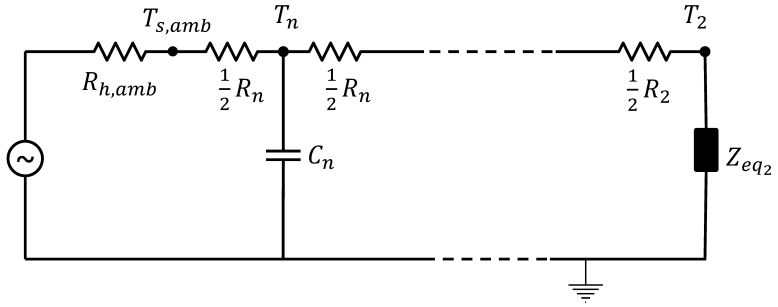

c.

Figure 3.2. N-layer RC Network Diagram. (a) Full circuit, (b) Collapsed circuit to first equivalent impedance, (c) Collapsed circuit to second equivalent impedance.

To validate the "folding" method model used in this part of the study [44], the seven wall configurations from Al-Sanea and Zedan [20] are modeled using this RC circuit methodology

and results are compared with those published. The seven wall configurations are shown in Figure A. 1. Each wall contains 200 mm concrete (grey) and 78 mm insulation (tan) distributed in varying configurations between two 15 mm layers of cement plaster (black) on both inner and outer surfaces. The overall wall thickness (308 mm) and total volume of each material is fixed, so the total resistance and capacitance values do not change regardless of how the layers are arranged.

The first family considers a single 78 mm layer of insulation placed towards the inside, middle, and outside of the wall. The second family splits the insulation into two 39 mm layers and distributes them at the inside/middle, inside/outside, and middle/outside positions. The final configuration positions one-third of the insulation (26mm) at the inside, middle, and outside, with concrete divided evenly between the three insulation layers. Because the decrement factor and time lag reported by Al-Sanea and Zedan [20] are equivalent to the magnitude ratio and phase lag produced in the frequency analysis, results may be compared directly. This data is provided in Table 1 for the decrement factor and magnitude ratio as a percentage, along with the time lag and phase lag, which is converted from radians to hours (considering a 24-hour period).

Table 1. Model Validation Results

Wall System	Decrement Factor (%)	Magnitude Ratio (%)	Time Lag (hours)	Phase (hours)
Wall 1a	1.35	1.51	6.13	5.92
Wall 1b	1.34	1.55	7.33	7.53
Wall 1c	0.74	0.90	6.71	6.10
Wall 2a	0.42	0.51	9.33	8.97
Wall 2b	0.24	0.33	8.19	6.76
Wall 2c	0.26	0.31	10.44	10.07
Wall 3	0.13	0.16	12.13	11.27

Table 1 shows a reasonable agreement between the models, considering the lumped parameter RC model has not been discretized independently for each layer. In general, any lumped parameter model necessarily sacrifices some accuracy to enable or expedite calculation. Here, the magnitude ratio from the RC model differs from the decrement factor results by 21% on average, while the time lag results differ by 7% on average. A lower percent error would be desirable, but further analysis reveals that the RC model consistently predicts performance trends. In addition, the ease and quickness of implementing numerous wall configurations using the RC model makes it ideal for analyzing general trends and investigating many different configurations.

The results show consistent trends with those from Al Sanea and Zedan [20]. Both models predict that Wall 1c has better insulating performance, with insulation positioned towards the outside, than Walls 1a and 1b with insulation positioned towards the inside and middle, respectively. The models also agree that Wall 3 has the best performance among all of the walls studied, and Walls 2b and 2c have similar performance, which improves over Wall 2a. In terms of time lag, similar trends are observed. Wall 3 in both models has the longest time lag among all seven studied. Comparing results demonstrates the ability of the RC model to accurately capture thermal performance trends produced by a numerical solution to the one-dimensional heat conduction equation. The RC “folding” model is used initially to investigate trends that have not been well covered in the past and suggest improvements over previous conclusions about wall assembly. Additional studies are conducted using a transmission matrix method.

3.4 TRANSMISSION MATRIX METHOD

The transmission line model or matrix method uses cascaded four-port or two-port pair (or two-port, for short) networks as a lumped parameter representation of a transmission line, or here, one-dimensional heat conduction. A single port network is shown in Figure 3.3. In the model used here, each port corresponds to a single R-C-R T-network. In Figure 3.2 (a), for example, *N* ports will represent the *N* inter-layer temperature nodes (T_i) shown.

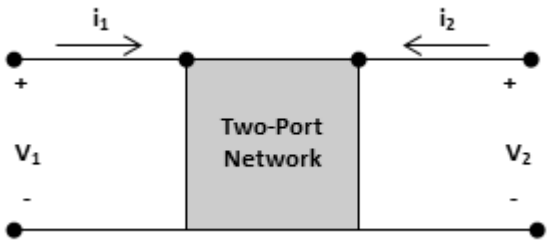

Figure 3.3. Two-port network diagram.

The method can be thought of as a transmission parameter method, in contrast to impedance, admittance, and scattering parameter methods, which all have different matrix parameters relating the input and output parameters (V_1, V_2, i_1, i_2). Kirchhoff's laws are used to derive the transmission matrix parameters for the network shown in Figure 3.4, where two current loops are shown and the sum of the voltages in each loop is zero.

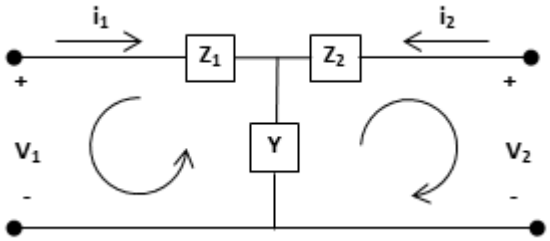

Figure 3.4. Deriving transmission matrix parameters from Kirchhoff's voltage law.

In the frequency domain where $s = j \cdot \omega$, the current '*i*' becomes 'I' and $V = I \cdot Z$ (impedances are represented as *Z* and admittances as *Y* in this notation). Then, two equations are written in terms of V_1, V_2, i_1, and i_2 in Equations (3.11) and (3.12).

$$V_1 - \frac{I_1}{Y} + \frac{I_2}{Y} - I_1 Z_1 = 0 \rightarrow I_2 = -YV_1 + \left(1 + YZ_1\right) I_1 \tag{3.11}$$

$$-V_2 - \frac{I_2}{Y} + \frac{I_1}{Y} - I_2 Z_2 = 0 \tag{3.12}$$

Solving for I_2 and V_2, the two equations can then be expressed in matrix form. Equation (3.13) is the transmission matrix representation for the circuit shown in Figure 3.4, where V_1 and i_1 are the network inputs and V_2 and i_2 are the network outputs.

$$\begin{bmatrix} V_2 \\ I_2 \end{bmatrix} = \begin{bmatrix} (1+YZ_2) & -(YZ_1Z_2 + Z_1 + Z_2) \\ -Y & (1+YZ_1) \end{bmatrix} \begin{bmatrix} V_1 \\ I_1 \end{bmatrix} \tag{3.13}$$

A thermally analogous RC network is shown in Figure 3.5 and its transmission matrix in Equation (3.14).

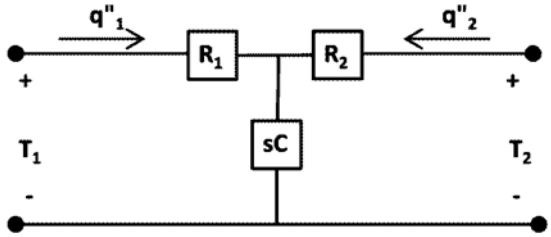

Figure 3.5. Analogous thermal RC T-network for one layer.

$$\begin{bmatrix} T_2 \\ q"_2 \end{bmatrix} = \begin{bmatrix} (1+sCR_2) & -(sCR_1R_2 + R_1 + R_2) \\ -sC & (1+sCR_1) \end{bmatrix} \begin{bmatrix} T_1 \\ q"_1 \end{bmatrix} \tag{3.14}$$

When the network includes non-resistive components, such as capacitors or inductors, the transmission matrix is comprised of complex valued elements.

The transmission matrix relates two input and two output parameters. The transfer function relating two parameters can be derived using Cramer's Rule and the principle of superposition. Define τ as the transmission matrix and apply Cramer's rule as shown in Equations (3.15)-(3.17). The transfer functions for the networks in Figure 3.4 and Figure 3.5 are also shown.

$$\tau = \begin{bmatrix} A & B \\ C & D \end{bmatrix} \rightarrow \begin{bmatrix} V_2 \\ I_2 \end{bmatrix} = \tau \begin{bmatrix} V_1 \\ I_1 \end{bmatrix} \rightarrow \begin{bmatrix} V_2 \\ I_2 \end{bmatrix} = \begin{bmatrix} A & B \\ C & D \end{bmatrix} \begin{bmatrix} V_1 \\ I_1 \end{bmatrix} \tag{3.15}$$

$$\begin{vmatrix} V_2 & B \\ I_2 & D \end{vmatrix} = V_1 \begin{vmatrix} A & B \\ C & D \end{vmatrix} \rightarrow V_2 D - I_2 B = V_1 \det(\tau) \tag{3.16}$$

$$\text{For } I_2 = 0: \ \frac{V_2}{V_1} = \frac{\det(\tau)}{D} = \frac{1}{D} = \frac{1}{1 + YZ_1} = \frac{1}{1 + sCR_1} \tag{3.17}$$

A transmission matrix can be derived for each network in the ladder relating intermediate nodes. The transmission model used here relates the temperatures between the resistors, such as T_{21} and T_{32}, as shown in Figure 3.6. (This is in contrast to the folding method that relates T_1 to T_2, for instance.)

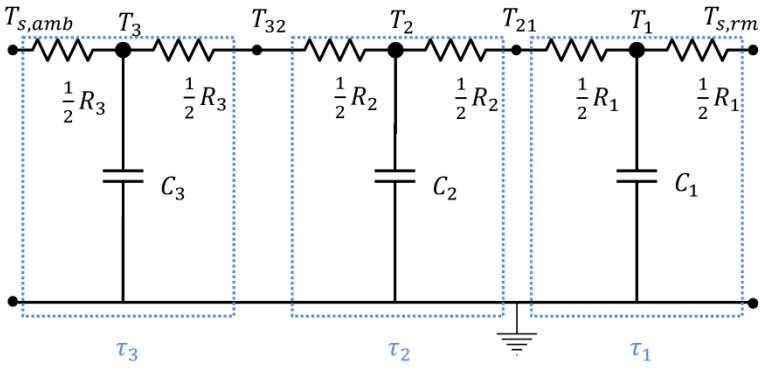

Figure 3.6. Transmission matrices τ_i for a three-node wall (i=1,2,3) represented as three RC T-networks.

Then the total transmission matrix relating input and output currents and voltages (ambient conditions are considered inputs and room conditions are considered outputs in this formulation), or temperature and heat flux values, is calculated in Equation (3.18) as the ordered product of each transmission matrix τ_i in the *N*-length ladder. (As in any matrix multiplication, the order of the operations matters.)

$$\tau_{total} = \prod_{i=1}^{N} \tau_i \tag{3.18}$$

The product of transmission matrices combined with the procedure in Equations (3.15)-(3.17) yields the overall transfer function (3.19), as in Equation (3.5), except the inside convection coefficient is accounted for in a subsequent step.

$$\tau_{total} = \tau_1 \cdot \tau_2 \cdots \tau_{n-1} \cdot \tau_n \rightarrow \frac{T_{s,rm}}{T_{s,amb}} \tag{3.19}$$

3.4.1 Adding Interior Convection

Based on a short-hand calculation and subsequent validation, the inside convection coefficient $R_{h,rm}$ is incorporated in the transmission matrix model via a simple formulation based on the elements of the overall transmission matrix (A, B, C, and D) that relate $T_{s,rm}$ to $T_{s,amb}$ as in Figure 3.2 (a). This formula is shown in Equation (3.20). To validate results with a finite volume

method, the outside convection coefficient $R_{h,amb}$ is taken to be very large, which assumes that the outside surface temperature is equivalent to the ambient temperature.

$$\frac{T_{s,rm}}{T_{s,amb}} = \frac{R_{h,rm}}{R_{h,rm}(D)+(-B)} \tag{3.20}$$

3.4.2 Refinement Using Higher Order Models

The transmission matrix method also allows material layers to be easily discretized for more accurate representations. Since each T-network represents one temperature node in a given layer of material, as many nodes may be used as necessary to model the heat conduction and temperature distribution in each layer. Figure 3.7 shows how a single network is represented in this discretized model, with the thermal resistance split around the thermal capacitance.

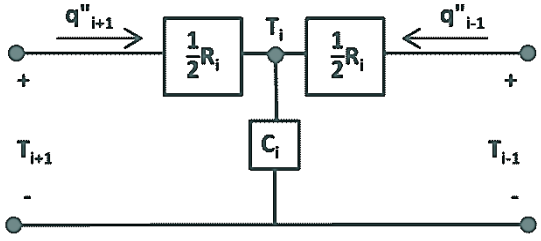

Figure 3.7. Single node RC T-network representation.

To validate the convergence or 'mesh independence' of the transmission method, a single 278 mm layer of concrete, then insulation, is discretized using the transmission matrix method

described here and compared to a finite volume solution, using $R_{h,amb}$ very large and $R_{h,rm}$ equal to 20 W/m^2·K. Table 2 shows the material properties used in the simulations.

Table 2. Material thermophysical properties.

	k (W/m·K)	ρ (kg/m^3)	C_p (J/kg·K)
Concrete	0.81	1618	840
Insulation	0.034	23	1280

Comparative results are presented for the magnitude ratio versus number of nodes in the transmission matrix model and elements in the finite volume model in Figure 3.8 for concrete and Figure 3.10 for insulation. Figure 3.9 and Figure 3.11 show the comparative phase lag results for the two methods. The two methods converge to the same magnitude ratio with sufficient layer discretization. The phase lag results are less precise but still comparable. With this refined RC modeling method, results from studying additional multi-layer wall configurations are more reliable and demonstrate a more absolute measure of performance than the trends found using the original, un-refined folding method (although this method could also be extended to discretize each layer accurately). Compared with their finite volume counterparts, the computational expense is much smaller for the transmission matrix method.

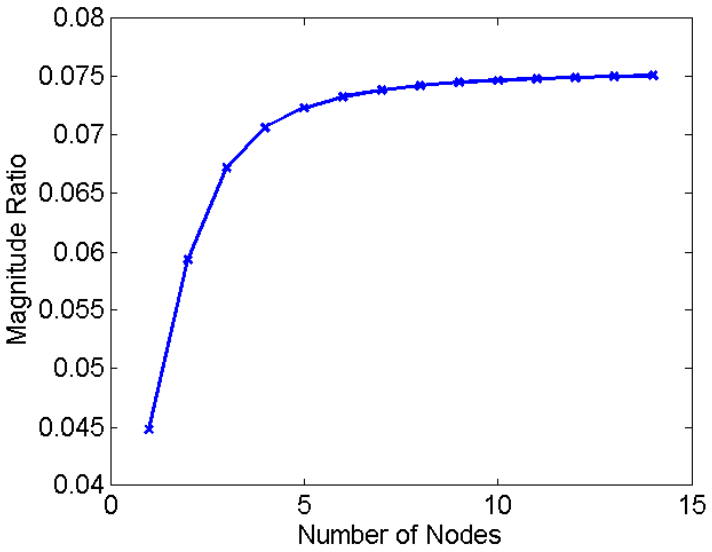

(a)

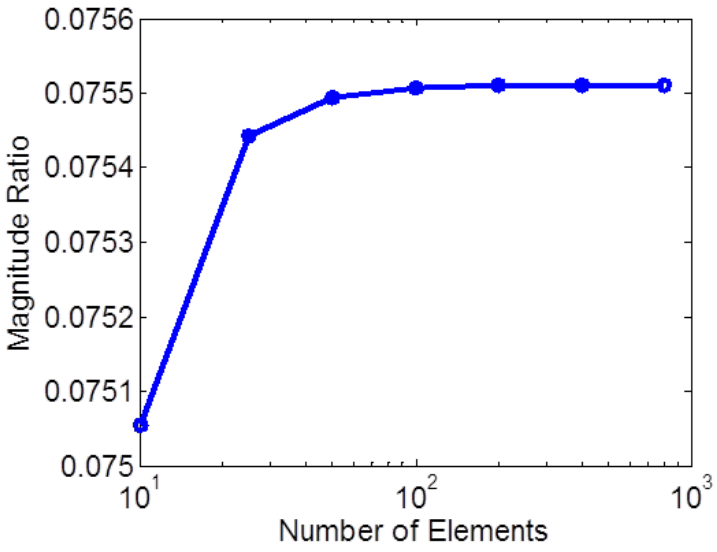

(b)

Figure 3.8. (a) Transmission matrix model convergence for 278 mm concrete: magnitude ratio.

(b) Finite volume model convergence for 278 mm concrete: magnitude ratio (M. Kimber).

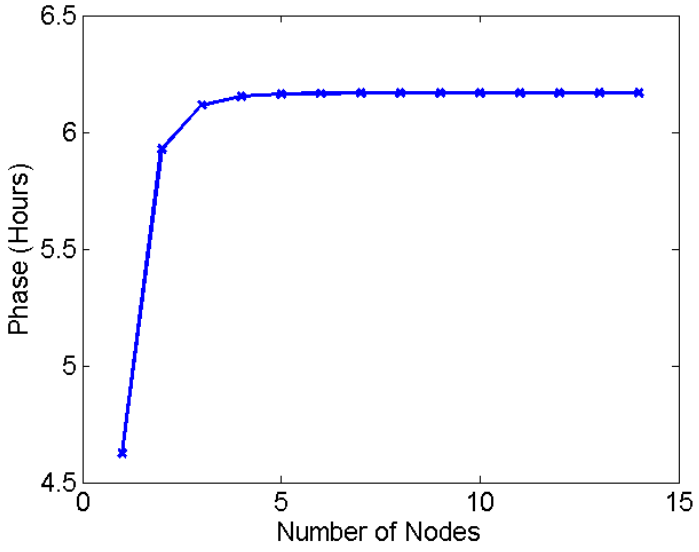

(a)

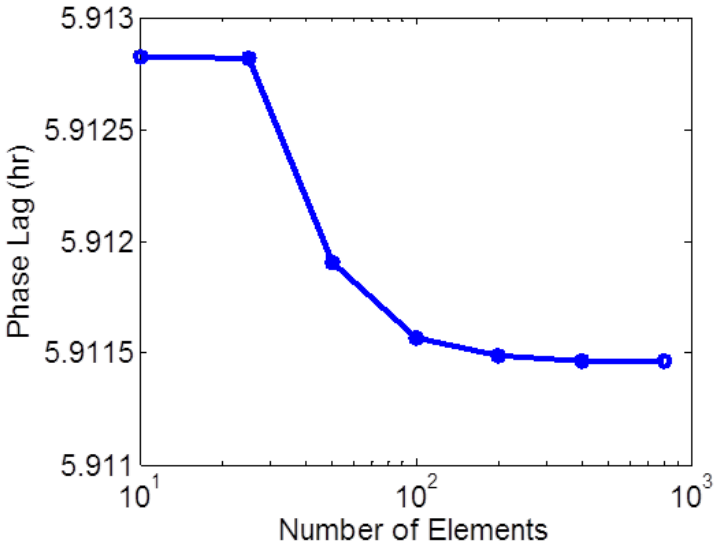

(b)

Figure 3.9. (a) Transmission matrix model convergence for 278 mm concrete: phase. (b) Finite volume model convergence for 278 mm concrete: phase (M. Kimber).

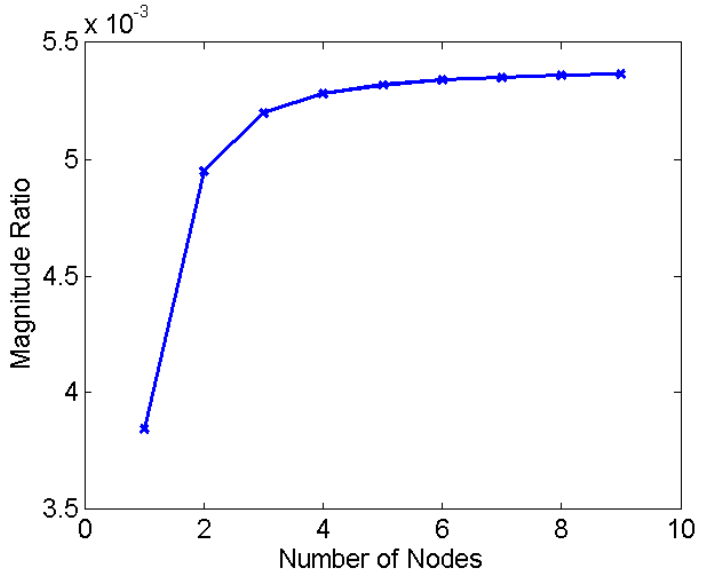

(a)

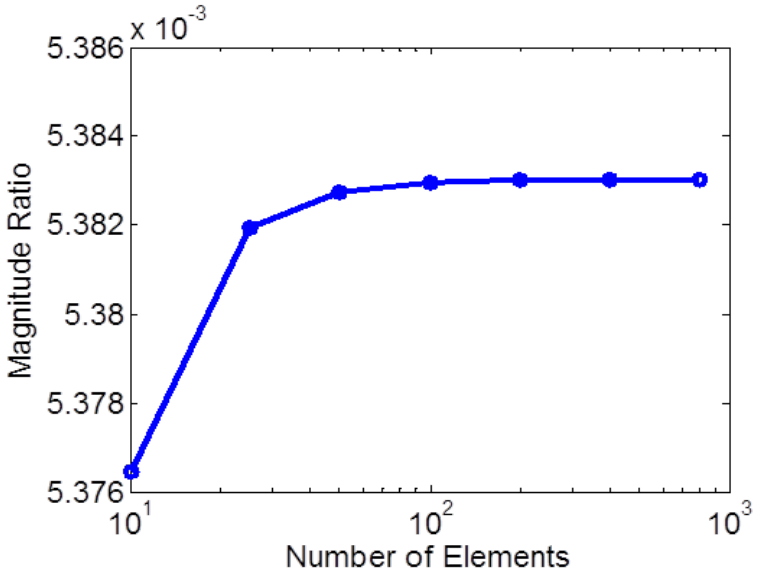

(b)

Figure 3.10. (a) Transmission matrix model convergence for 278 mm insulation: magnitude ratio. (b) Finite volume model convergence for 278 mm insulation: magnitude ratio (M. Kimber).

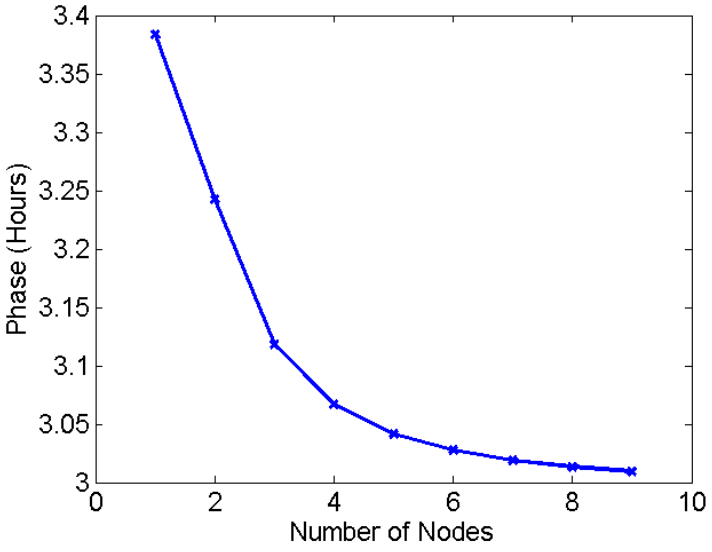

(a)

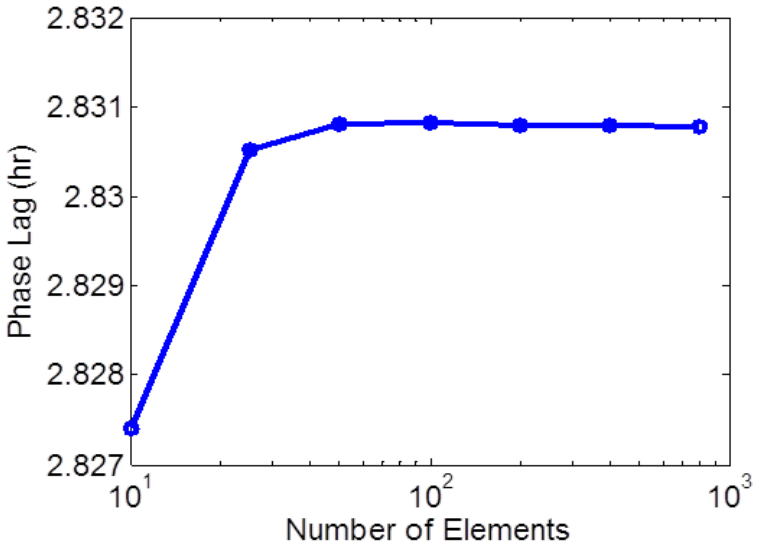

(b)

Figure 3.11. (a) Transmission matrix model convergence for 278 mm insulation: phase. **(b)** Finite volume model convergence for 278 mm insulation: phase (M. Kimber).

4.0 INITIAL STUDY OF MULTI-LAYER WALLS USING RC FOLDING METHOD

External walls provide an important barrier between occupied building spaces and variable ambient conditions. The focus of this chapter is to provide fundamental insight into configuring wall layers for improved insulating performance, evaluating a larger set of configurations and using a generalized procedure, compared to what has been presented in the literature. In this analysis, the walls are decoupled from any specific climatic data or building orientation, and results provide insight into the frequency response of each wall system as an assembly of multiple insulation and thermal mass layers. The problem of concern is illustrated in Figure 4.1. Suppose a wall is to be comprised of fixed amounts of insulation (e.g., fiberglass) and thermal mass (e.g., concrete). For a particular wall design, the left hand side is subject to an oscillatory ambient temperature (i.e., outdoor environment). The corresponding internal surface temperature (filtered by the wall) is seen on the right hand side (i.e., inside surface of a room). Two examples of potential wall designs are also shown in Figure 4.1. Any particular layer exhibits thermal resistance and capacitance behavior, which is influenced by the material properties, namely thermal conductivity (k), density (ρ), and heat capacity (C_p), and the thickness (L) of each layer. However, since the same amount of each material is used for any wall design, the total resistance and capacitance remain constant, regardless of how it is divided or arranged. Since, in this chapter, a fixed amount of insulating material and thermal mass will be used for each wall

design, the primary variables left to define are the number of layers, the thickness of the layers, and the order in which the layers are arranged.

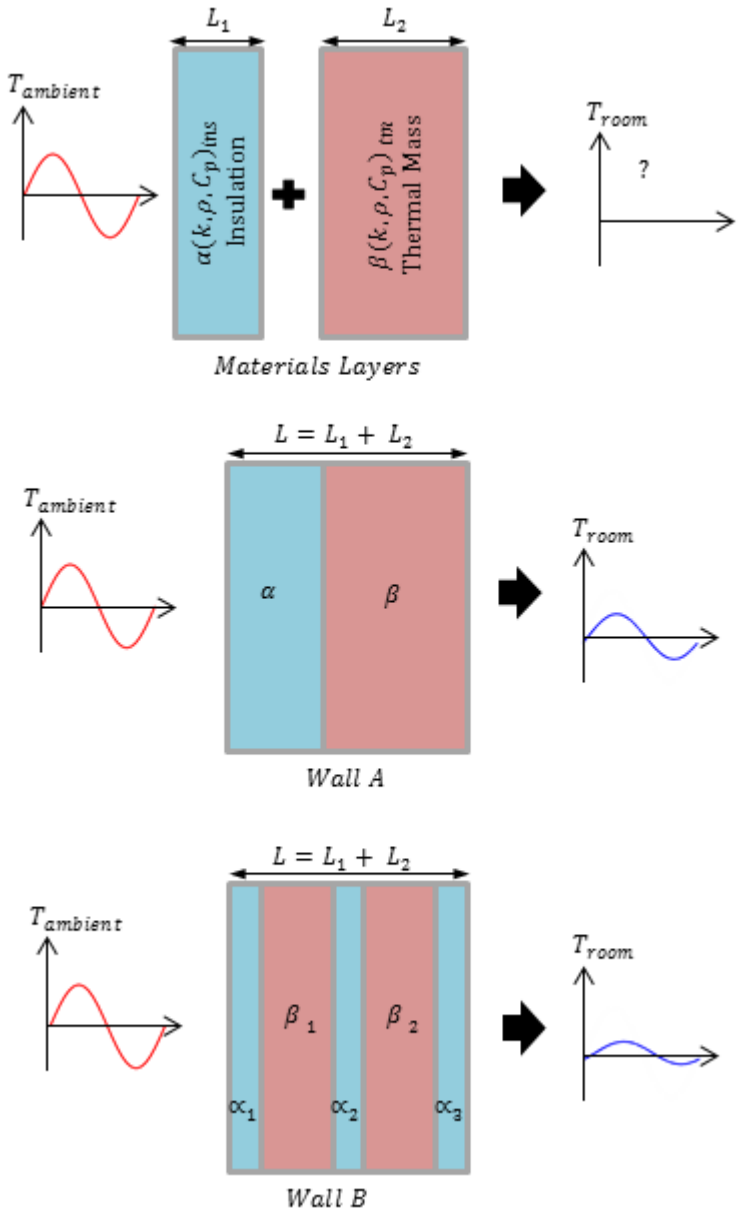

Figure 4.1. Assembling wall layers for improved thermal performance.

The "folding" method described in Chapter 3 is used to model one-dimensional heat conduction through the wall and determine the magnitude ratio and phase of the frequency response evaluated at the frequency corresponding to a period of one day (ω_{day} = 7.27 x 10^{-5} rad/s). Justification for using this frequency is presented in Appendix B. The two temperatures used to quantify the wall system transfer function are the inside and outside surfaces of the wall (i.e., two surfaces exposed to the indoor and outdoor environments, respectively). The frequency response is evaluated to assess (1) the effect of configuration (2) the effect of weighting insulation and/or mass towards each side of the wall compared to distributing layers evenly, and (3) the effect of increasing the overall number of insulation and thermal mass layers.

4.1 MULTI-LAYER WALL STUDY

Specific objectives of this multi-layer wall study are to distinguish between the performance of an insulation/mass/insulation configuration compared to mass/insulation/mass and insulation towards the inside compared to insulation towards the outside, to investigate the effect of distributing layers un-evenly, and to evaluate the effect of increasing the overall number of insulation and thermal mass layers. In order to understand the thermal behavior trends for all possible multi-layer wall arrangements, four basic patterns are studied, with each pattern being studied as a family of configurations. A total of thirty-three wall configurations are evaluated based on four primary configurations, shown in Figure 4.2.

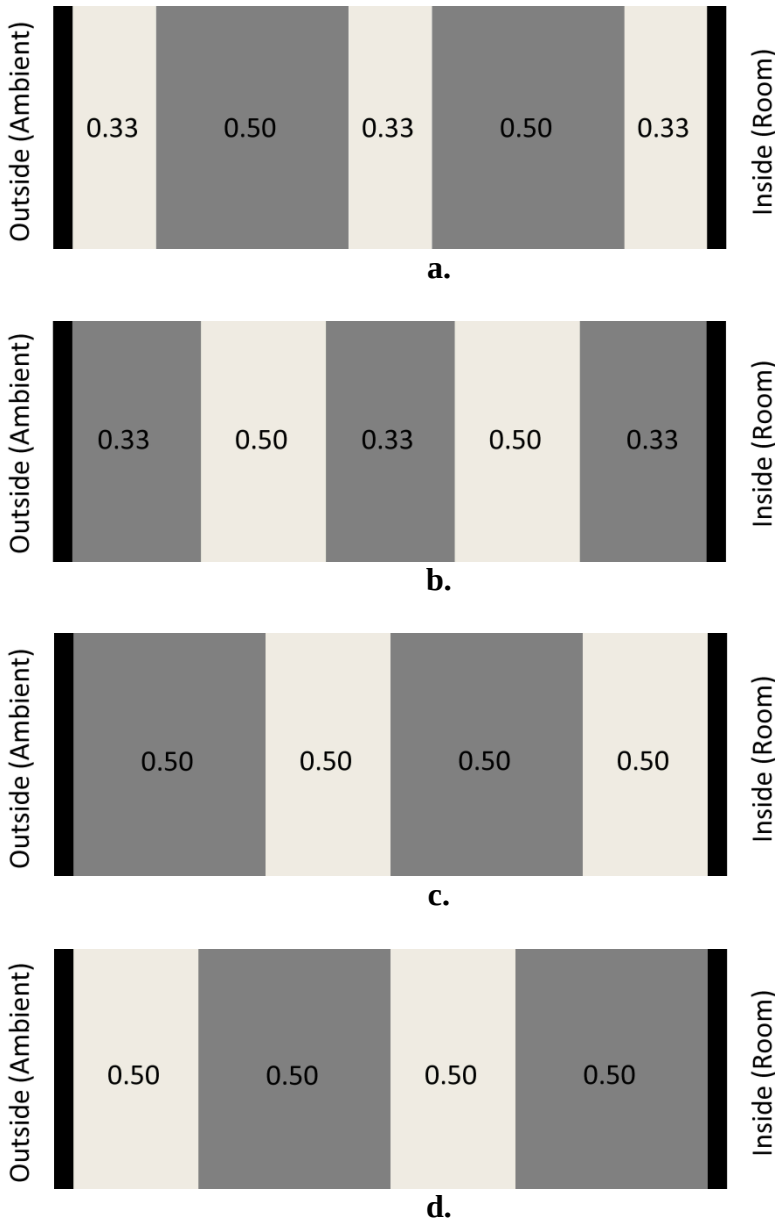

Figure 4.2. Four Wall Configurations: (a) Wall 0, (b) Wall 1, (c) Wall 2, (d) Wall 3. The shading represents material (light grey = insulation, dark grey = concrete), and the numbers represent percentage of that component (insulation or concrete) in each layer.

Each wall is the same total thickness, and has thin layers of cement plaster at the outermost layers. The four basic patterns are defined by how the insulation and concrete are

positioned. Wall 0 has seven total layers, including the plaster layers, with insulation at the outer layers. The fixed volume of insulation is divided into three equally sized layers (~33% each), and the fixed volume of concrete is split evenly between two layers (50% each). This distribution is reversed in Wall 1, which has seven total layers with concrete at the outer layers. Wall 2 has six total layers with insulation at the outside layer and concrete at the inside layer. Wall 3 reverses the insulation and concrete layers from Wall 2. Insulation and concrete are divided evenly in Walls 2 and 3, fifty percent for each layer in the primary configurations. Variations of these four primary or base configurations are extended to investigate different weighting scenarios for the insulation and concrete layers.

Any weighting distribution might be selected for study with infinitely many scenarios possible. For this study, scenarios are studied in which each base configuration (0.0, 1.0, 2.0, and 3.0 as defined in Fig. 4.2), is extended using different volumetric weightings. Specifically, configurations are constructed to investigate alternatively weighting insulation, concrete, or both insulation and concrete by 80% of each material volume towards the outside, middle, or inside of the wall. Table 3 shows the configurations for all walls studied. For example, Wall 0.1 weights 80% of the insulation towards the outside with the remaining 20% divided evenly between the middle and inside. Similarly, Wall 1.1 weights 80% of the concrete towards the outside. Wall 1.2 weights 80% of the concrete towards the middle, and Wall 1.3 shifts it to the inside. Walls 1.4 and 1.5 alternate weighting the two insulation layers towards the outside or inside, while Walls 1.6 and 1.7 alternate weighting concrete and insulation layers towards the outside or inside together.

The four base configurations and the various weighting scenarios are designed to clarify wall assembly guidelines regarding layer thickness, or distribution, and material position. Wall

0.0, with evenly distributed layers, is extended to investigate the effect of increasing the total number of layer divisions. As with the other wall variations, Walls 0.8, 0.9, and 0.10 have the same total volume of insulation and concrete, thus maintaining the same overall resistance and capacitance. However, each wall configuration 0.8, 0.9, and 0.10 divides the two materials into a greater number of thinner layers. One might expect further divisions to continually improve performance, but results will be discussed that suggest otherwise.

Table 3. Weighting variations for each of three wall configurations and extended Wall 0 configurations (8,9, and 10). Layer thicknesses are displayed as percentages of total wall insulation or thermal mass.

Wall 0	CP	INS	MASS	INS	MASS	INS	CP	...	INS	CP	...	INS	CP	...	INS	CP
0.0	Ambient Conditions	0.33	0.50	0.33	0.50	0.33	Room Conditions									
0.1		**0.80**	0.50	0.10	0.50	0.10										
0.2		0.10	0.50	**0.80**	0.50	0.10										
0.3		0.10	0.50	0.10	0.50	**0.80**										
0.4		0.33	**0.80**	0.33	0.20	0.33										
0.5		0.33	0.20	0.33	**0.80**	0.33										
0.6		**0.80**	**0.80**	0.10	0.20	0.10										
0.7		0.10	0.20	0.10	**0.80**	**0.80**										
0.8		0.25	0.33	0.25	0.33	0.25	0.33	0.25								
0.9		0.20	0.25	0.20	0.25	0.20	0.25	0.20	0.25	0.20						
0.10		0.167	0.20	0.167	0.20	0.167	0.20	0.167	0.20	0.167	0.20	0.167				

Wall 1	CP	MASS	INS	MASS	INS	MASS	CP
1.0	Ambient Conditions	0.33	0.50	0.33	0.50	0.33	Room Conditions
1.1		**0.80**	0.50	0.10	0.50	0.10	
1.2		0.10	0.50	**0.80**	0.50	0.10	
1.3		0.10	0.50	0.10	0.50	**0.80**	
1.4		0.33	**0.80**	0.33	0.20	0.33	
1.5		0.33	0.20	0.33	**0.80**	0.33	
1.6		**0.80**	**0.80**	0.10	0.20	0.10	
1.7		0.10	0.20	0.10	**0.80**	**0.80**	

Wall 2	CP	INS	MASS	INS	MASS	CP
2.0	Ambient Conditions	0.50	0.50	0.50	0.50	Room Conditions
2.1		**0.80**	0.50	0.20	0.50	
2.2		0.20	0.50	**0.80**	0.50	
2.3		0.50	**0.80**	0.50	0.20	
2.4		0.50	0.20	0.50	**0.80**	
2.5		**0.80**	**0.80**	0.20	0.20	
2.6		0.20	0.20	**0.80**	**0.80**	

Wall 3	CP	MASS	INS	MASS	INS	CP
3.0	Ambient Conditions	0.50	0.50	0.50	0.50	Room Conditions
3.1		0.50	**0.80**	0.50	0.20	
3.2		0.50	0.20	0.50	**0.80**	
3.3		**0.80**	0.50	0.20	0.50	
3.4		0.20	0.50	**0.80**	0.50	
3.5		**0.80**	**0.80**	0.20	0.20	
3.6		0.20	0.20	**0.80**	**0.80**	

4.2 MULTI-LAYER STUDY RESULTS

Figure 4.3, Figure 4.4, Figure 4.5, and Figure 4.6 illustrate the (a) magnitude ratio and (b) phase results for each material weighting configuration of the four wall families. Figure 4.3 (a), for example, shows the magnitude ratio results for Wall 0.0 through 0.7 from the RC model frequency analysis, and Figure 4.3 (b) shows the respective phase results. Each bar is shaded and labeled to indicate which material is weighted (no weighting or evenly distributed, insulation weighting, concrete weighting, or both in a combined weighting) and in what direction the weighting is applied (outside, middle, or inside). Refer to Figure 4.2 and Table 3 for more detailed descriptions of each wall configuration.

Wall 0.0 with evenly distributed layers and insulation at the outside, middle, and inside, has a lower magnitude ratio than any of the other Wall 0 weighting configurations (0.1 through 0.7) and outperforms all other configurations when considering magnitude and phase. For the Wall 0 family, weighting insulation towards the inside performs better than weighting towards the middle or outside, but not as well as distributing the three layers evenly. Weighting insulation and concrete together (either on the inside or outside) has the highest magnitude ratio or worst insulating performance. Results also show that among the Wall 0 variations, the two configurations, 0.4 and 0.5, that maintain insulation evenly at the inside and outside and simply shift the concrete between the two middle layers performs better than any configuration that deviates more dramatically from the 0.0 base configuration.

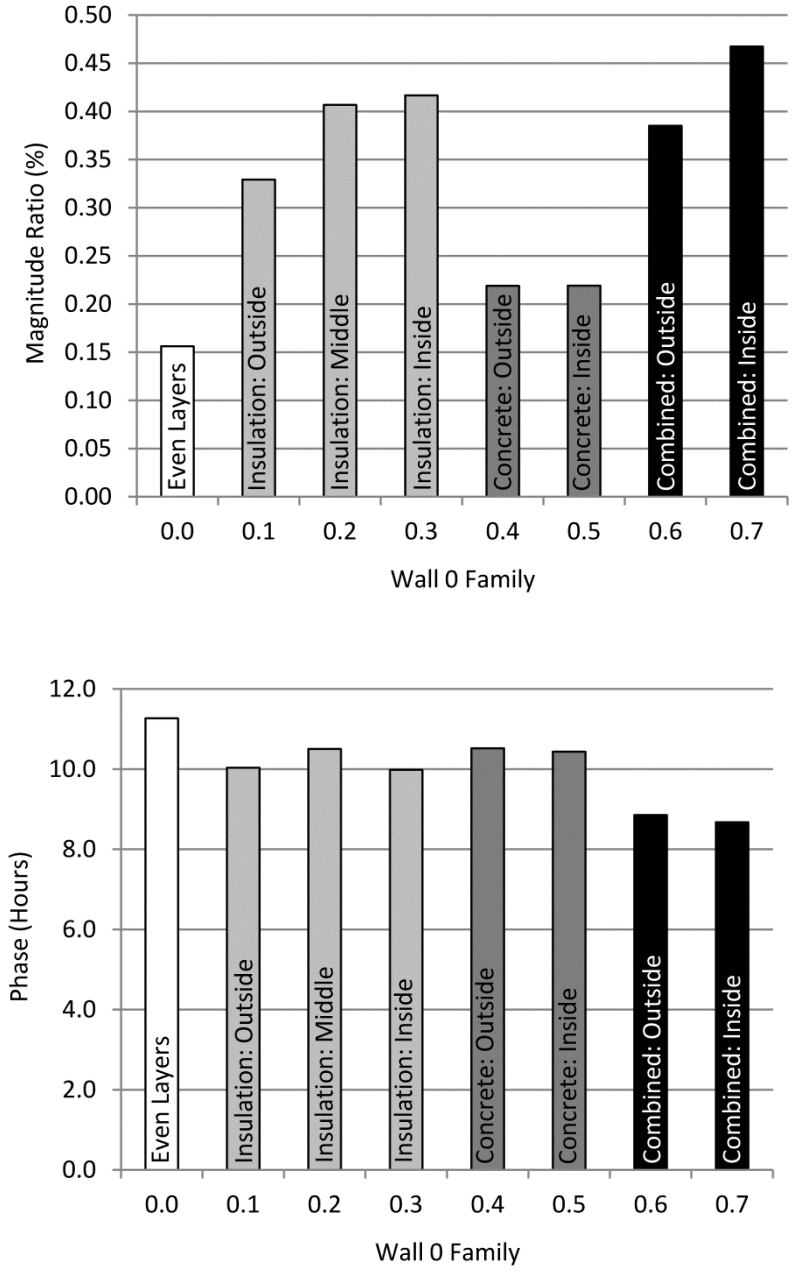

Figure 4.3. (Top) Magnitude ratio and (bottom) phase results for Wall 0 weighting configurations.

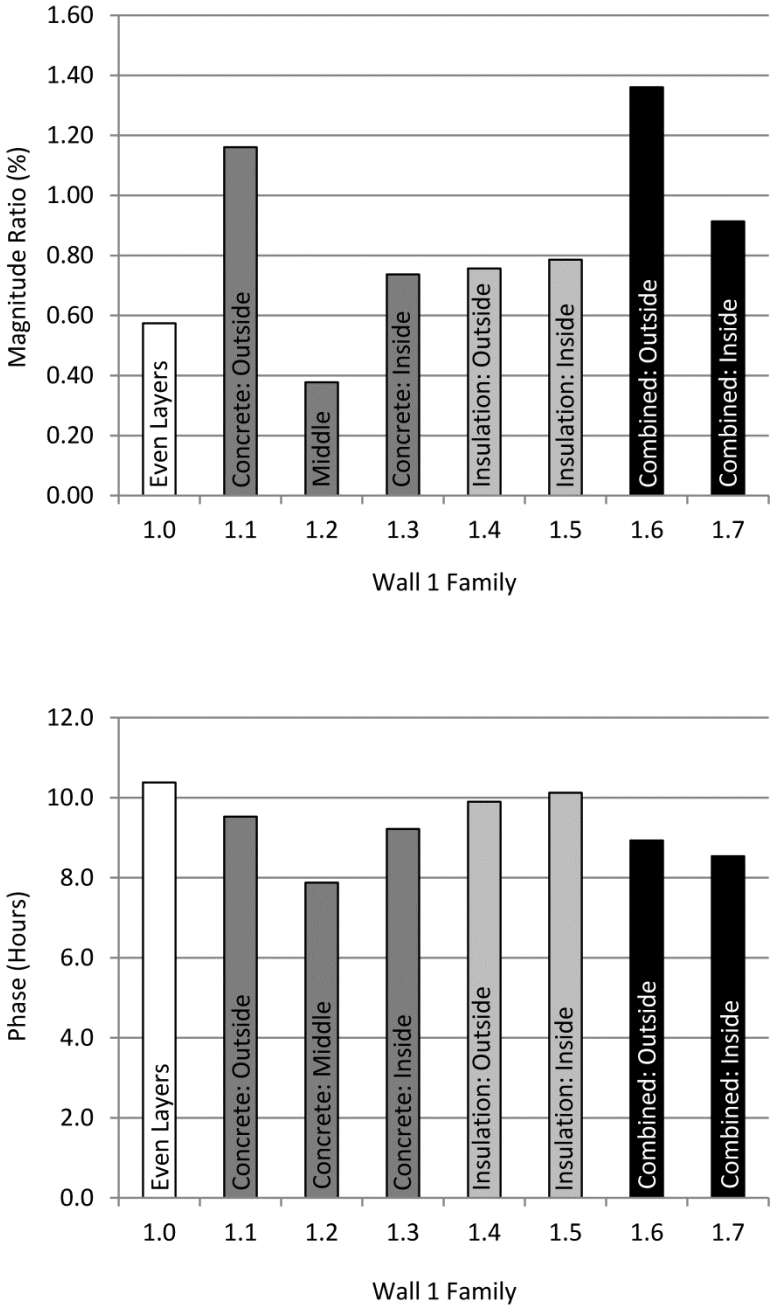

Figure 4.4. (Top) Magnitude ratio and (bottom) phase results for Wall 1 weighting configurations.

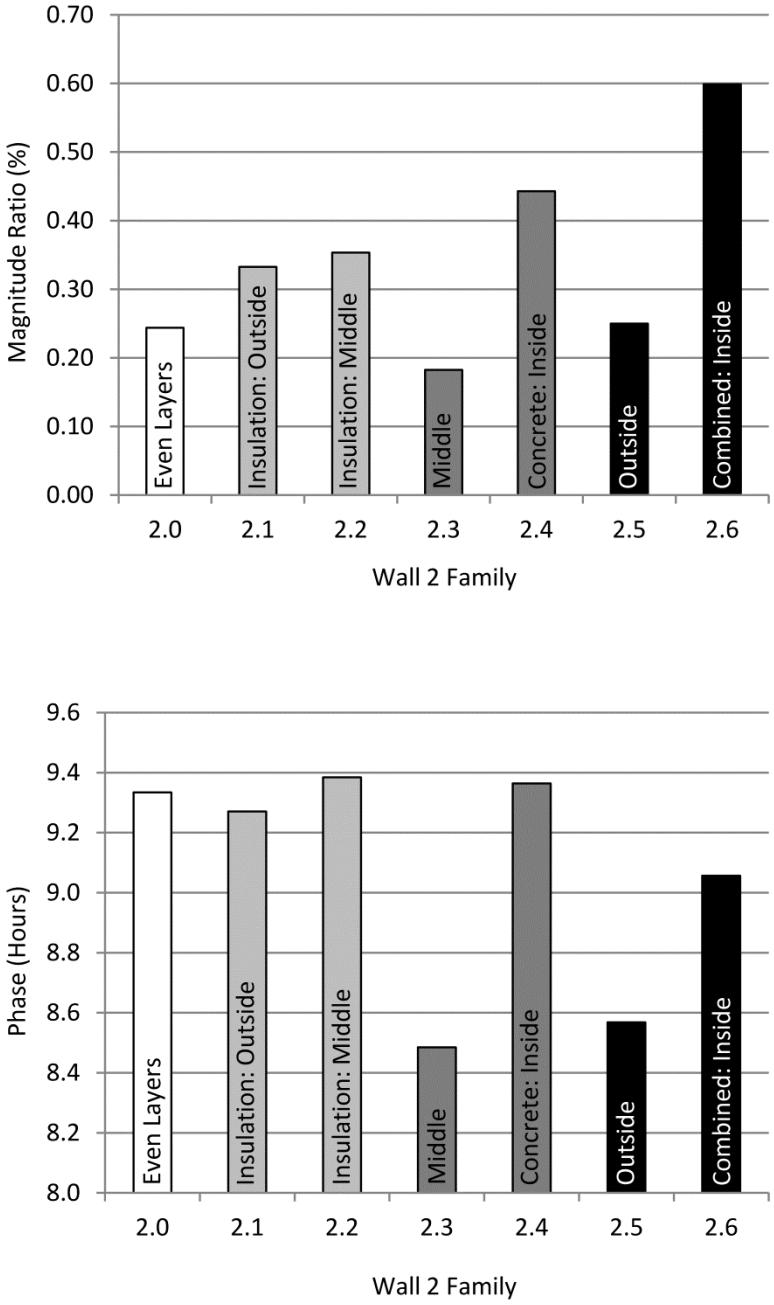

Figure 4.5. (Top) Magnitude ratio and (bottom) phase results for Wall 2 weighting configurations.

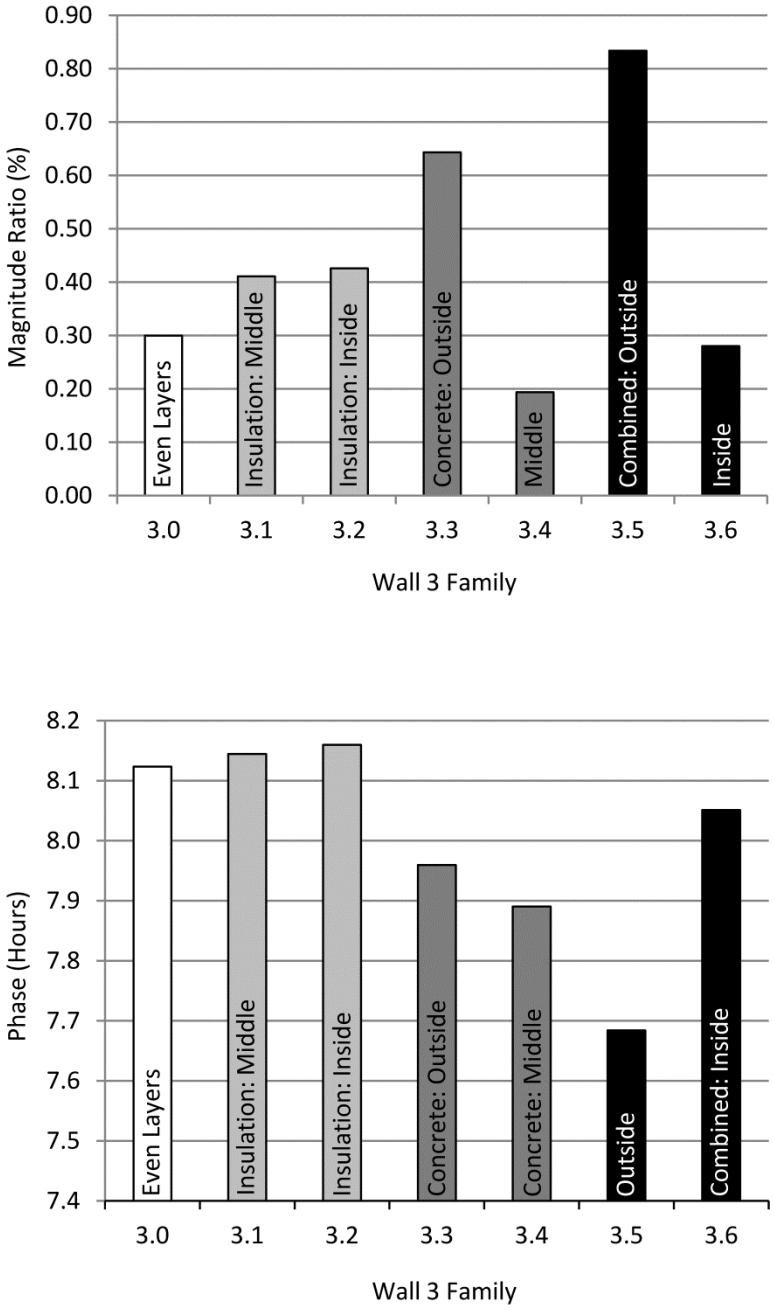

Figure 4.6. (Top) Magnitude ratio and (bottom) phase results for Wall 3 weighting configurations.

Wall 1 results also favor a configuration that resembles the 0.0 assembly, namely that concrete is weighted towards the middle of the wall with insulation on both sides. The best

performing configuration for Wall 1 (Wall 1.2) occurs when 80% of the concrete is weighted towards the middle layer, leaving only 10% of the concrete at the inside and outside positions. If the outer concrete layers were considered negligible, this configuration resembles a three layer version of the top performing five layer Wall 0.0, indicating a configuration favoring insulation at the outside and inside and concrete in the middle. The assemblies with concrete or both concrete and insulation weighted towards the inside and outside show the highest magnitude ratio, with the exception of Wall 1.3. These wall configurations – 1.1, 1.3, 1.6, and 1.7 – weight 80% of the concrete towards either the inside or outside. Walls 1.4 and 1.5, that weight insulation only, show some improvement, although 1.0 and 1.2 are still better with the concrete distributed evenly or weighted towards the middle.

Among the four layer Wall 2 and 3 configurations (Figure 4.5 and Figure 4.6), 2.2 and 3.2 have the highest phase lag, and 50% of the concrete is positioned toward one of the outer most layers. Walls 2.3 and 2.5 weight 80% of the concrete towards the middle of the assembly, and show the lowest phase lag among Wall 2 configurations. This suggests that increasing concrete at an outer layer helps increase the phase lag performance of the wall assembly. Among Wall 1 configurations, Wall 1.2 provides the lowest phase lag and has just 10% of concrete at both outermost layers. This lack of concrete at the outer layers resulting in decreased phase lag supports the indication that increasing concrete at an outer layer increases phase lag. However, all of the Wall 3 configurations have relatively low phase lag results (around 8 hours) among the four families of wall configurations, and other results show some inconsistency in this trend. Such discrepancy suggests that the model accuracy may need improvement in order to capture phase lag trends among different wall families as well as different weighting configurations within a family.

When magnitude ratio is considered, Walls 2.3 and 3.4 show the best performance among Wall 2 and 3 variations. This indicates that weighting concrete towards the middle of the assembly is best. This is consistent with Wall 1 results, where Wall 1.2 has the lowest magnitude ratio and concrete weighted towards the middle. Wall 0 results agree as well, where Walls 0.0, 0.4, and 0.5 show concrete weighted towards the middle layers, with at least one third of the insulation on either side, and relatively low magnitude ratios. Walls 2.5 and 3.6 also weight 80% of the concrete towards the middle and have comparatively low magnitude ratios. The evenly distributed configurations 2.0 and 3.0 also perform comparatively well, while the worst performing Wall 2 and 3 configurations - 2.6 and 3.5 - weight 80% of the concrete towards one of the outer most layers, leaving only 20% towards the middle.

Since Wall 0.0 shows the best overall thermal performance among the thirty variations, it is selected as the configuration to extend for further analysis. The configuration is extended by dividing the insulation and concrete into a greater number of thinner layers. Wall 0.0 has five layers of insulation and concrete, increasing to 7, 9, and 11 in Walls 0.8, 0.9, and 0.10, respectively. Magnitude and phase results comparing these four evenly distributed Wall 0 configurations with an increasing number of layers are plotted in Figure 4.7 and Figure 4.8. Figure 4.7 shows that rather than decreasing continuously as the number of layers increases, the magnitude ratio appears to reach a minimum with a smaller number of divisions. Wall 0.8 has the lowest magnitude ratio (M=0.14%) of all the configurations studied. Insulation and concrete are distributed evenly throughout the seven layers, and insulation is located at the inner and outer most positions.

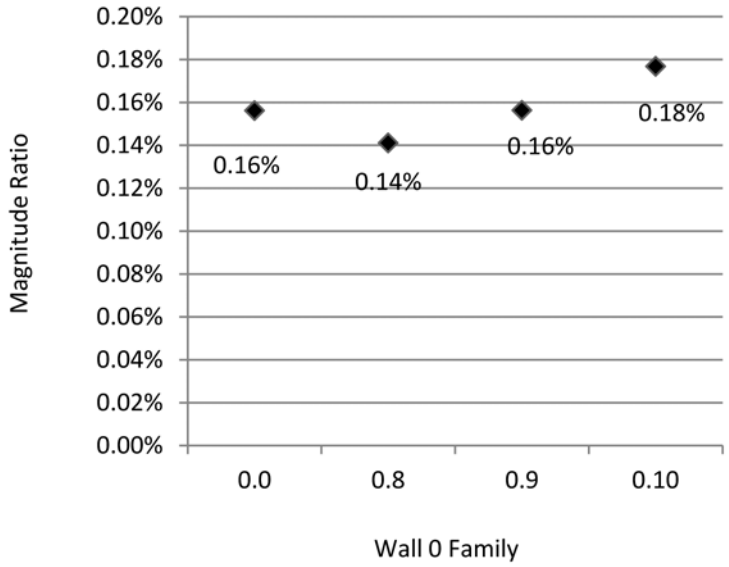

Figure 4.7. Magnitude ratio (%) for Wall 0 extended configurations shown versus respective wall configurations. Each subsequent wall configuration represents an increase in the total number of insulation and concrete layers.

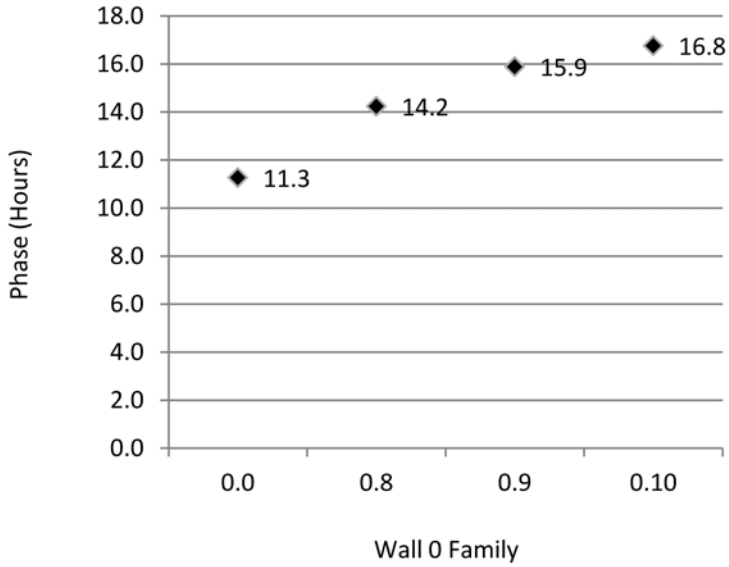

Figure 4.8. Phase (hours) for Wall 0 extended configurations shown versus respective wall configurations. Each subsequent wall configuration represents an increase in the total number of insulation and concrete layers.

In the evenly-distributed configurations, phase lag shows a continuously increasing trend as the number of layers increases. In terms of the RC model, dividing each thermal mass layer into a greater number of layers increases the number of poles in the transfer function of the model, since the impedance of each capacitance layer adds an integrator. The increased number of poles increases the negative slope of the phase response, resulting in a longer phase lag at the same frequency. Previous work has also shown, generally, that phase lag increases with an increasing number of layers. Even though some results suggest that concrete at an outer layer helps increase the phase lag, complete analysis shows that phase lag is not compromised when design focuses on reducing the magnitude ratio. The assembly that minimizes the magnitude ratio among the primary thirty configurations considered also maximizes the phase lag.

The degree to which maximizing the phase lag is desirable may be debated in the same way that maximizing the decrement factor is not always beneficial, as explained in the Masoso study [25], where it is shown that increased insulation may actually lead to higher annual energy consumption based on annual heating and cooling loads. Similarly, maximizing the decrement factor may not always be beneficial from a practical standpoint, unless meeting specific thermal performance criteria while reducing material usage is considered.

It is important to note that the analysis described herein need not include region specific climate data. Although the absolute thermal performance might be dependent on this factor as shown in [12], the qualitative relationships between the number of layers and optimal configuration is expected to be maintained. In other words, the same wall might not perform exactly the same in different climates, but a wall that insulates better than its alternative in one climate will still insulate better than its alternative in a different climate. Also expected to have an impact is the solar insolation, which would suggest another voltage source is needed in the

RC circuit or a sol-air method may be used to incorporate the effect within the outside air temperature.

To summarize this chapter, a lumped parameter RC model is used to simplify and expedite solution of the one-dimensional heat equation for a multi-layer wall. Results indicate the model is sufficiently accurate, having reasonable agreement with benchmarks found in the literature. The first part of the analysis explores various weighting arrangements developed from four primary configurations; a total of thirty-three configurations are studied. Frequency response analysis results suggest placing insulation at both inside and outside layers and positioning thermal mass towards the middle of the assembly will result in the best insulating performance. In the second part of the analysis, the wall with the best performance from the first set of results, Wall 0.0, is extended by splitting insulation and mass layers into an increasing number of divisions. These results suggest that an optimum number of layers exists where the thermal performance is maximized.

This trend is illustrated via a heuristic optimization procedure described in Chapter 5. The formal optimization presented in Chapter 5.3 will clarify whether distributing the thermal mass evenly among the inner layers is best or if a different configuration yields better thermal performance (in terms of magnitude ratio and phase lag).

5.0 OPTIMIZATION OF MULTI-LAYER WALLS USING TRANSMISSION MATRIX AND MATLAB OPTIMIZATION METHODS

The previous work raises certain questions. First is the need to refine the RC model to ensure the accuracy of results. This is accomplished by increasing the number of nodes or T-networks used to represent each layer. The transmission matrix method is chosen over the folding method, because the matrix format is judged to be advantageous for storing, computing, and manipulating modeling information, while maintaining physical relevance to the wall system. This refined method is validated using a finite volume calculation. Results comparing the transmission matrix method and a finite volume method are shown in Chapter 5.1. Using the refined transmission matrix method, the thirty three configurations from Chapter 4 are re-evaluated to confirm the results originally reported based on the folding method, and the results of the refined method do indeed confirm previous results. Within each family, Walls 0.0, 1.2, 2.3, and 3.4 produce the lowest magnitude ratio, or decrement factor, and Wall 0.0 achieves the minimum among all considered. For simplicity, the term magnitude ratio is used exclusively in lieu of the equivalent term decrement factor for the remainder of this chapter.

Other questions raised by previous work focus, in general, on how to illustrate the existence of optimal multi-layer configurations and how to realize an optimal multi-layer wall design. Specifically, the work in Chapter 4 is based on varying the total number of layers and the distribution of fixed amounts of material in a multi-layer wall. In this chapter, the analysis is

extended to accommodate different material combinations, the relative proportion of each material used, and the overall wall thickness. This work aims to determine the effect each parameter has on reducing magnitude ratio and increasing phase lag. The results provide insight, tools, and guidelines for designing multi-layer insulation systems that satisfy a given application demand.

The original question regarding number and arrangement of layers is expanded in Chapter 5.1, starting with the four basic families and evenly distributed layers. This heuristic optimization approach initially considers increasing the total number of layers with fixed overall thermal resistance and capacitance. In Chapter 5.2, the design space is expanded to include different proportions of two materials, specifically insulation and concrete, so the overall thermal resistance and capacitance of the wall are no longer fixed. The overall thermal resistance and capacitance are allowed to vary as the proportion of the two materials in each configuration is altered. A variety of materials in different combinations are analyzed in Chapter 5.2 and simplified analysis tools are introduced to enable quick and easy material selection in a design process. In Chapter 5.3, the Matlab Genetic Algorithm and Pattern Search optimization methods are utilized to explore layer distribution and reinforce the results and conclusions developed using the heuristic studies. These results resolve outstanding questions regarding the best distribution of materials – specifically, whether symmetric, evenly distributed layers yield a lower magnitude ratio than asymmetric or unevenly distributed layers. Finally, in Chapter 5.4, overall wall thickness is addressed. First, the RC model is refined using the transmission matrix method and validated using a finite volume solution.

5.1 NUMBER OF LAYERS

To confirm the existence of an optimal configuration based on total number of layers, and to further explore the effect of layer number and distribution on magnitude ratio and decrement factor, the four primary configurations studied in Chapter 4 are extended. Maintaining the overall configuration and fixed thermal resistance and capacitance for each wall, the total number of layers is increased, as shown in Figure 5.1. Each wall is 278 mm thick with 78 mm of insulation and 200 mm of concrete. The thin cement plaster layers at the outermost positions in the walls examined in Chapter 4 are no longer included.

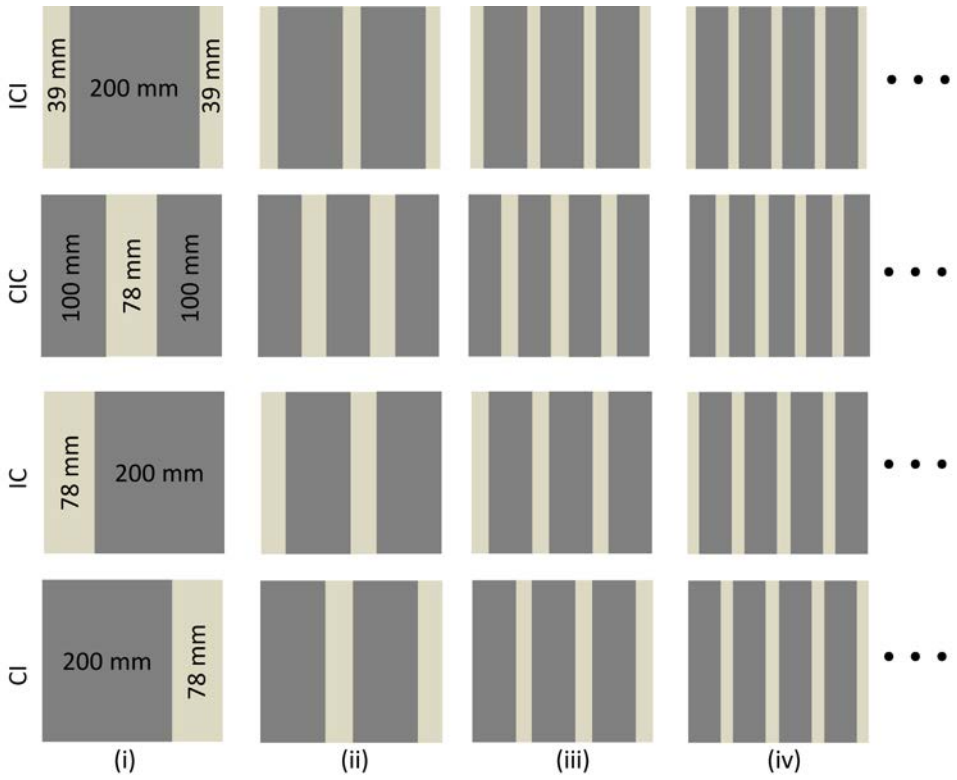

Figure 5.1. Four primary configurations of insulation (I) and concrete (C): ICI, CIC, IC, and CI, form four families. Sub-dividing material layers increases the total number of layers in each wall (i,ii,iii,iv…).

The transmission matrix method is compared with a finite volume solution. Both models independently discretize each layer. Unlike the analysis in Chapter 4, in which each layer was represented by a single RC node, in this analysis the number of nodes is increased to ensure model accuracy. The number of nodes per layer in the transmission matrix method is increased until the relative error percentage of magnitude ratio between discretized layer models (one node vs. two nodes, six nodes vs. seven nodes, for example) is less than or equal to 0.01% for each layer. This will be referred to as the *residual convergence error* in the transmission matrix method. As a result, each layer is modeled using at least two nodes, or T-networks. All results presented in the remainder of this dissertation are based on these converged layers, or in other words, the model is mesh-independent. If a residual convergence error greater than 0.01% is used, it will be noted.

The magnitude ratio for each family is plotted versus total number of wall layers for the transmission matrix method and finite volume modeling in Figure 5.2 (a) and (b), respectively. Phase lag results for each method are shown in Figure 5.3 (a) and (b). Between the two methods, there is between 1 and 8.7% difference in discrete magnitude ratio values and between 1 and 5% difference in discrete phase lag values. (The maximum root mean square error between the magnitude ratios of the two methods, among the four curves, is 2.43e-04 while that of the phase lag is 2.98e-01).

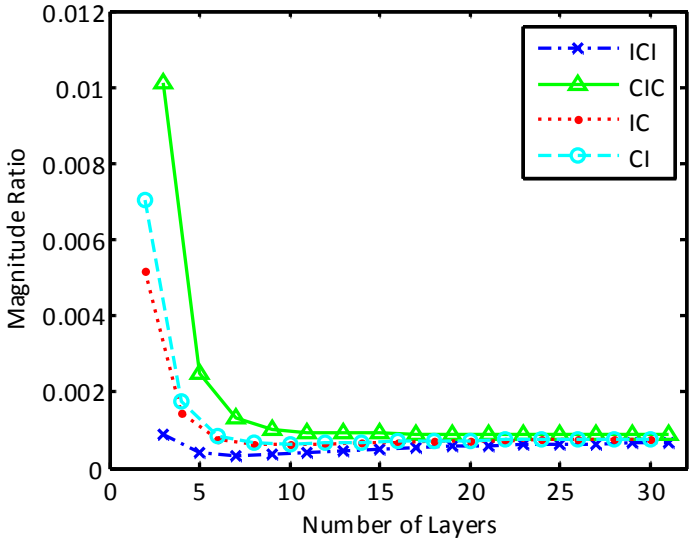

(a)

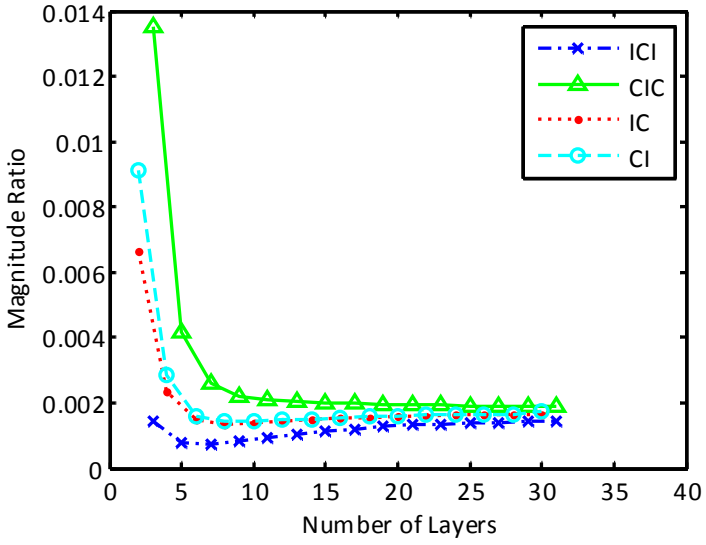

(b)

Figure 5.2. (a) Transmission matrix results: magnitude ratio versus total number layers for four families. (b) Finite volume results: magnitude ratio versus total number layers for four families (M. Kimber).

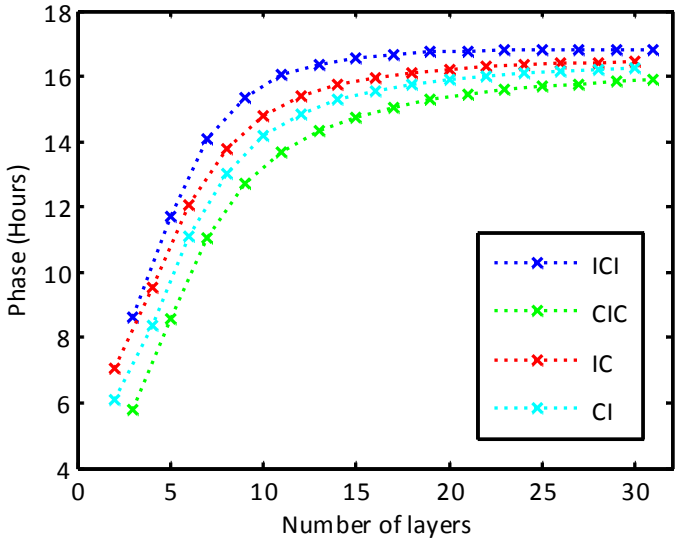

(a)

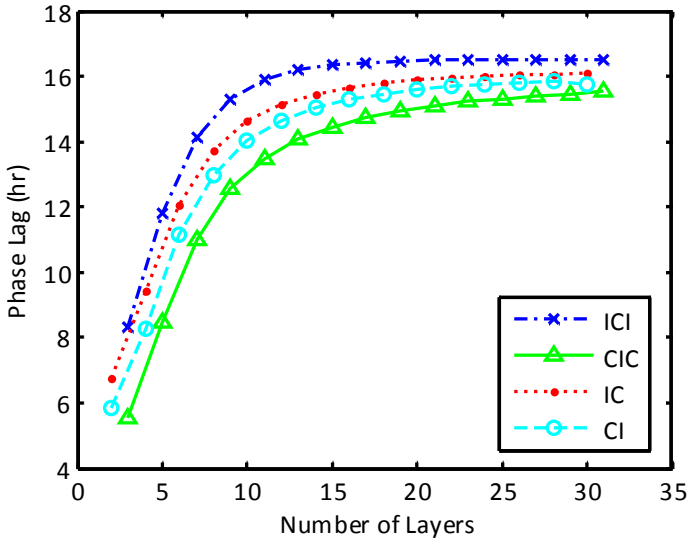

(b)

Figure 5.3. (a) Transmission matrix results: phase versus total number layers for four families. (b) Finite volume results: phase versus total number layers for four families (M. Kimber).

These magnitude ratio plots show that three out of the four configuration families have an optimal configuration that minimizes the magnitude ratio, whereas the fourth, CIC, shows a

monotonic change in performance. It may be noted that as the number of layers increases, the composition of the wall approaches a near-homogeneous form, an equivalent composite of the two original materials. Given the same two materials and four different configuration families, the optimal configuration of one family, ICI, achieves a lower magnitude ratio than all the others. Therefore, within the roughly 120 wall configurations studied, one optimal configuration was found that minimizes the magnitude ratio based on increasing the total number of layers in the wall. The phase lag appears to increase and reach a maximum value, but this maximum does not appear to coincide with the magnitude ratio minimum. The optimal configuration for magnitude ratio may achieve a desirable time lag, nonetheless, if it is close to 12 hours or otherwise suitable to the application (i.e. frequency of interest).

Increasing the total number of layers for each of the four primary configurations demonstrates that the number and distribution of layers within a wall may be selected to minimize the resulting magnitude ratio (or to maximize phase lag). These heuristic results show that the ICI family achieves a lower magnitude ratio than the other families. This result is further examined in Chapter 5.3 when material distribution is explored using numerical optimization search methods. In the work that follows, results based on the ICI family alone are presented, and the effect of other design parameters on magnitude ratio are discussed. It will be shown that the optimal number of layers depends on the materials used and the relative proportion of each material in the wall.

5.2 PROPORTION OF MATERIALS AND MATERIAL COMBINATIONS

5.2.1 Proportion of Insulation to Concrete

To this point, the overall wall thickness and proportion of materials has remained fixed in order to highlight the effect of layer distribution (in terms of the four basic families) and number of layers while keeping the overall resistance and capacitance of the wall fixed. Eliminating cement plaster from the outer surfaces, the results shown in Figure 5.2 and Figure 5.3 represent a 278 mm thick wall with 200 mm of concrete and 78 mm of insulation, or roughly 28% insulation. Now, the proportion of materials (insulation and concrete) is altered incrementally (without changing wall thickness), as shown in Figure 5.4, allowing the overall thermal resistance and capacitance to vary. The proportion of insulation in each wall is increased from five percent to ninety-five percent. A step size of either 1% or 0.1% is used to increment the percentage of insulation in these calculations.

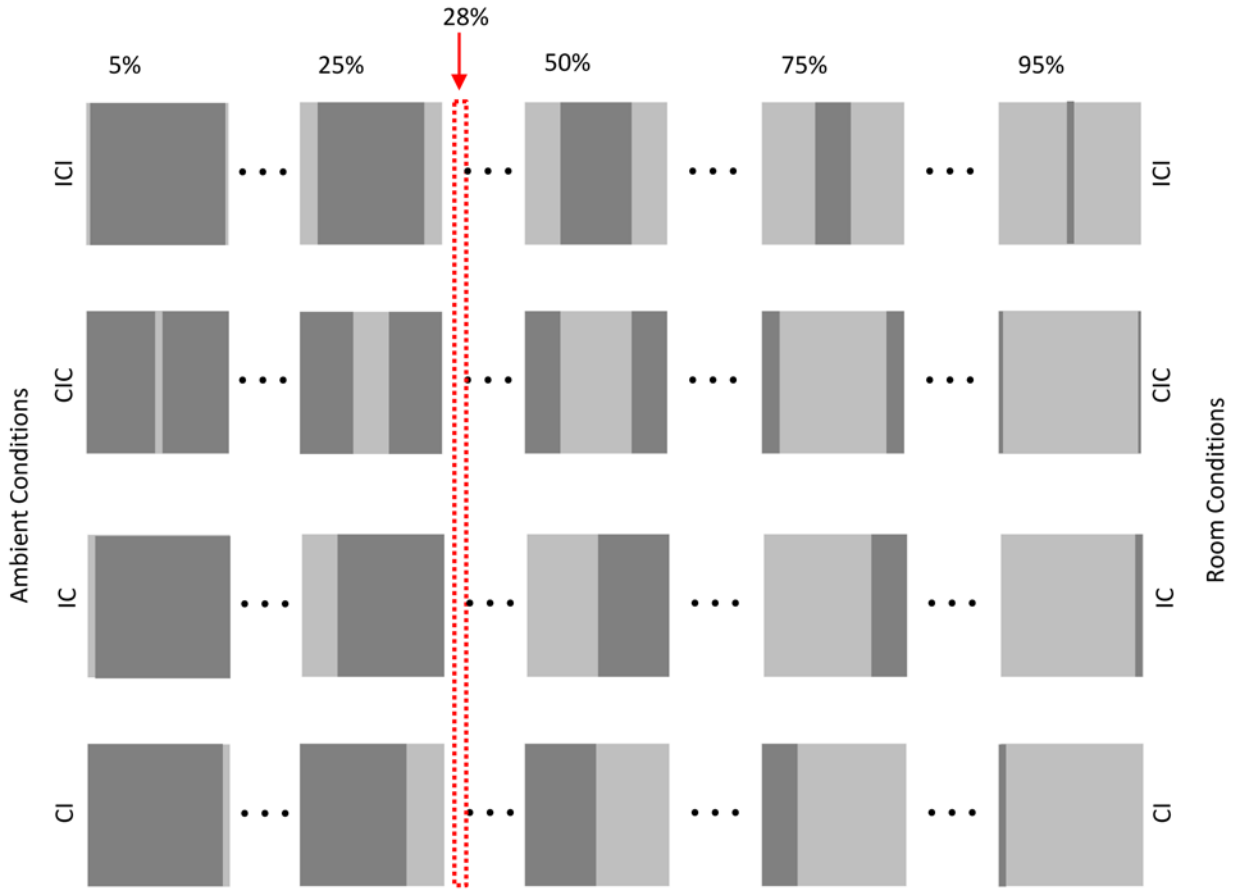

Figure 5.4. The proportion of insulation to concrete ranges from 5 to 95% insulation for each of the four families ICI, CIC, IC, and CI. Cases studied previously are noted as the set with 28% insulation.

The magnitude ratio and phase lag are calculated using the refined transmission matrix method for the wall configurations and proportions of insulation and concrete shown in Figure 5.4 and for increasing number of layers, as shown in Figure 5.1. These results are shown in Figure 5.5 for family ICI.

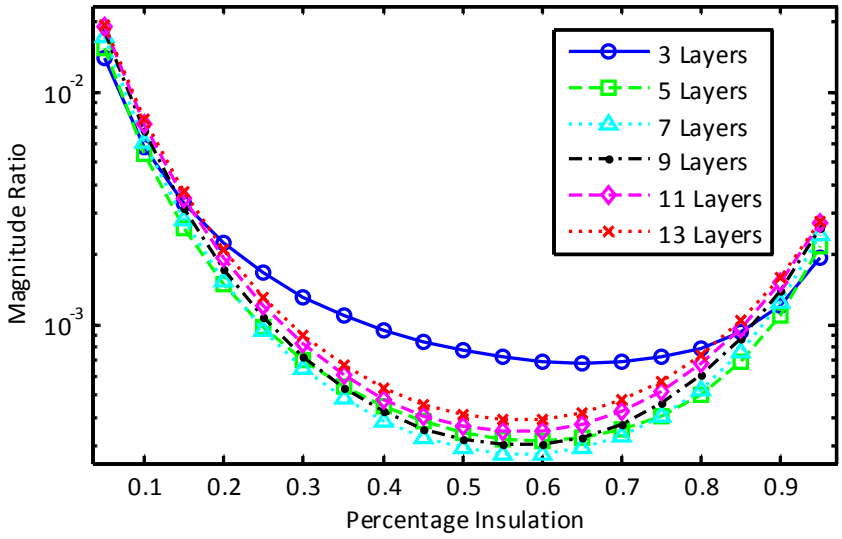
3 Layers
5 Layers
7 Layers
9 Layers
11 Layers
13 Layers
Magnitude Ratio
10^{-2}
10^{-3}
0.1
0.2
0.3
0.4
0.5
0.6
0.7
0.8
0.9
Percentage Insulation

(a)

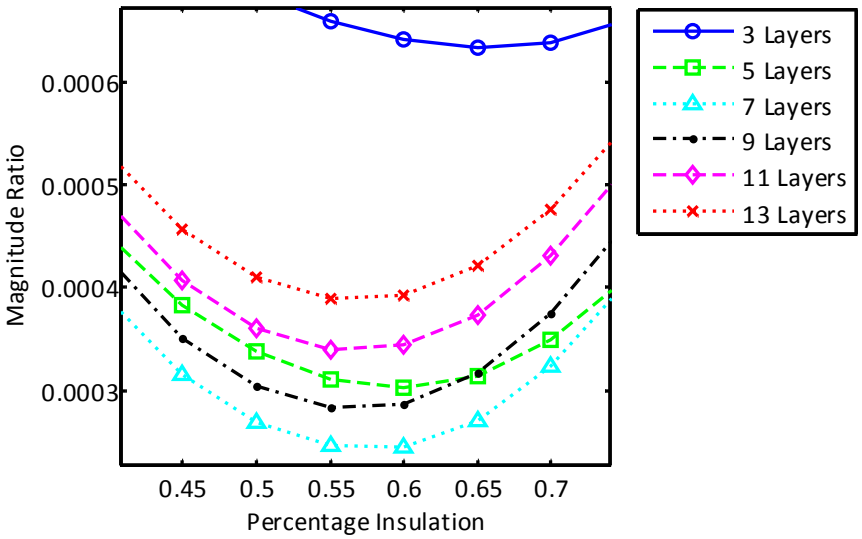
3 Layers
5 Layers
7 Layers
9 Layers
11 Layers
13 Layers
Magnitude Ratio
0.0006
0.0005
0.0004
0.0003
0.45
0.5
0.55
0.6
0.65
0.7
Percentage Insulation

(b)

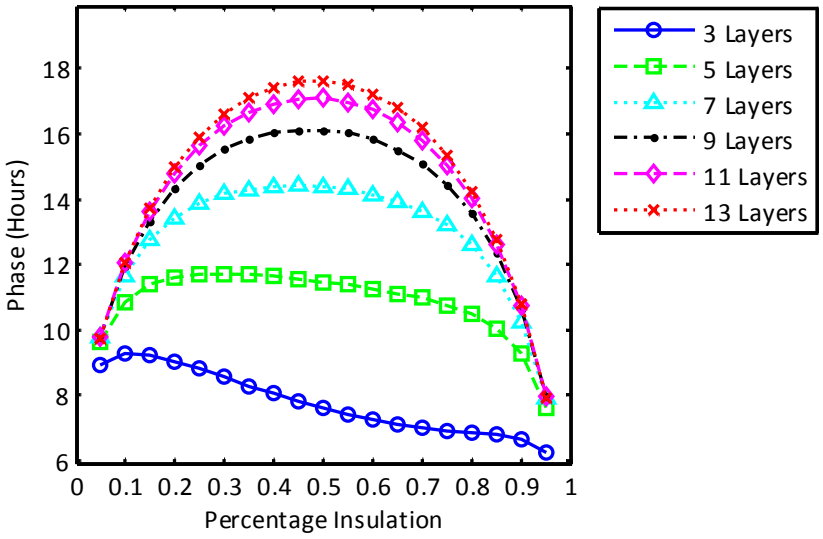

(c)

Figure 5.5. (a) Magnitude ratio for six ICI curves, (b) Close-up view showing minimum magnitude ratio of the six ICI curves, (c) Phase lag for six ICI curves.

The number of layers is increased, yielding six curves, while the overall width is fixed at 278 mm. The first wall has three layers, the next five layers, then seven, and so on, maintaining the basic ICI configuration (3-layer ICI, 5-layer ICICI, and so on through a 13-layer configuration). The magnitude ratio is minimized by the wall with seven layers. The magnitude ratio then increases with 9, 11, and 13 layers (not shown in Fig. 5.5, but predicted in Figure 5.2, the magnitude ratio settles near the 13-layer curve as the number of layers continues to be increased). In other words, the magnitude ratio begins to increase as the number of layers continues to increase beyond the optimal number. As the number of layers continues to increase, the magnitude ratio approaches the performance of an equivalent composite wall.

The percentage insulation that minimizes the magnitude ratio changes depending on the number of layers used, with a range of 56.5% to 65.5% insulation being optimal for the layer numbers analyzed. For the seven layer configuration, the percentage insulation that minimizes

the magnitude ratio is 58.6% ($M = 2.77\times10^{-4}$). The maximum phase is shown to continue to increase with increasing number of layer divisions, but the improvement diminishes between each subsequent increase in number of layers. Similar to magnitude ratio, the percentage insulation that maximizes the phase lag also changes with number of layers. For the cases analyzed, the maximum phase lag was found to be 48.3% (which occurs for the thirteen-layer case). The corresponding time delay is about 17.6 hours. The phase lag corresponding to the minimum magnitude ratio, the wall with seven layers and 58.6% insulation, is about 14 hours.

For the purposes of designing multi-layer walls for building applications, it is important to evaluate potential energy savings against additional costs that might be associated with increased complexity in manufacturing or installation. It is apparent in Figure 5.5 (a) that there is a greater reduction in magnitude ratio between the 3- and the 5-layer walls than there is between the 5- and 7-layer walls. The differences are listed in Table 4.

Table 4. Improvement in magnitude ratio and change in optimal proportion of insulation for increasing number of layers in multi-layer walls with ICI configuration.

Number of Layers	*Magnitude Ratio (M)*	*Optimal Proportion of Insulation (%)*	*Reduction in Magnitude Ratio Compared to 3 Layers (%)*
3	6.8×10^{-4}	65.5	-
5	3.2×10^{-4}	59.5	53
7	2.8×10^{-4}	58.6	59

There is a 53% reduction in magnitude ratio between the 3- and 5-layer walls and a 59% reduction between the 3- and 7-layer walls, or only a 13% reduction from the 5-layer to the 7-layer configuration. The optimal proportion of insulation changes slightly as the number of layers is increased. To simplify wall construction and still achieve major reduction in magnitude

ratio, it may be best to use a 5-layer design rather than the 7-layer design, for this 278 mm wall made of insulation and concrete. A design methodology is presented in Chapter 6 where these potential trade-offs will be discussed in more detail.

It is also informative to consider how the optimal percentage of insulation changes as the total number of layers changes. In other words, what proportion of materials (insulation and concrete have been considered so far) minimizes the magnitude ratio for a given configuration and number of layers? To illustrate this, the four configuration families are considered again, and the overall wall thickness is still fixed, but the overall thermal resistance and capacitance is allowed to vary. Figure 5.6 (a) shows the percentage of insulation that minimizes the magnitude ratio for each wall, distinguished by the number of layers in the wall, as shown along the x-axis. Similarly, Figure 5.6 (b) shows the percentage of insulation that maximizes the phase lag for the total number of layers shown. The lower limits (two or three layers) are not shown in order to highlight the convergence trend seen as the number of layers increases.

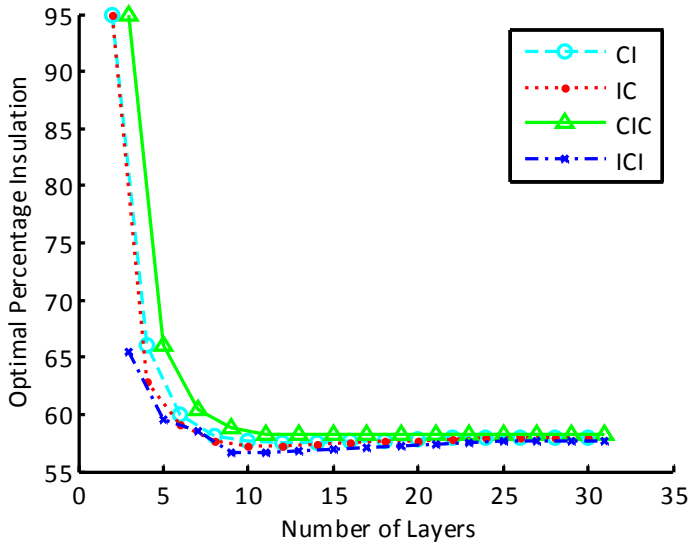

(a)

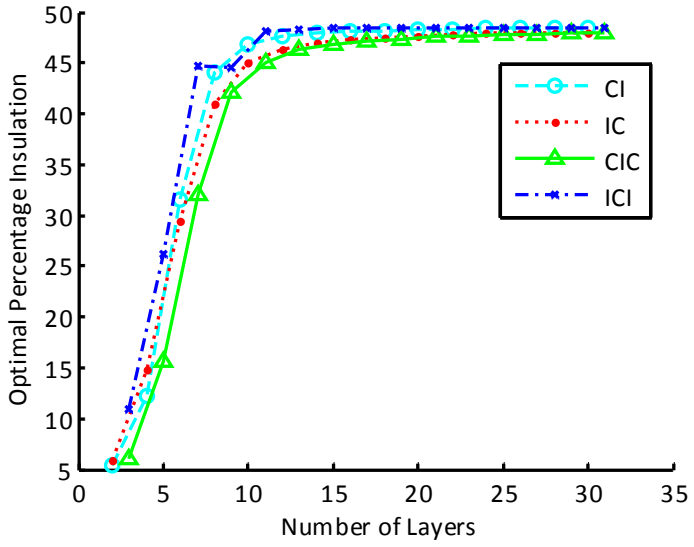

(b)

Figure 5.6. (a) The percentage insulation that minimizes the magnitude ratio for the configuration family and total number of layers shown. (b) The percentage insulation that maximizes the phase lag for the configuration family and total number of layers shown.

These results are an indication of what the best proportion of each material would be if insulation and concrete were combined to form a composite wall. With fewer layers, more insulation helps reduce the magnitude ratio while more concrete helps increase the phase lag. Moreover, because the proportion of materials is varied, the overall R-value of the wall changes. Thus, design trade-offs likely exist. The design methodology presented in Chapter 6 will address these potential trade-offs in more detail.

Having expanded the search space to include both number of layers and proportion of materials, conclusive trends have been identified. Four primary configuration families with a range of five to ninety-five percent insulation-to-concrete and an increasing number of layers (from the original two or three layers that identify each family) were considered. The ICI family

was found to be the most effective configuration of the four families at minimizing the magnitude ratio and maximizing the phase lag. The 7-layer ICI wall with approximately 59% insulation-to-concrete yields the lowest magnitude ratio among the entire heuristic search set. The search space for an optimal multi-layer wall configuration is further expanded in Chapter 5.2.2 to include different materials, beyond the insulation and concrete considered previously. Using different materials and determining the best combination of materials is explored both numerically and analytically.

5.2.2 Effective Properties of Different Materials

The combination of insulation and concrete is examined further, using the methodology presented in Salazar [46] for calculating the effective thermal properties of a composite wall. Effective thermal conductivity is shown in Equation (5.1) and effective heat capacity per unit volume is shown in Equation (5.2), where v_1 represents the volumetric proportion of one material and v_2 represents the volumetric proportion of the second material. The single-layer composite wall is based on a multi-layer wall with many layers arranged in series like one of the wall configurations in Figure 5.1 towards the far right, shown as *(iv)*… and onward. This layer arrangement results in serial heat conduction and accounts for the form of Equations (5.1) and (5.2).

$$k_{eff} = \left[\frac{v_1}{k_1} + \frac{v_2}{k_2} \right]^{-1} \tag{5.1}$$

$$\left(\rho \cdot C_p\right)_{eff} = v_1\left(\rho \cdot C_p\right)_1 + v_2\left(\rho \cdot C_p\right)_2 \tag{5.2}$$

Equation (5.3) shows the dependence between v_1 and v_2, the sum of which must equal one, or one hundred percent of the total volume of material in the wall, since the wall is comprised of two and only two materials.

$$v_2 = 1 - v_1 \tag{5.3}$$

The effective properties k_{eff} and $(\rho C_p)_{eff}$ are calculated for 99 composite walls ranging from one percent insulation to ninety-nine percent insulation compared to concrete, with a total of 101 walls, including the two cases with one hundred percent of either insulation or concrete. The effective thermal conductivity of each equivalent composite wall is plotted against the effective thermal diffusivity of the same wall in Figure 5.7. The result is a “K-D” performance curve (K for conductivity and D for diffusivity) with end-points demarcating the non-composite walls made of one hundred percent of either material.

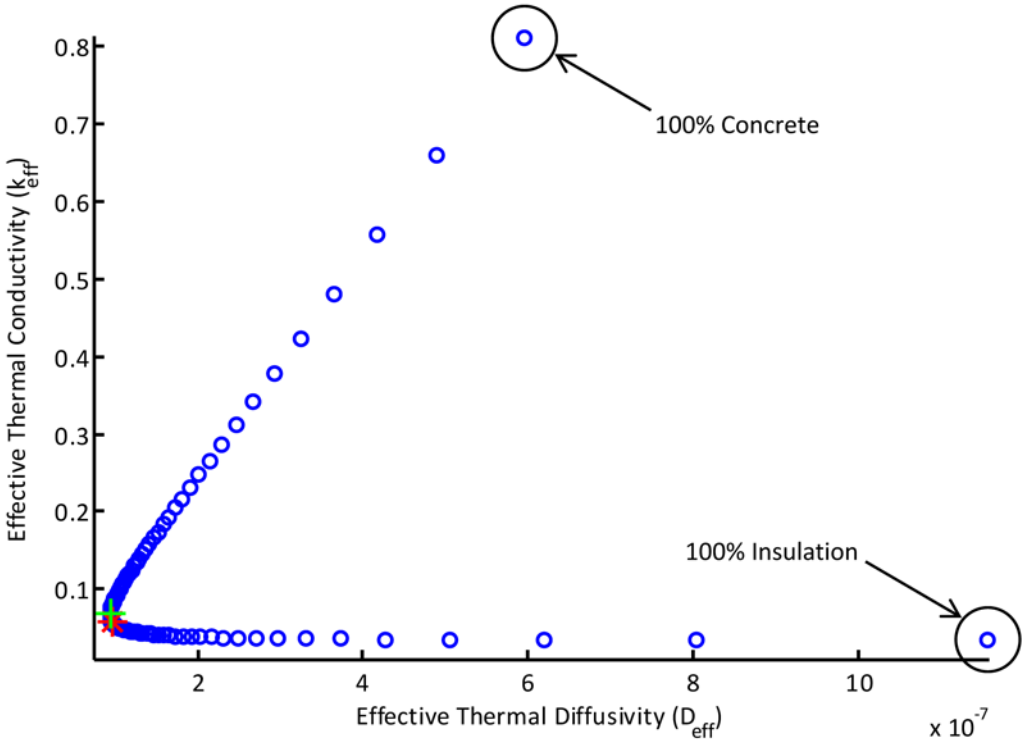

Figure 5.7. Effective thermal conductivity of an equivalent composite wall based on varying proportions of insulation and concrete is plotted against effective thermal diffusivity of the same wall. Star data point (red) is minimum magnitude ratio and cross data point (green) is maximum phase lag from previous analyses.

The red star near the apex of the curve designates the percentage insulation (roughly 58%) found in Chapter 5.2.1 for which the magnitude ratio is minimized for a multi-layer wall. The green cross designates the percentage insulation (roughly 48%) found in Chapter 5.2.1 for which the phase lag is maximized. From these results, a rough correlation is apparent between the minimum effective diffusivity and the optimized dynamic response. To explore this further, additional material combinations are analyzed. The results are shown in Figure 5.8 for six different materials – insulation, concrete, air (assuming conduction only), polymer, aluminum, and copper – in seven different combination pairs. Insulation and concrete have been considered thus far.

The air and polymer options are added to the material list as representative components of a smart insulation concept [47]. In the insulating state of this concept, thin alternating layers of polymer and air limit thermal transport to conduction only. Then, the polymer layers can collapse, eliminating the thin layers of air, to form a conductive state. (The smart insulation concept enables one state or the other depending on thermal conditions and desired behavior, such as heat gain or loss.) Aluminum and copper represent materials with high thermal conductivity and capacitance. As a result, a wide range of materials and thermal properties are covered with the paired combination of these six materials.

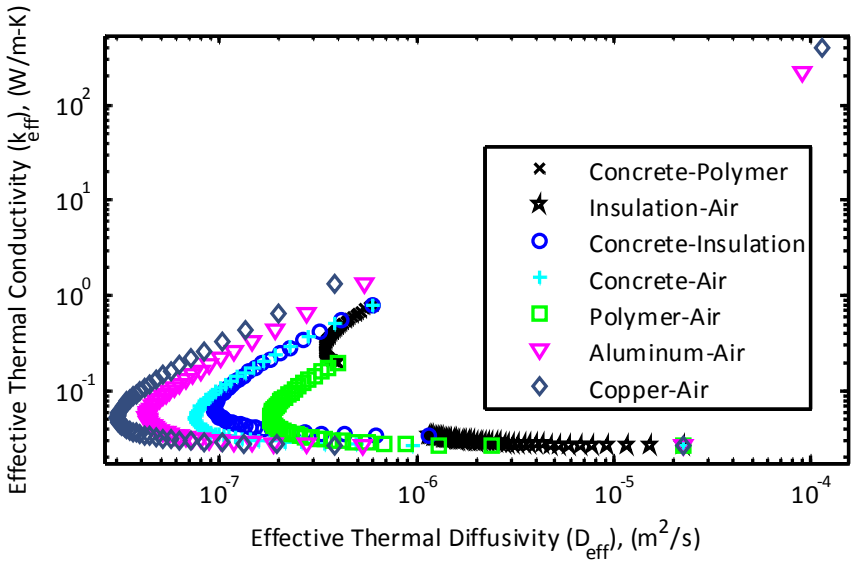

(a)

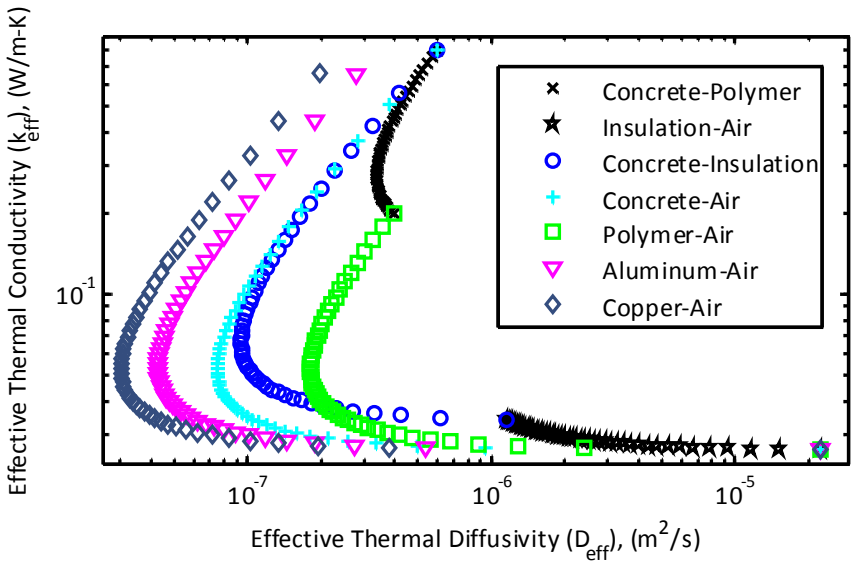

(b)

Figure 5.8. (a) Effective thermal conductivity is calculated for the equivalent composite of each of seven pairs of six different materials and plotted against its associated effective thermal diffusivity. (b) The far ends of the aluminum and copper curves are not shown, so the apex of each curve is shown more clearly.

Figure 5.8 (a) shows the full curve for seven different material combinations, while Figure 5.8 (b) does not include upper extremes of the aluminum-air and copper-air curves (i.e. 100% aluminum and copper) in order to display the apex of all seven curves more clearly. The first material in each pair is represented by the upper end of its respective curve, while the second material in each pair is the lower end. Five different combinations use air as the second material, so the symbols representing each pair overlap in the lower right-hand corner marking the thermal properties of a hypothetical wall made of 100% air. Among the seven material combinations considered, pairing copper and air produces the lowest effective thermal conductivity and the lowest effective thermal diffusivity.

Recall that the primary goal of this work is to determine design features of multi-layer walls that minimize heat transfer, as characterized by the performance criteria magnitude ratio. A

brute force approach requires taking a large set of simulations to arrive at the optimal solution. But with the approach illustrated in Figure 5.8, an initial design tool exists that can aid in the selection of materials and material proportions and ultimately help minimize magnitude ratio. The advantage to this approach is the fact that it can be accomplished analytically. Two analytical methods are proposed and compared to the transmission matrix method in Chapter 5.2.3 to gauge their effectiveness in minimizing the magnitude ratio for different material combinations.

5.2.3 Material Selection for Minimum Magnitude Ratio

As before, the magnitude ratio of a multi-layer wall, now comprised of various material combinations, is determined using the refined transmission matrix method, which assumes that heat transfer occurs by conduction only. Even for layers of air, the model still represents one-dimensional conduction. Using thin layers of air and low emissivity coatings on non-air surfaces may realistically reduce the effects of heat transfer via convection and radiation.

From Figure 5.7, it is apparent that the data points for minimum magnitude ratio and maximum phase lag occur at or near the volume ratio where the effective diffusivity is smallest. Therefore, analytical tools could be developed which reveal the “optimal” volume ratio without the need to conduct many sets of simulations. Two such methods are proposed and each yields a different “optimal” result. These will be compared to a full transient analysis using the transmission matrix method, as previously described. While the transmission matrix method is relatively quick compared to a numerical method like finite difference, running numerous combinations is ultimately somewhat time-consuming, especially when accelerated, or fast-pace, design-build type schedules demand efficient methods and limit time available for detailed

analyses. The first analytical approach is to simply minimize the effective thermal diffusivity of an equivalent composite wall based on the thermal properties of two different materials. The volumetric proportion of materials that minimizes the effective thermal diffusivity is determined, where the proportion of the first material ranges from 0 to 100% of the total wall volume.

The second method independently normalizes each K-D performance curve in Figure 5.8 and then determines the percentage of the first material in the two-material combination that minimizes the distance between the origin and the associated normalized curve. This simultaneously minimizes the effective diffusivity and the effective conductivity of the material combination (the motivation for which may be better understood when the concept of ideal diffusivity is introduced). In the following sections, the two analytical methods are presented and then compared to a full transmission matrix analysis for accuracy.

5.2.3.1 Minimizing Effective Diffusivity

An analytical solution is developed to minimize the effective thermal diffusivity of an equivalent, single-layer composite wall comprised of two different materials (i.e., "layering" is not accounted for, only composite properties). First, the effective thermal properties are expressed in terms of the properties of two different materials as in Equations (5.1) and (5.2). The effective thermal diffusivity (D_{eff}) is the ratio of effective thermal conductivity and effective heat capacity per unit volume, expressed in Equation (5.4).

$$D_{eff} = \frac{k_{eff}}{\left(\rho \cdot C_p\right)_{eff}} \tag{5.4}$$

The partial derivative of the effective thermal diffusivity with respect to the volume ratio of material one (v_1) is set to zero, as shown in Equation (5.5), to determine an optimal proportion of material that minimizes the effective diffusivity.

$$\frac{\partial D_{eff}}{\partial v_1} = 0 \tag{5.5}$$

Equation (5.5) is evaluated analytically and two solutions are found to exist. However, only one solution is valid based on the physical interpretation of the results (a negative solution is invalid).

Equation (5.6) shows the optimal proportion of one material, valid between zero and one, that minimizes the effective thermal diffusivity of an equivalent, single-layer composite wall made of two materials.

$$v_{opt} = \frac{1}{2}\left(\frac{\left(\rho \cdot C_p\right)_2}{\left(\rho \cdot C_p\right)_2 - \left(\rho \cdot C_p\right)_1} - \frac{k_1}{k_2 - k_1} \right) \tag{5.6}$$

The effective thermal diffusivity is also quickly calculated for varying proportions of any two materials using Equations (5.1), (5.2), and (5.3). As a result, this method is extremely quick and simple compared to running numerous iterations of the transmission matrix method.

5.2.3.2 Minimizing Normalized Distance

The curves shown in Figure 5.8 for different material combinations show that the volume ratio that yields minimum magnitude ratio (and maximum phase lag) appears to coincide with the apex of the curve. This suggests that simultaneously minimizing effective thermal

conductivity and effective thermal diffusivity may be advantageous. For this reason, the objective becomes determining what proportion of two materials minimizes the distance between the K-D performance curve and the origin. It may be reasoned that the best possible combination of two materials is the idealistic union of the lowest thermal conductivity (k_{low}) of the pair and largest heat capacity per unit volume ($\rho C_{p,high}$) of the two materials, as shown in Equation (5.7). This combination produces an ideal thermal diffusivity, shown in Equation (5.8) and validated in Chapter 5.3. Although this is unachievable with any physical combination of the two materials, it provides a useful parameter to normalize the curves.

$$k_{low} = \min\left(k_1, k_2\right); \qquad \left(\rho \cdot C_p\right)_{high} = \max\left(\left(\rho \cdot C_p\right)_1, \left(\rho \cdot C_p\right)_2\right) \tag{5.7}$$

$$D_{ideal} = \frac{k_{low}}{\left(\rho \cdot C_p\right)_{high}} \tag{5.8}$$

The first step in this method, after repeating the calculations in Equations (5.1), (5.2), and (5.3), is to normalize each effective diffusivity curve by its respective ideal diffusivity (D_{ideal}). A distance function is formalized in Equations (5.9), (5.10), (5.11), and (5.12), based on the effective, normalized properties of an equivalent composite wall.

$$x_n = D_{eff,\,n} = \frac{D_{eff}}{D_{eff,\,ideal}} = \frac{k_{eff,\,n}}{\left(\rho \cdot C_p\right)_{eff,\,n}} \tag{5.9}$$

$$y_n = k_{eff,\,n} = \frac{k_{eff}}{k_{eff,\,low}} \tag{5.10}$$

$$H = x_n^{\,2} + y_n^{\,2} \tag{5.11}$$

$$d_n = \sqrt{H} \tag{5.12}$$

The proportion of the two materials that minimizes the distance function (d_n) may be expressed analytically or can be determined either visually or using a minimum function. The method is implemented here using Matlab, but a spreadsheet program may also be used.

5.2.3.3 Comparing Minimization Methods

The two minimization methods are now compared to each other and repeated iterations using the transmission matrix method. Recall that the transmission matrix method calculates the magnitude ratio directly, thereby determining the proportion of two materials that results in a minimum magnitude ratio. The two minimization methods are used to identify an optimal proportion of two materials based on other performance criteria, namely minimum effective diffusivity and minimum normalized distance. The proportion of materials selected from these two methods is then used to select a corresponding minimum magnitude ratio (based on number of layers, such as the ICI wall which is minimized for 7 layers, as shown in Figure 5.5) from the results of the transmission matrix method. The relative merit of each method is based on the accuracy of the resulting magnitude ratio and the computational ease and efficiency of the method itself.

To help visualize the similarity in the proportion of materials selected by each method, Figure 5.9 (a) shows the effective thermal diffusivity of the insulation-concrete material combination, with a close-up showing the apex of the curve in Figure 5.9 (b). The curve is based on a range of 0-100% of insulation and, the curve is normalized by its respective idealistic composite material properties (Equation (5.7)). The two methods described here are shown for comparison along with minimum magnitude ratio and maximum phase lag. Each approach selects an optimal proportion of materials for its respective objective: minimizing effective diffusivity, minimizing normalized distance, minimizing magnitude ratio, or maximizing phase lag, the latter two are based on layered walls while the former two are based on a single-layer composite wall.

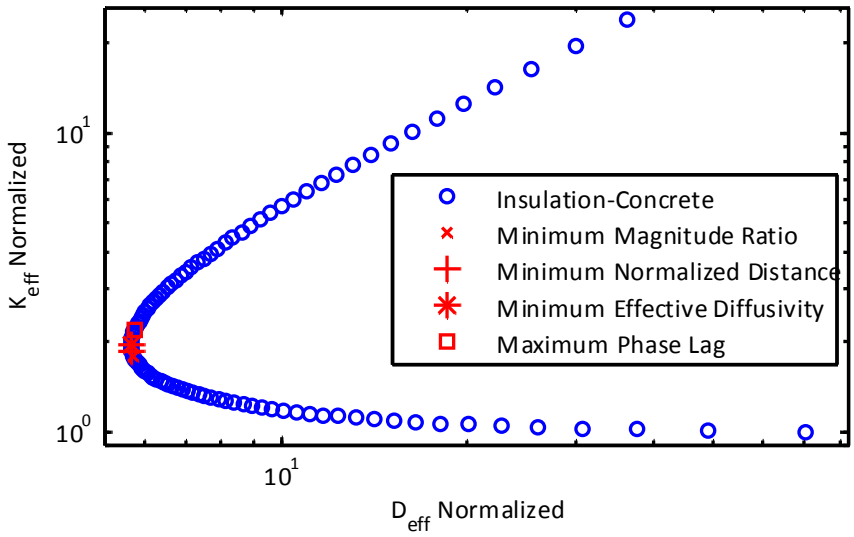

(a)

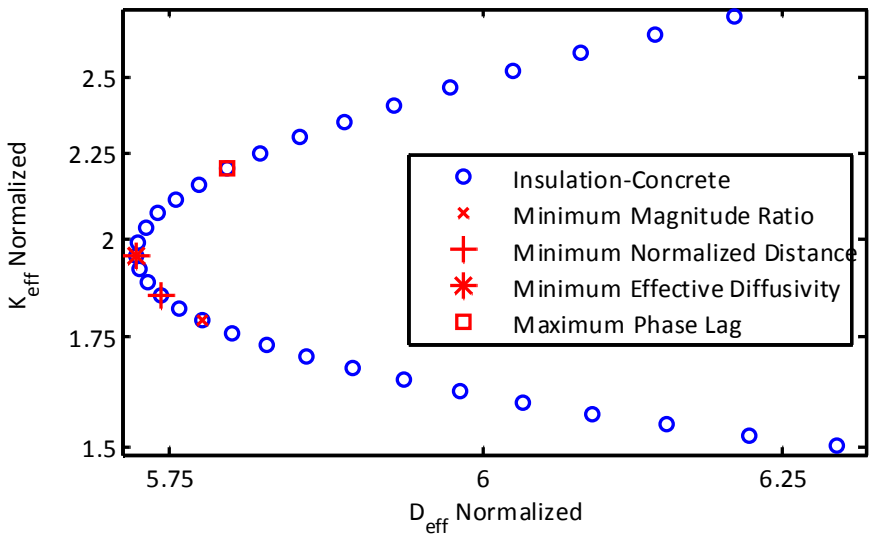

(b)

Figure 5.9. (a) Normalized effective thermal conductivity versus normalized effective thermal diffusivity for 0 to 100% of insulation in the insulation-concrete pair. (b) Close-up showing curve apex with four descriptive data points.

The magnitude ratios are compared in Table 5 for three different material combinations. Because the difference in magnitude ratio is relatively small, potentially negligible, the best design method will favor that which is easiest to implement and fastest to produce results.

Table 5. Compare magnitude ratio results from two different minimization methods with transmission matrix results for minimum magnitude ratio and maximum phase lag, for three different material combinations (percentage of first material selected by method).

Material Combination	Magnitude Ratio (M)			
	Minimum Magnitude Ratio *(% Material 1)*	Method 1: Minimum Effective Diffusivity *(% Material 1)*	Method 2: Minimum Normalized Distance *(% Material 1)*	Maximum Phase Lag *(% Material 1)*
Polymer-Air (*mean 53% polymer*)	1.91 e-03 (*43%*)	2.13 e-03 (*57%*)	2.02 e-03 (*53%*)	2.25 e-03 (*60%*)
Insulation-Concrete (*mean 52% insulation*)	2.78 e-04 (*59%*)	3.00 e-04 (*49%*)	2.87 e-04 (*52%*)	3.06 e-04 (*48%*)
Aluminum-Air (*mean 50% aluminum*)	5.90 e-05 (*44%*)	6.21 e-05 (*50%*)	5.97 e-05 (*47%*)	8.43 e-05 (*59%*)

Recall, the transmission matrix method begins with a 3-layer wall based on the ICI configuration for the concrete (C) – insulation (I) material combination. The configurations for the other two material combinations, polymer (R) – air (A) and aluminum (L) – air (A), are implemented as RAR and LAL, respectively. While in theory, ARA would be better than RAR based on the demonstrably better ICI arrangement with insulating material at outermost layers, it is unrealistic to construct a wall with outer layers made of air, so the solid material is assumed to occupy the outermost layers. As before, the proportion of the two materials and the total number of layers are modified to represent different possible multi-layer wall configurations, each of which is evaluated using the transmission matrix method. Of the whole set, one configuration minimizes the magnitude ratio.

Before comparing these methods in Table 5, it is worth noting that the K-D performance curves shown in Figure 5.8 are indicative of the magnitude ratio resulting from the material

combinations associated with each curve. In other words, the relation of the curves based on effective diffusivity corresponds to differences in magnitude ratio. Generally, a lower effective diffusivity produces a lower magnitude ratio. For example, Table 5 shows that the lowest magnitude ratio of a wall made from layers of polymer and air will be greater than that made with concrete and insulation, and that made of aluminum and air will have the lowest magnitude ratio of the three. Similarly, Figure 5.8 shows that the effective diffusivity of aluminum-air is less than that of concrete-insulation, which is still less than that of polymer-air. Thus, the K-D curve is useful for comparing different material combinations and may be used to determine an optimal material combination, based on effective diffusivity, to minimize magnitude ratio. With a combination of materials selected, the next step is to determine the optimal proportion of each material to use for minimizing magnitude ratio. To this end, the methods listed in Table 5 are compared based on magnitude ratio.

The difference in magnitude ratio between the transmission matrix solution and minimizing effective diffusivity is about 7.5% for the concrete-insulation material combination, about 11% for the polymer-air combination, and about 5% for aluminum-air. The difference in magnitude ratio between the transmission matrix solution and minimizing normalized distance is about 3% for the concrete-insulation material combination, about 6% for the polymer-air combination, and about 1% for aluminum-air. These results indicate that the proportion of materials selected to minimize the effective diffusivity (Method 1) is not as accurate as minimizing the normalized distance (Method 2) or using a full search (transmission matrix solution), but the differences are reasonably small. If the differences in magnitude ratio are considered sufficiently small, the ease and simplicity of calculation favors Method 1 (minimizing

effective diffusivity) over the transmission matrix or even Method 2 (minimizing normalized distance).

The difference in material proportion, for the three material combinations shown, ranges from about 40% to 60% of the first material in the pair (polymer, insulation, or aluminum). The mean proportion of all twelve cases is about 52% of the first material. If the differences in magnitude ratio among all methods considered are sufficiently small, then any proportion of the two materials within the range 40-60%, or close to 50%, may be selected to produce desired thermal performance results (in terms of magnitude ratio and phase lag). For multi-layer wall design, this range or target may be considered a starting point and other factors, such as R-value or cost, may be used to fine-tune the material proportion selected for design. Chapter 5.2.3.5 will develop additional insight regarding Method 1, minimizing effective diffusivity, and the thermal properties of favorable material combinations. First, a method for eliminating unfavorable material combinations is presented.

5.2.3.4 K-D Performance Curve Analysis

Given the relative accuracy of Method 2 (minimizing normalized distance) in predicting the proportion of two materials that minimizes magnitude ratio, and that this method stems from the general trend observed in a K-D performance curve, this trend is explored further. Specifically, a material combination that does not generate a curve with a clear apex approaching the origin will not provide the balance of insulating and capacitive properties necessary for achieving lower magnitude ratios and higher phase lags. Figure 5.7 and Figure 5.8 show these curves, and the trend showing an apex is evident for a material combination such as concrete and insulation. In contrast, a material combination with similar thermal properties such as air and insulation, shown in Figure 5.8, does not demonstrate this behavior. Because the nature of the

curves in Figure 5.8 indicates which materials make poor combinations, a test is developed to quickly rule out these undesirable material combinations.

A new term (c) is defined in Equation (5.13) to represent the heat capacity per unit volume of a given material.

$$c_i \equiv \left(\rho \cdot C_p\right)_i \tag{5.13}$$

Based on the volumetric proportion of material (v_1) that minimizes effective diffusivity (Equation (5.6)) and the physical limitations of the problem ($0 < v_1 < 1$), two constraints are derived. The first limitation – the proportion of one material (v_1) must be greater than or equal to zero, that is, not less than zero percent of the total volume of material in the wall – leads to the constraint defined in Equation (5.14).

$$c_1 k_1 + c_2 k_2 \geq 2 c_2 k_1 \tag{5.14}$$

The second limitation, that the proportion (v_1) must also be less than or equal to one, or one hundred percent of the total volume of material in the wall, leads to the constraint defined in Equation (5.15).

$$c_1 k_1 + c_2 k_2 \geq 2 c_1 k_2 \tag{5.15}$$

Any two materials whose thermal properties do not satisfy these two constraints will perform poorly in combination, so the respective combinations may be eliminated from further

consideration in the design process. Table 6 shows results for this test, based on six materials and a total of thirty-six material combinations. The six materials are concrete (C), polymer (R), insulation (I), air (A), aluminum (L), and copper (U).

Table 6. Material combinations for K-D test and results represented in a symmetrical matrix indicate poor (grey background with bold text) and viable (white background) material combinations.

CC	RC	IC	AC	**LC**	UC
CR	**RR**	IR	AR	LR	UR
CI	RI	**II**	**AI**	LI	UI
CA	RA	**IA**	**AA**	LA	UA
CL	RL	IL	AL	**LL**	**UL**
CU	RU	IU	AU	**LU**	**UU**

The test produces a binary result, where zero indicates a material combination fails one or both of the constraint equations. These poor combination results are shown in Table 6 with a shaded background and bold text. Combining two of the same material is somewhat meaningless, but even so, such a combination will not help reduce magnitude ratio. Four combinations are eliminated based on the method described here, including the two already shown in Figure 5.8, concrete-polymer (CR) and insulation-air (IA), as well as concrete-aluminum (CL) and aluminum-copper (LU). The other material combinations will not all be ideal. Rather, the K-D test indicates that the combination of two materials will produce a wall with effective thermal properties that are better than either material individually, in terms of reducing magnitude ratio. For the combinations that violate constraint equations (5.14) and/or (5.15), one material alone will perform better than the combination of the two.

5.2.3.5 Design Implications of Minimum Effective Diffusivity

Minimizing effective thermal diffusivity has been shown to be a viable surrogate method for determining which material combinations will minimize magnitude ratio. A method has also been presented for eliminating poorly performing material combinations. The aim of this section is to develop a clearer relation between minimum effective diffusivity and optimal material combinations and proportions in the form of generalized design steps. So, to extrapolate on the findings thus far, two terms representing the ratio of thermal conductivities, k_R, and the ratio of heat capacities per unit volume, $(\rho C_p)_R$, are introduced in Equations (5.16) and (5.17).

$$k_R = \frac{k_1}{k_2} \tag{5.16}$$

$$\left(\rho C_p\right)_R = \frac{\left(\rho C_p\right)_1}{\left(\rho C_p\right)_2} \tag{5.17}$$

It may be noted that in a combination of two materials, the material with the lower thermal conductivity (i.e., the "insulating" material) will also have a lower volumetric heat capacity ($\rho \cdot C_p$). Thus, both k_R and $(\rho C_p)_R$ are valid between 0 and 1. The expression for v_{opt} in Equation (5.6) is re-cast in Equation (5.18) to express the optimal volumetric proportion of material in terms of these new ratio terms.

$$v_{opt_R} = \frac{1}{2}\left[\frac{1}{1-\left(\rho \cdot C_p\right)_R} - \frac{k_R}{1-k_R}\right] \tag{5.18}$$

By forcing v_{opt} to equal 1, an expression can be developed for k_R in terms of $(\rho \cdot C_p)_R$ that represents a lower bound of material combinations where an optimum exists (within the physical constraints of $0 \leq v_{opt} \leq 1$). Similarly, an upper bound can be determined by forcing v_{opt} equal to 0. These relationships are mathematically expressed according to Equation (5.19).

$$\left(2 - \frac{1}{\left(\rho \cdot C_p\right)_R}\right) \leq k_R \leq \frac{1}{2 - \left(\rho \cdot C_p\right)_R} \tag{5.19}$$

Graphically, these bounds form a region that represents a viable design space for combining two materials, as shown in Figure 5.10. According to the design space region, the relationship between k_R and $(\rho \cdot C_p)_R$ is coupled, but unrestricted, below values of 0.5, but if either ratio is greater than 0.5, then the other term becomes restricted.

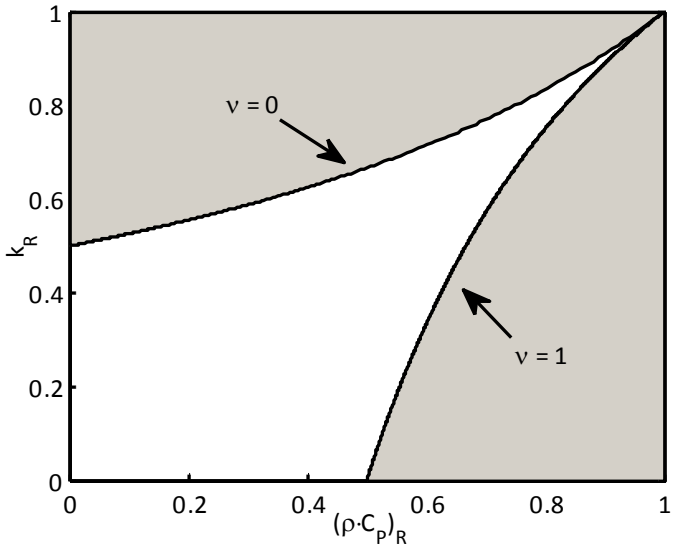

Figure 5.10. Design space for selecting material combinations, based on a two-material composite wall analysis. The acceptable range lies between the two curves shown (unshaded region).

The ratios k_R and $(\rho \cdot C_p)_R$ also become more restricted as their values increase towards 1. As the thermal properties of two materials come closer to one another, or become more alike, the combination actually approaches a single material. Then, there is no optimal proportion. In other words, when either k_R or $(\rho \cdot C_p)_R$ approaches unity, the other must also approach unity, meaning the composite is actually a single material. Also, if a combination of two materials exists outside of this bounded region, then it is better to remove one of the materials altogether and pursue a single material design.

A contour plot is developed by forcing v_{opt} to assume discrete values between 0 and 1. This is shown in Figure 5.11 along with seven data points representing real material combinations. Log scaling is used to help differentiate the data.

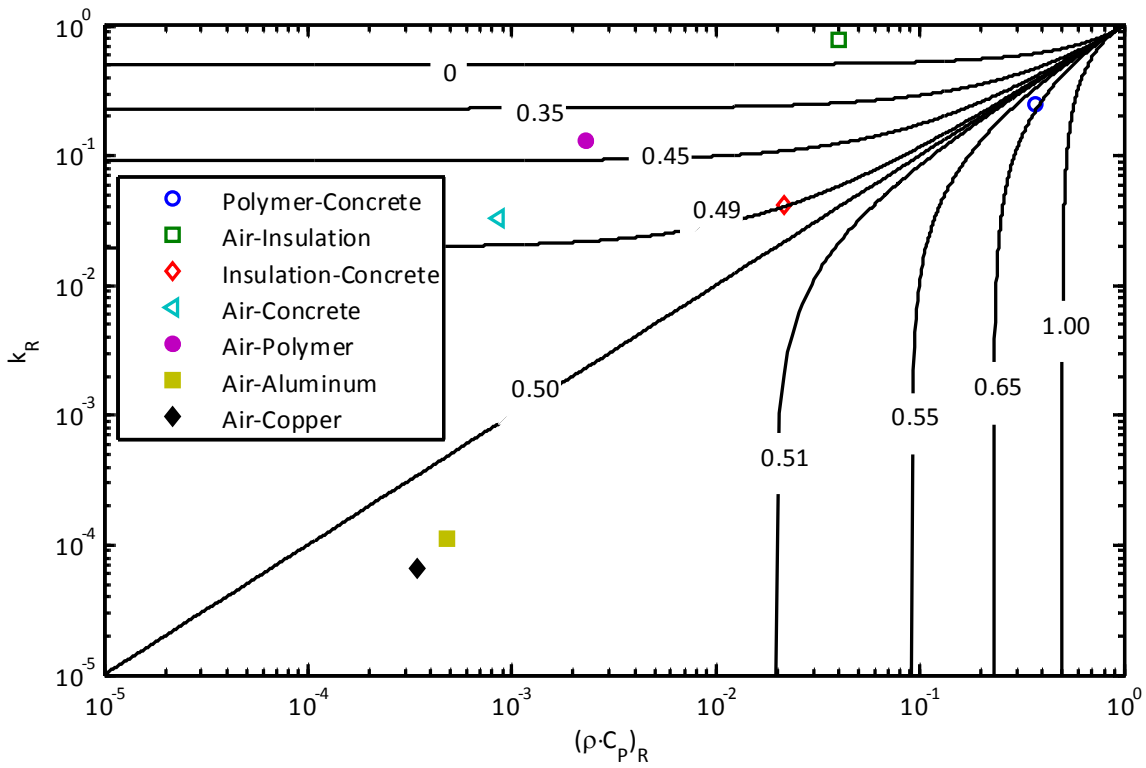

Figure 5.11. Contours of v_{opt} values with data points representing specific material combinations.

The datum for the air-insulation composite actually lies outside the bounding curve for v_{opt} = 0, meaning this material combination is in the reject region outside of the design space highlighted in Figure 5.10. It is also worth noting that with the log scaling used, there is an extensive design space with a relatively small window of v_{opt} values. For example, three of the six viable material combinations (insulation-cement, air-copper, and air-aluminum) fall within 0.49 and 0.51 with a fourth (air-cement) just outside of this range.

For $k_R = (\rho \cdot C_p)_R$, the contour shows that v_{opt} = 0.5, which suggests that equal volumes of each material is required to achieve optimal performance. As the previous figure (Figure 5.10) hints, it is apparent in Figure 5.11 that for larger values of k_R and $(\rho \cdot C_p)_R$, or values of k_R and $(\rho \cdot C_p)_R$ closer to 1, the optimal proportion (v_{opt}) may take on values in the full range between 0 and 1. However, as the values of k_R and $(\rho \cdot C_p)_R$ get smaller, the optimal proportion of the two materials approach 0.5, or 50% by volume of each material (because the contours below 0.49 and above 0.51 diverge). The contours in Figure 5.11 are reproduced in Figure 5.12 for a different perspective.

The contours are not valid for the full range of k_R and $(\rho \cdot C_p)_R$ values between zero and one, so the values beyond this range are plotted as zero. In Figure 5.12 (a), the optimal proportion is shown for fixed values of $(\rho C_p)_R$ and a range of k_R values. The optimal volumetric proportion (v_{opt}) changes from about 0.5 or 0.55 to 0 as k_R approaches 0.5. In Figure 5.12 (b), the optimal proportion for fixed values of k_R and a range of $(\rho \cdot C_p)_R$ values, changes from about 0.45 or 0.5 to 1 as $(\rho \cdot C_p)_R$ approaches 0.5. In both Figure 5.12 (a) and (b), v_{opt} approaches 0.5 as the respective ratios tend towards zero, which suggests k_1 is much less than k_2 and $(\rho \cdot C_p)_1$ is much less than $(\rho \cdot C_p)_2$. While it is informative to relate v_{opt}, k_R, and $(\rho \cdot C_p)_R$, it is worth relating these

directly back to the minimized, or optimal, effective thermal diffusivity, D_{opt} or α_{opt}, to fully understand the implications of the analysis and ensure reliable design decisions.

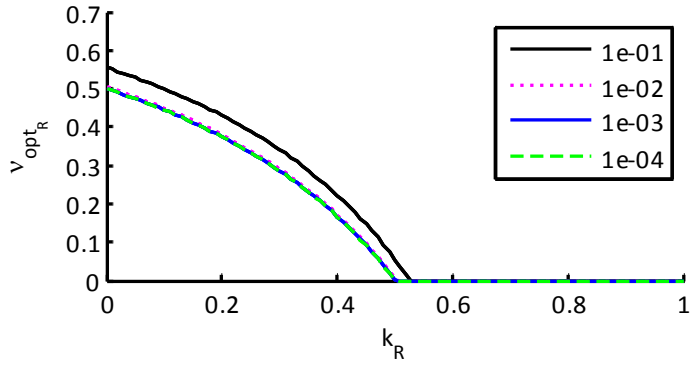

(a)

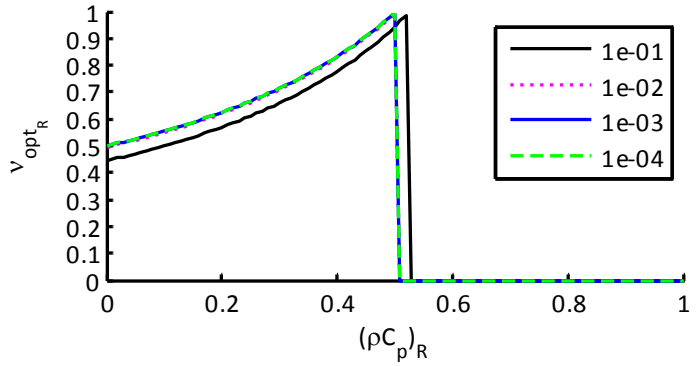

(b)

Figure 5.12. (a) The optimal volumetric proportion v_{opt} of insulation, shown for four values of $(\rho \cdot C_p)_R$ corresponding to contour lines from Figure 5.11 and k_R between 0 and 1. (b) v_{opt} of insulation, shown for four values of k_R corresponding to contour lines from Figure 5.11 and a range of $(\rho \cdot C_p)_R$ between 0 and 1.

In Equation (5.6), the proportion of one material (v_{opt}) that minimizes the effective diffusivity is presented and restricted between zero and one. When this result is substituted back into the equation for effective diffusivity (Equation (5.4)), the result is an analytical expression

for minimum effective diffusivity based on the combination of two materials, as shown in Equation (5.20).

$$\alpha_{opt} = D_{eff,\,\min} = \frac{4 \cdot k_1 \cdot k_2 \cdot (k_1 - k_2) \cdot \left((\rho C_p)_1 - (\rho C_p)_2 \right)}{\left(k_1 \cdot (\rho C_p)_1 - k_2 \cdot (\rho C_p)_2 \right)^2} \tag{5.20}$$

Next, k_R and $(\rho \cdot C_p)_R$ are used to simplify the expression in Equation (5.20). The expression is then normalized by the ideal diffusivity of the material pair, $\alpha_{ideal} = k_1/(\rho C_p)_2$. Equation (5.21) shows the resulting dimensionless, minimum effective thermal diffusivity, which may described as a normalized diffusivity, α_{norm}.

$$\alpha_{norm} = \frac{\alpha_{opt}}{\alpha_{ideal}} = \frac{D_{eff,\,\min}}{D_{ideal}} = \frac{4(1-k_R)\left(1-(\rho \cdot C_p)_R\right)}{\left(1-k_R \cdot (\rho \cdot C_p)_R\right)^2} \tag{5.21}$$

This formulation is used to generate Figure 5.13 and Figure 5.14. Collectively, these figures lend insight into the thermal properties of a favorable material combination and the optimal proportion of each material to use in a multi-layer wall (optimal for minimizing magnitude ratio).

First, in Figure 5.13, contours of α_{norm} are overlaid with the bounded region from Figure 5.10 where the reject space is shaded. In general, one must use caution in applying the dimensionless form, α_{norm}. The mathematical range for Equation (5.21) allows α_{norm} to be as small as zero and as large as 4, but the lower bound is actually 1 for a physical system. This is apparent in Figure 5.13, where the bounding curves of v_{opt} intersect with the contours of α_{norm} equal to 1. This bound is only reached as both k_R and $(\rho \cdot C_p)_R$ approach unity and the two-material

composite actually approaches a single material. This suggests that α_{norm} equal to 1, or $\alpha_{opt} = \alpha_{ideal}$, is a lower bound, and not the most desirable relation in terms of pairing materials for improved performance. In fact, it represents a single ideal material rather than an optimal combination of two materials.

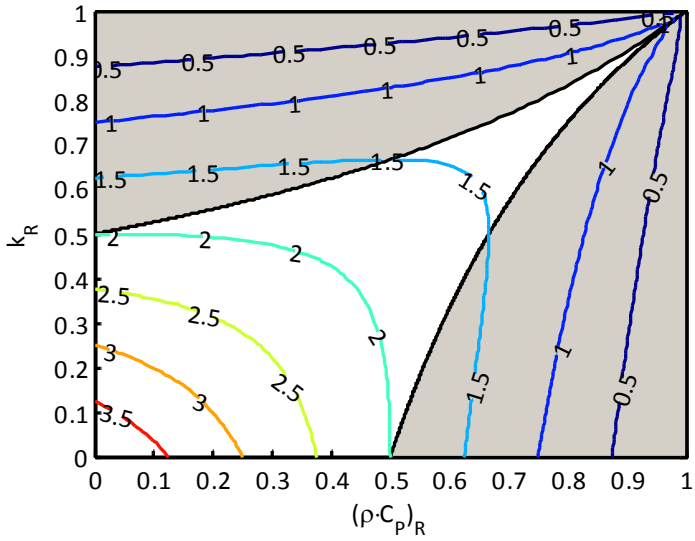

Figure 5.13. Contours for α_{norm} (the ratio of α_{opt} to α_{ideal}). The unshaded region represents the acceptable design space for a composite wall based on the combination of two materials.

Thus, when evaluating the relative performance of different material combinations, the target is not necessarily to find material combinations for which α_{opt} is equal or nearly equal to α_{ideal}. Rather, α_{norm} approaches its upper bound, 4, as k_R and $(\rho \cdot C_p)_R$ approach 0, which also coincides with $v_{opt} = 0.5$, as shown in Figure 5.11 and Figure 5.12. In Figure 5.14, α_{opt} is plotted against α_{ideal} for the seven material combinations considered previously, along with the bounding curves for α_{norm}. Log scaling is used again to help differentiate the data. Each datum lies within

the two bounding curves of $\alpha_{opt} = 4 \cdot \alpha_{ideal}$ and $\alpha_{opt} = 1 \cdot \alpha_{ideal}$ with the exception of air-insulation, which has been shown to lie outside of the acceptable design space.

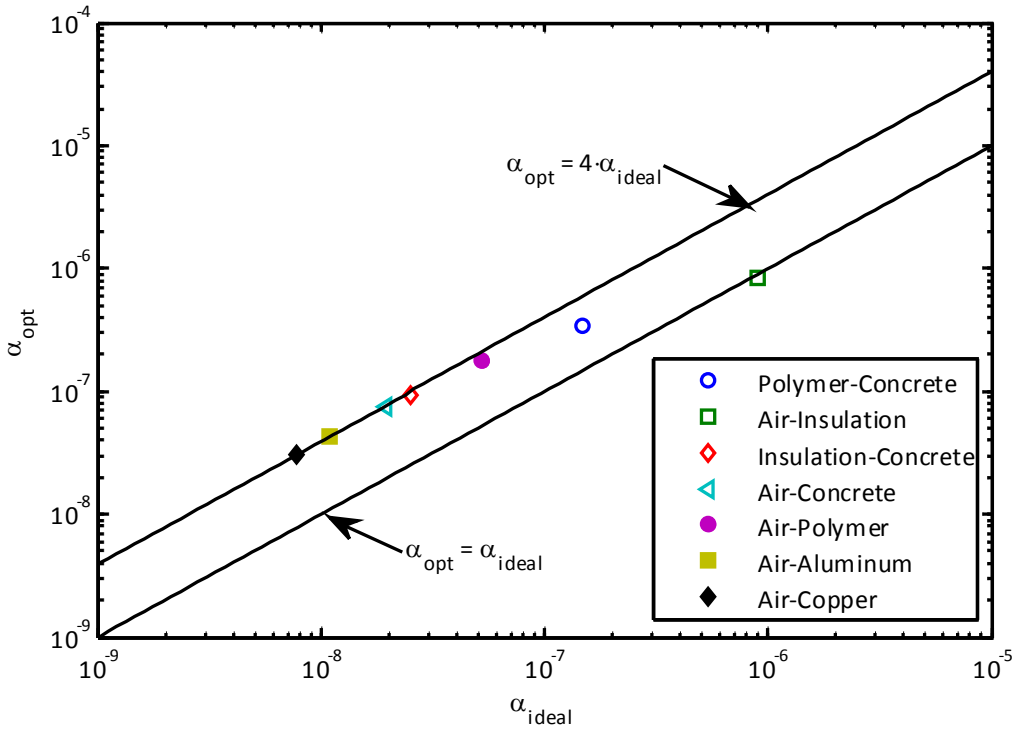

Figure 5.14. α_{opt} versus α_{ideal} with the ratio α_{norm} of seven material combinations and the bounding curves for $\alpha_{opt} = \alpha_{ideal}$ and $\alpha_{opt} = 4 \cdot \alpha_{ideal.}$

It is also apparent that the material combinations with the lowest optimal diffusivity fall on, or close to, the $\alpha_{opt} = 4 \cdot \alpha_{ideal}$ bounding line, which occurs when k_R and $(\rho \cdot C_p)_R$ approach zero. The correlation between the best performing combinations in Figure 5.14 and the values for k_R and $(\rho \cdot C_p)_R$ in Figure 5.11 make it clear that simultaneously minimizing k_R and $(\rho \cdot C_p)_R$ will maximize the performance achievable with the physical combination of two real materials. These simple analytical calculations coincide with minimizing α_{opt} and, correspondingly, minimizing magnitude ratio.

In this Chapter, the relations between thermal properties and material proportions have been explored to develop greater insight into the nature of pairing materials for desirable thermal properties and performance. Additionally, design tools have been developed for selecting optimal material combinations and proportions of each material. So far, this work has addressed three of the five design parameters identified for minimizing magnitude ratio in multi-layer wall design, namely, number of layers, material combinations, and material proportions. To a certain extent, the distribution of materials in the wall has also been addressed. Specifically, the work in Chapter 4 suggests an optimal distribution is based on the ICI family with an insulating material at both the innermost and outermost layers and a thermally massive material located towards the middle of the wall. However, the search is not yet sufficiently exhaustive to justify concluding that evenly distributed layers are best for minimizing magnitude ratio. Therefore, a formalized search is developed to help answer this question more decisively.

5.3 MATERIAL DISTRIBUTION

Material distribution is addressed heuristically in Chapter 4 by evaluating different configuration families and a discrete set of walls with unevenly distributed layers. However, it is not conclusive whether evenly distributed and symmetric layers are an optimal layer arrangement for minimizing magnitude ratio. Therefore, a formal optimization is developed to determine the material distribution and overall wall composition that minimizes magnitude ratio for a steady, sinusoidal input. The work presented here will simultaneously indicate optimal material distribution for minimum magnitude ratio and validate the trends observed in Chapter 5.2 for optimal material combinations.

As in the work presented previously, material thermophysical properties are assumed to be constant, homogeneous, and isotropic through each layer, and one-dimensional heat conduction is the dominant heat transfer mode through the multi-layer wall. Since this work is not focused on developing optimization methods, a suitable method is selected from the Matlab Optimization Toolbox. The objective function to be minimized is the overall magnitude ratio of the wall, which depends on the five design parameters that form the overall wall composition.

Recall from Chapter 3 that the overall transmission matrix is calculated as the ordered product of intermediate, or even elemental, transmission matrices. An elemental transmission matrix represents a single impedance (*Z*) or admittance (*Y*). The matrices are upper triangular and lower triangular, respectively. With this in mind, it can be shown that the determinant of any transmission matrix is unity [48]. As a result of this property and the relation derived in Equations (3.15)-(3.17), the overall network transfer function can be expressed in terms of one element of the overall transmission matrix, element D, as shown in Equations (5.22) and (5.23).

$$\tau_{total} = \begin{bmatrix} A & B \\ C & D \end{bmatrix} \tag{5.22}$$

$$\frac{T_{s,rm}}{T_{s,amb}} = \frac{\det(\tau_{total})}{D} = \frac{1}{D} \tag{5.23}$$

As a result, the objective function is essentially a polynomial (*p*) of order *N* equivalent to the denominator of the overall network transfer function. Equation (5.24) shows the objective function in terms of three design parameters x_1, x_2, and x_3.

$$\text{Minimize } f(x_1, x_2, x_3) = -D_t = p_N(x_1, x_2, x_3) \tag{5.24}$$

The order N of the polynomial is determined by the number of nodes, or capacitors, in the network. The total number of nodes (N) is determined within the refined transmission matrix method, which ensures model accuracy. The number of nodes is also related to the number of layers in the wall. Due to the methodology of the refined transmission matrix method, there are at least two nodes per layer, regardless of thickness or properties.

For this work, it is important to choose a sufficiently large number of possible layers, or what will be referred to as wall "slices". If neighboring slices are the same material, then they form an n-slice layer. The total number of slices must be large to avoid over-constraining the problem by restricting the solution to an even or an odd number of layers, or to any specific distribution. A large number of total possible layers is defined, dividing the wall into many very thin slices, as illustrated in Figure 5.15.

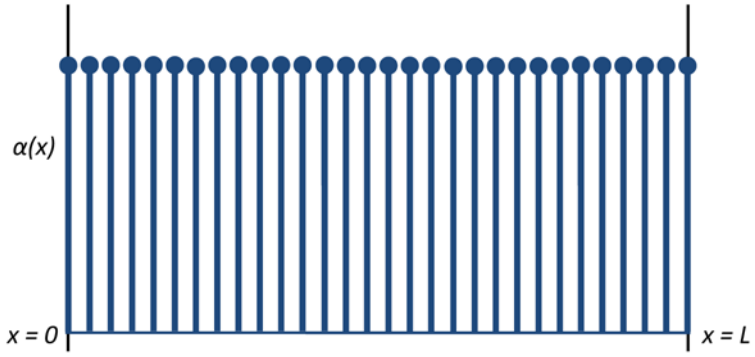

Figure 5.15. A wall, length (L), with a large number of very thin slices. Identical slices form a single n-slice layer of the same material.

Three cases are considered using this basic strategy. First, using only two materials, insulation and concrete, an optimal distribution is determined. For this case, the problem is essentially selecting between two sets of material properties for each slice. Each material may be identified by its thermal diffusivity, shown for this case in Equation (5.25).

$$\alpha = \alpha_i \text{ for } i = 1,2 \tag{5.25}$$

This problem is described more in Chapter 5.3.1.1 along with the approach used and resulting material distributions. The second case, described more in Chapter 5.3.1.2, is an extension of the first, where a discrete number (n) of different materials is considered, as in Equation (5.26).

$$\alpha = \alpha_i \text{ for } i = 1,2,...\text{n} \tag{5.26}$$

By considering multiple materials and a large number of slices, the optimization search selects both the best combination of materials and the best distribution of those materials. For this reason, it informs the overall wall composition.

Finally, an optimal multi-layer configuration is determined where each slice may assume a value of thermal conductivity (k) or heat capacity per unit volume (ρC_p), within a specified range of known values, as shown in Equations (5.27) and (5.28).

$$k_{lb} \le k \le k_{ub} \tag{5.27}$$

$$\left(\rho C_p\right)_{lb} \le \left(\rho C_p\right) \le \left(\rho C_p\right)_{ub} \tag{5.28}$$

This study is described more in Chapter 5.3.2.1. Results affirm previous conclusions about minimizing effective diffusivity and reducing magnitude ratio via layering.

In the first two cases, the variables used in the optimization method are selected from a set of integer values. Therefore, the Matlab optimization function is selected to account for integer-valued variables as well as the general form of the objective function. Since the transmission matrix method involves matrix multiplication, the resulting transfer function used to determine magnitude ratio contains quadratic or nonlinear terms. Based on the format of the objective function, the use of integer valued variables, and some experimentation, the Genetic Algorithm and Pattern Search methods are selected from the optimization functions available in Matlab.

5.3.1 Matlab Genetic Algorithm

Matlab's Genetic Algorithm (GA) solver is a stochastic procedure that does not guarantee the same solution every time. It uses random number generators to complete a stochastic search. The process mimics natural selection from the area of evolutionary biology. Rather than calculating a single point at each iteration in the solver, a set of points is calculated. Each set of points is called a population, and each iteration is called a generation. The initial population is seeded randomly, or it can be set in whole or in part by the user. Similarly, subsequent generations are produced randomly (based on pseudorandom numbers) from the current generation using three strategies to evolve one generation to the next. First, not all individuals within a current population may contribute to the next population. Individuals are chosen using "selection rules" to be "parents" for the next generation. Pairs of two parents from the current generation are combined using "crossover rules" to form children, who are individuals for the

next generation. Individual parents may be randomly changed using the algorithm's "mutation rules" before combining with another individual to form children. By setting solver options, this selection process may be tweaked to modify the algorithm performance.

In the evolutionary language Matlab uses for its genetic solver, the term "fitness function" is used to mean the objective function. An individual may be considered a "genome," or "genes" if it is a vector, and the population refers to an array of individuals. Each individual has a fitness value, which is the value of the fitness function for that individual. The minimum of the individual fitness values is the best fitness value of its population. While some "elite" individuals with lower fitness values are selected to pass directly to the next generation, the mutation and crossover methods are used to form children to populate the remainder of the next generation. The process continues until a stopping criterion is reached, such as a specified number of generations or fitness limit threshold. Another stopping criterion is the number of stall generations, which stops the algorithm when the "average relative change in the fitness function value" is less than a specified tolerance [49]. Stall generations is the stopping criterion invoked exclusively while using the Genetic Algorithm for this analysis.

The creation, crossover, and mutation functions unique to this algorithm allow the solver to obtain integer variables. Given that the objective function has nonlinear terms and that discrete material choices constrain design variables to be integers, Matlab's GA solver is a good fit for this optimization problem.

The fitness function is formulated using the transmission matrix method to select material layers that will minimize magnitude ratio. Initially, only insulation and concrete are considered for each slice. Then, each slice is selected from among seven different materials, including insulation (I), concrete (C), cement plaster (P), air (A), polymer (R), aluminum (L), and copper

(U). Each material has a known value of thermal diffusivity, $\alpha = k/(\rho C_p)$. Finally, the thermal conductivity (k) and heat capacity per unit volume (ρC_p) are selected independently for each slice, producing a thermal diffusivity for an unknown, idealistic material.

5.3.1.1 Optimal Material Distribution with Insulation and Concrete Only

The heuristic search method used in Chapter 5 identifies a 7-layer, ICI wall with about 59% insulation as the optimal multi-layer configuration using insulation and concrete. Matlab's Genetic Algorithm is used to confirm the optimal distribution of insulation and concrete in a multi-layer wall for minimizing magnitude ratio. Now, rather than evaluating multiple walls with fixed layers of alternating materials, a single wall is divided into numerous very thin slices whose thermal properties will be individually selected.

The overall wall length and total number of slices is fixed, thereby setting the thickness of each individual slice within the wall. The overall resistance and capacitance of the wall is not restricted, but each slice is restricted to assume one material. In this case, each slice must assume one of two integer values, representing the thermal diffusivity (α) of either insulation or concrete. Recall, if neighboring slices are the same (here, either insulation or concrete) they form an n-slice layer.

An example illustrating this method is shown in Figure 5.16, which represents a solution using a sample wall with overall length (L) and 30 individual slices. One of two different values for thermal diffusivity (α) are selected at each slice. The sample solution shown in Figure 5.16 represents a 5-layer distribution of two materials. Six slices are clustered together to form each thicker layer, for an effective total of five 6-slice layers, in this illustrative example.

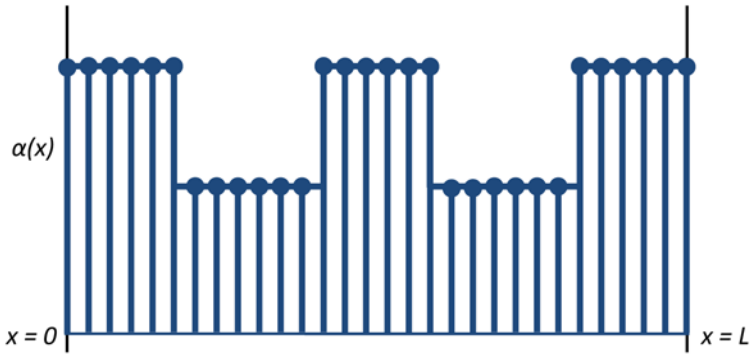

Figure 5.16. Hypothetical solution for material distribution using only two materials.

A 0.5% residual convergence error (described in Chapter 5.1) is used in the transmission matrix method here, which is called within the fitness function. The population size for the GA solver is set to equal the total number of wall slices. In addition, a “Crossover Fraction” value of 0.85 is set in the solver options, which differs slightly from the default value based on experimentation. Integer valued variables and lower and upper bounds are specified. All other options are the default solver settings.

Preliminary results show a trend towards clustering slices, as illustrated in Figure 5.16, which suggests that a larger number of generations is required for the algorithm to converge. However, increasing the number of generations and stall generations within the algorithm was found to be ineffective, so instead, an alternative procedure is developed. Using a loop, the total number of generations run using the Genetic Algorithm is effectively increased, and the best fitness value continues to improve.

This method uses the Genetic Algorithm to randomly create an initial population, and the algorithm runs until a stopping criterion is met. Since the number of generations and the stall generations are limited, the algorithm typically stops based on the stall generation limit. Then, 10% of the initial population for the next GA run is set based on the final individual with the best

fitness value from the GA run that just stopped. So, each subsequent run uses the best result from the previous run to seed 10% of its initial population. The loop executes the Genetic Algorithm as many times as specified. For example, if each GA run stops after 100 stall generations, and the loop executes 5 times, then 500 total effective generations are used to find the best fitness value and converged layer clusters.

For a very large number of slices, the clustered slices do not always converge perfectly. Where a cluster of slices is nearly converged, each slice is the same material for several consecutive slices, except that one very thin slice in the middle somewhere is a different, often similar, material. This slice is referred to as an outlier.

In the first case considered, the overall wall thickness is 278 mm with a total of 70 slices, making each individual slice just under 4 mm thick. Results are shown in Table 7 for the 278 mm wall with 70 total slices which assume the thermal properties of either insulation or concrete.

Table 7. Genetic Algorithm results, from 15,000 effective generations, for 278 mm wall. Seven effective layers of insulation and concrete are selected for a wall with 70 total slices.

Total Number Slices	Magnitude Ratio (Final Value)	Proportion of Insulation to Concrete (% Insulation)	Layer						
			1	2	3	4	5	6	7
70	2.77e-04	57	11I	10C	10I	10C	9I	10C	10I

After 15,000 effective generations running the GA solver, the 70 slices are clustered into seven effective layers with no outliers. The layers are symmetrically distributed and almost perfectly even. There are three layers of concrete and four layers of insulation, with insulation at the inner and outermost layers. With approximately 57% insulation to concrete and a magnitude

ratio M=2.77e-04, the Genetic Algorithm result confirms the heuristic search results presented previously (also a 7-layer ICI configuration with 58.6% insulation and $M = 2.77\times10^{-4}$).

To further validate conclusions regarding optimal material distribution, the method used here is repeated using a larger number of materials. This result will affirm prior conclusions by indicating an optimal wall composition based on the five design parameters: wall thickness, number of layers, materials, material proportion, and material distribution. Overall wall thickness is fixed and materials are limited to those within the set provided, but all other parameters are selected based on lowering the fitness function in the GA solver.

5.3.1.2 Optimal Wall Composition (Material Combination and Distribution)

Two cases are evaluated using fixed overall wall thicknesses of 100 mm and 140 mm and seven possible materials: insulation (I), concrete (C), air (A), aluminum (L), cement plaster (M), polymer (R), and copper (U). Each wall is evaluated for 30, 50, and 70 total slices.

A 0.5% residual convergence error is used again, as is the methodology used in the first case that considered only insulation and concrete. Both wall thicknesses arrive at solutions of alternating layers of air and copper, with air at the outermost layers. Since the model simply views air as an insulating material, the best insulating material within the set is selected. The 100mm wall results in five effective layers, and the 140 mm wall results in seven effective layers.

A small number of outliers in the slice clusters that form each effective layer are identified in Table 8 for the 100 mm wall and Table 9 for the 140 mm wall. These tables also show the magnitude ratio associated with each wall configuration, the proportion of air to copper, and the layer distribution by material and total number of layers within each material cluster. An evenly distributed five layer wall is also shown in Table 8 to compare with the

Genetic Algorithm results for the 100 mm wall. Similarly, an evenly distributed seven layer wall is shown in Table 9 to compare with the GA results for the 140 mm wall. The differences in magnitude ratio that result from slight alterations in material distribution are small, and in the majority of cases, the evenly distributed layers result in a lower magnitude ratio for the same number of total slices.

Table 8. Genetic Algorithm results, from 15,000 generations, for 100 mm wall. Five effective layers of air and copper are selected for three different sets of wall slices: 30, 50, and 70.

Total Number Slices	Magnitude Ratio (Final Value)	Proportion of Air to Copper (% Air)	Layer				
			1	2	3	4	5
30	3.30e-03	63	7A	5U	5A	6U*	7A
50	3.18e-03	62	11A	9U	8A	10U	12A
70	3.47e-03	65.7	22A**	12U**	11A	11U*	14A
5	3.20e-03	60	1A	1U	1A	1U	1A

*one outliers, **two outliers (A, L, or U)

Table 9. Genetic Algorithm results, from 15,000 generations, for 140 mm wall. Seven effective layers of air and copper are selected for three different sets of wall slices: 30, 50, and 70.

Total Number Slices	Magnitude Ratio (Final Value)	Proportion of Air to Copper (% Air)	Layer						
			1	2	3	4	5	6	7
30	7.42e-04	57	5A	5U	3A	3U	3A	5U	6A
50	7.61e-04	60	7A	3U	4A	8U	9A	9U	10A
70	7.67e-04	61	13A	12U**	8A	6U	7A	10U	14A
7	7.16e-04	57	1A	1U	1A	1U	1A	1U	1A

*one outliers, **two outliers (A, L, or U)

5.3.2 Matlab Pattern Search

The third and final case is used to determine optimal thermal properties with no constraint requiring that those properties must correspond to a known material. In this case, fictitious values of thermal diffusivity are allowed, because thermal conductivity (k) and heat capacity per unit volume (ρC_p) are no longer coupled, but selected individually for each individual slice. Results ultimately show an idealistic material and help explain the benefits of layering two materials.

This final case was implemented using the Genetic Algorithm, but the solver does not converge well and results in too many outliers. Through experimentation, the Pattern Search solver was found to yield better results. The GA solver in Matlab has a hybrid function option that allows a secondary search method to be invoked after the Genetic Algorithm stops. Initially, the Pattern Search function was called after the GA solver. The Pattern Search method is effective on its own, though, so it is used directly instead of the Genetic Algorithm.

A pattern search algorithm is, generally, a direct search method that does not rely on a gradient and does not require that the objective function be continuous. Matlab's Pattern Search solver uses a method called *polling* to find a local minimum of an objective function. (The italicized text indicates language used in the Matlab description of the Pattern Search algorithm.)

The objective function is evaluated for a set of points around the *current point*, based on a *mesh size*. If the minimum of this set is lower than the *current point*, then the *mesh size* is doubled and a new pattern is established around the *current point*. If the minimum of the set is not lower than the *current point*, then the *mesh size* is reduced by half and a new pattern is set around the same *current point*, unless the reduction in *mesh size* is below a threshold that stops the search.

As before, Matlab's Pattern Search calculates the magnitude ratio of the multi-layer wall as the objective function to be minimized. A starting point is also specified for the search. Linear equality and inequality constraints can be used and upper and lower bounds can be set to constrain the solution parameters. A nonlinear constraint function may also be specified along with a number of options, which are set by specifying an options structure. In this analysis, the default options are used, where 2N vectors comprise the default generalized Pattern Search, and N is the number of independent variables in the objective function.

5.3.2.1 Ideal Material Combinations and Layering Effect

One wall with an overall thickness of 140 mm and 70 total wall slices is considered. Rather than selecting among seven different materials, the method chooses from among seven different values of thermal conductivity (k) and seven different values of heat capacity per unit volume (ρC_p), thereby doubling the total number of optimization variables. The lower bound on k is the minimum thermal conductivity of the materials in the set considered previously: insulation (I), concrete (C), air (A), aluminum (L), cement plaster (P), polymer (R), and copper (U). The upper bound on k is the maximum value of thermal conductivity of the seven materials within this set. The lower bound on k is the minimum value within the set. The bounds on ρC_p are set in a similar manner. The Pattern Search executes successfully, stopping based on the default *mesh size* tolerance.

The result using Matlab's Pattern Search algorithm is shown in Figure 5.17 with uniform values for k and ρC_p across the wall. The lowest bound for k, the thermal conductivity of air (k_{air}), is selected for every slice, and the highest bound for ρC_p, that of copper ($(\rho \cdot Cp)_{copper}$), is selected for every slice. The result is a 70-slice, single layer wall, where every slice minimizes thermal diffusivity, $\alpha = k/(\rho C_p)$. For this wall, the resulting magnitude ratio is M = 1.43e-05,

which is an order of magnitude smaller than the results shown in Table 9, whose configurations rely on layering different materials.

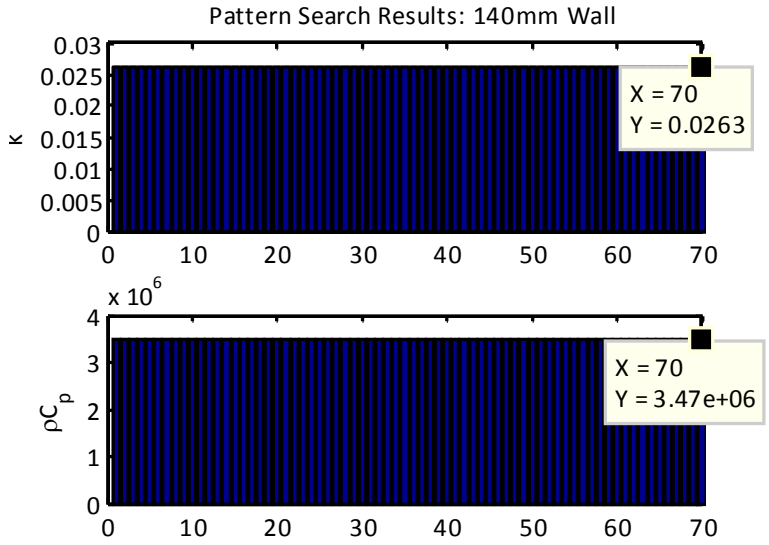

Figure 5.17. Results for thermal conductivity (k) and heat capacity per unit volume (ρC_p) using *patternsearch.m* from Matlab.

This indicates that using just a single layer of an ideal material is better than layering different, known materials. Layering different material combinations is a physical method that allows a multi-layer wall to approach an idealistic composition. This concept is illustrated in Figure 5.18, which shows that layering approaches the performance of an ideal composite, but it reaches a threshold beyond which layering is no longer beneficial. Specifically, Figure 5.18 shows the magnitude ratio of the ICI configuration for an increasing number of layers.

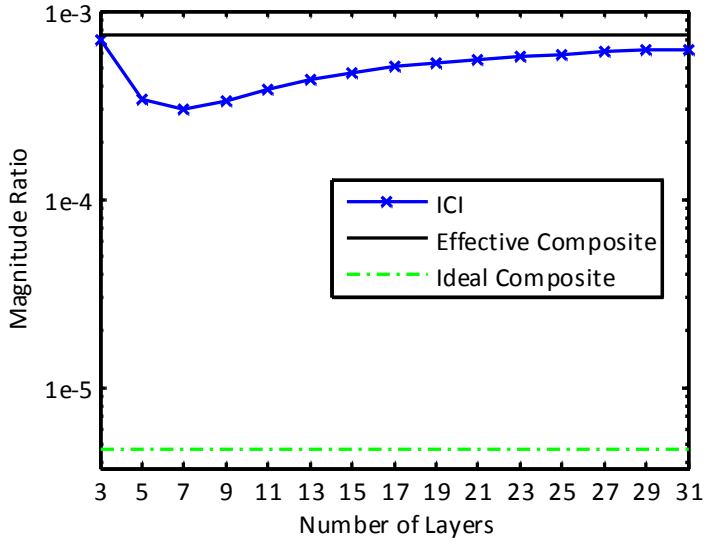

Figure 5.18. Magnitude ratio for ICI family with increasing number of layers, an effective composite, and an ideal composite, showing the effect layering has on reducing magnitude ratio and approaching an idealistic material composition.

The magnitude ratio of a single layer wall made of an effective composite for each proportion of insulation to concrete is also shown near its minimum. Finally, a flat line shows the magnitude ratio resulting from a single layer wall made of an ideal composite, using the thermal conductivity of insulation ($k_{insulation}$) and the heat capacity per unit volume of concrete ($(\rho \cdot C_p)_{concrete}$). From 5.2.1, the ICI wall with seven layers and about 58.6% insulation is the minimum magnitude ratio ($M = 2.77\times10^{-4}$) achieved using the two materials, insulation and concrete, with layering. The magnitude ratio achieved using an ideal combination of the two materials is $M = 4.17\times10^{-6}$, two orders of magnitude less than that achieved by layering insulation and concrete.

As in Chapter 5.2.3, the best possible combination of two materials is the idealistic union of the lowest thermal conductivity (k_{low}) and largest heat capacity per unit volume ($\rho C_{p,high}$). Such a combination produces an ideal thermal diffusivity, as shown in Equation (5.8). Until materials

scientists develop methods for minimizing thermal diffusivity, wall design may rely on different material combinations and multi-layer configurations to approach this ideal. Chapter 5.4 considers how these and the other design parameters considered may change, depending on the overall thickness of the wall.

5.4 WALL THICKNESS

Having addressed number of layers, materials, material proportion, and material distribution, the fifth design parameter – wall thickness – is discussed here. Wall thickness may be pre-determined by the specific application or design constraints. Regardless, the optimal number of layers and proportion of materials will depend on the materials used and the overall thickness of the wall.

To illustrate the effect of overall thickness on optimal layer number and material proportion, insulation and concrete are used while the total number of layers and the percentage of insulation are varied, as described previously. The magnitude ratio and phase lag for each set of parameters is calculated for an overall wall thickness ranging from 50 mm to 300 mm. Figure 5.19 shows the frequency response (magnitude ratio and phase lag) and design parameters of a multi-layer ICI wall for this range of overall thickness. The minimum magnitude ratio for a given wall thickness is shown in Figure 5.19 (a), while Figure 5.19 (b) shows the corresponding phase lag in hours. Figure 5.19 (c) shows the percent insulation that minimizes the magnitude ratio for a given wall thickness, and Figure 5.19 (d) shows the number of layers that minimizes the magnitude ratio for a given wall thickness.

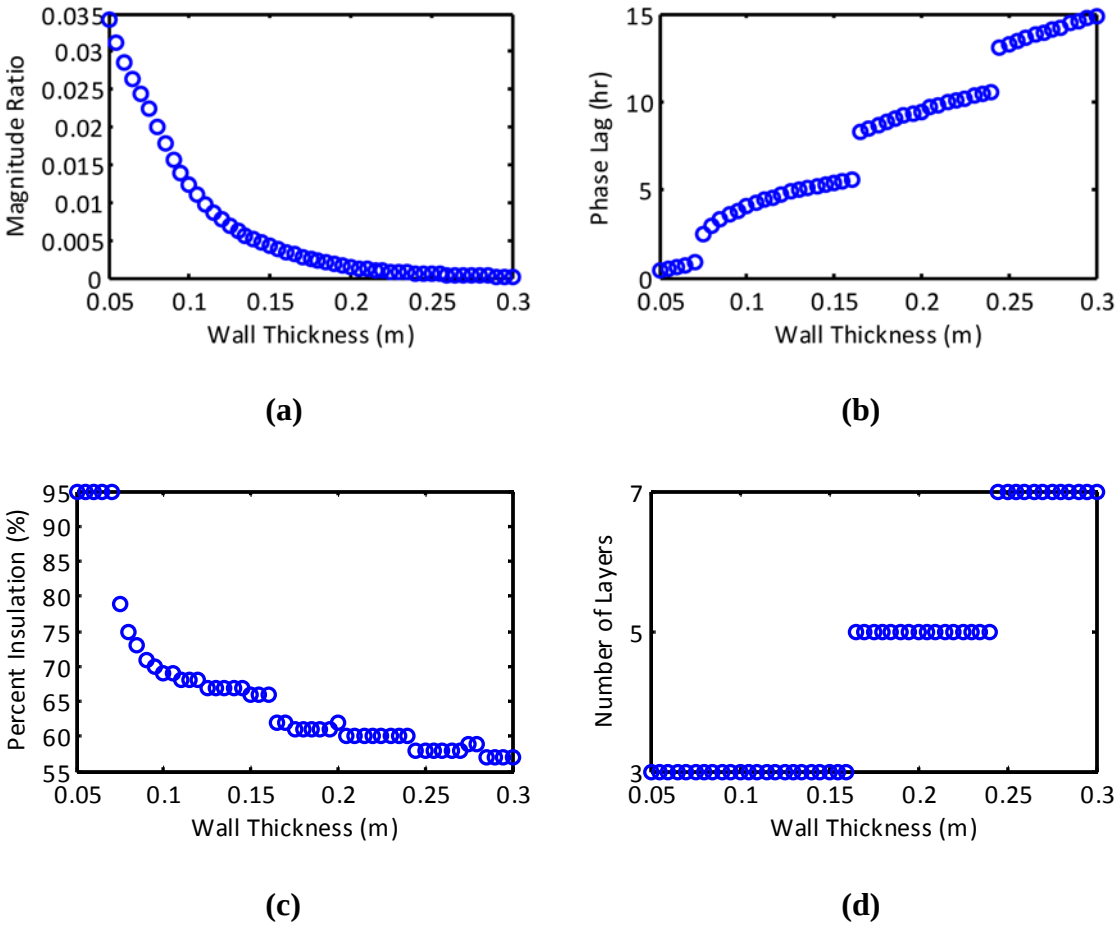

Figure 5.19. (a) Minimum magnitude ratio for given wall thickness. (b) Phase lag corresponding to minimum magnitude ratio for given wall thickness. (c) Percent insulation that minimizes magnitude ratio for given wall thickness. (d) Number of layers that minimizes magnitude ratio for given wall thickness.

As expected, a larger overall wall thickness yields a lower magnitude ratio and a longer phase lag. Figure 5.19 (c) and (d) show how the optimal proportion of materials and the optimal number of layers also depends on the overall wall thickness. For a combination of insulation and concrete, a thicker wall requires less insulating material and a larger number of layers. A thinner wall requires more insulating material and fewer layers of insulation and concrete.

It is likely that design goals such as R-value and constraints such as cost will dominate the selection of building materials and dictate the overall wall thickness. With these design

parameters set, the optimal number layers and proportion of materials can be determined and combined with the guidelines for material distribution to create an optimized multi-layer wall that will minimize magnitude ratio for a specific application. Based on previous results, it is also likely that the corresponding phase lag will be acceptable for a building application. The results and tools developed in Chapter 5 are synthesized into a guide for multi-layer wall design, which is presented in Chapter 6. A sample case study is provided to illustrate the process.

6.0 MULTI-LAYER WALL DESIGN GUIDE FOR BUILDING APPLICATIONS

A five step process is outlined here for designing multi-layer walls that minimize magnitude ratio (decrement factor), based on the five design parameters explored in this thesis. Design choices are based on common residential construction practices, relevant codes and standards, and the tools and recommendations presented in this work. Additional methods to analyze material costs or impacts may be used in addition to the steps outlined here. The process starts with setting the (1) Overall Thickness, then selecting (2) Materials and (3) Proportion of Materials, and finally discussing the practical aspects of implementing (4) Material Distribution and (5) Number of Layers. The overall wall thickness, selected material combination, and relative proportion of each material will determine the overall wall R-value, which does not depend on the number of layers or distribution of materials. To illustrate this design process, a sample multi-layer wall is designed for a residential application in Pittsburgh, Pennsylvania. In Chapter 7, the performance of this wall is compared with that of a standard residential wall, and the associated energy saving potential is estimated.

6.1 OVERALL THICKNESS

Step one this design process is to set the overall wall thickness. Generally, for both static (R-value) and dynamic (magnitude ratio and phase lag) performance, thicker walls are better.

Wall thickness will depend on the type of building, whether it is residential, commercial, or industrial, as well as local conventions, costs, and climate. Some regions are known for certain types of design based on architectural or aesthetic features. A good thermal design will evaluate these features rather than relying solely on local custom.

For this residential application in Pittsburgh, Pennsylvania, wall thickness will be based on common U.S. residential construction and material availability in Western Pennyslvania. According to the American Wood Council (AWC), “Studs in exterior walls of one and two story buildings are at least nominal 2x4 inches with the 4-inch dimension forming the basic wall thickness” [50]. Details from AWC, ASHRAE and others illustrate that wood frame construction typically starts at the exterior face with a 1/2 inch (12.7 mm) layer of plywood, stucco, siding, or similar material, followed by a vapor barrier or thin sheathing layers. This is followed by a 3-1/2 inch (88.9 mm) cavity for 2x4 construction or 5-1/2 inches (139.7 mm) for 2x6 constructions. The cavity may be filled with insulation or insulation may be combined with an air gap. The interior layer is often a 1/2 inch (12.7 mm) of gypsum board or drywall [45].

Vapor barriers and sheathing often have negligible thermal resistance and capacitance compared to other materials (or they may be required regardless of other design features), so they are omitted from the material selection process presented in Chapter 6.2. In some cases, siding materials are designed to be insulating, but thermal capacitance is small, so they might be considered an outer insulating layer. Building materials for 2x4 and 2x6 constructions are both readily available from most U.S. hardware stores. Since thicker is better, this design will opt for a 2x6 wall construction. Therefore, the overall design wall thickness is set to be 5-1/2 inches (139.7 mm), plus an outer layer of siding with sheathing underneath and an interior layer of gypsum or plaster board.

6.2 MATERIALS

The second step in this design process is to determine what materials are available and then find the best pair. In Western Pennsylvania, it is common to see both massive and wood-frame construction, so a variety of materials are considered here. Ten materials, specifically, are outlined in Table 10. There are five insulating materials (numbered 1-5 in the table), two plaster board materials (6-7), two masonry materials (8-9) and one wood material (10). Thermal properties are taken from Chapter 26 of the ASHRAE Fundamentals reference [45].

Table 10. Thermal properties of ten building materials.

	Materials and Thermal Properties	***k*** **(W/m·K)**	***ρ*** **(kg/m^3)**	C_p **(kJ/kg·K)**
1	Glass-fiber batts, 85-90 mm (3.35-3.54 inches)	0.043	12	0.84
2	Glass fiber board	0.036	160	0.84
3	Expanded polystyrene extruded (smooth skin)	0.026	32.5	1.47
4	Spray applied: Polyurethane foam (low density)	0.042	7	1.47
5	Air [1]	0.0263	1.16	1.007
6	Gypsum or plaster board	0.16	640	1.15
7	Cement plaster, sand aggregate	0.72	1860	0.84
8	Brick, fired clay	0.895	1920	0.8
9	Gypsum/fiber concrete (87.5% gypsum, 12.5% wood chips)	0.24	800	0.84
10	Eastern white pine wood (12% moisture content)	0.1	400	1.63

[1](Thermophysical properties of air at 300 K and atmospheric pressure [51].)

To eliminate poor combinations, Equations (5.14) and (5.15) may be applied, or simply avoid pairing similar materials, such as two different types of insulation. To determine the best pair among a set of materials, the ideal diffusivity (α_{ideal}) of each possible combination is evaluated and the combination that minimizes α_{ideal} is selected. Recall (according to the analysis following Figure 5.11), for optimal designs, α_{opt} will be close or equal to $4 \cdot \alpha_{ideal}$. In other words, α_{norm} is greater than 1 and close to 4. The ideal diffusivity (α_{ideal}) for the ten different materials considered and 25 possible material combinations is shown in Table 11. To populate this table, α_{ideal} is calculated using the thermal conductivity (k) of the insulating materials (1-5) and the heat capacitance (ρC_p) of the more massive materials (6-10).

Table 11. α_{ideal} for 25 possible material combinations.

	ρC_p	**6**	**7**	**8**	**9**	**10**
k	$\alpha_{ideal} \times 10^{-8}$ **(m^2/s)**	Gypsum or plaster board	Cement plaster, sand aggregate	Brick, fired clay	Gypsum / fiber concrete	Eastern white pine wood
1	Glass-fiber batts (85-90mm)	5.84	2.75	2.80	6.40	6.60
2	Glass fiber board	4.89	2.30	2.34	5.36	5.52
3	Expanded polystyrene extruded	3.53	1.66	1.69	3.87	3.99
4	Spray applied: polyurethane foam	5.71	2.69	2.73	6.25	6.44
5	Air gap	3.57	1.68	1.71	3.91	4.03

A combination of polystyrene (3) and cement plaster (7) minimizes the set, with three other combinations following closely. The six pairs of insulating and massive materials with the lowest values of α_{ideal} among the twenty-five considered are listed in Table 12 along with α_{norm}, the ratio of α_{opt} to α_{ideal}.

Table 12. Ratio of α_{opt} to α_{ideal} (α_{norm}) for the six material combinations with the lowest α_{ideal} values.

Insulating Material	**Massive Material**	$\boldsymbol{\alpha_{norm}}$
polystyrene	cement plaster	3.7459
air gap	cement plaster	3.8512
polystyrene	brick	3.7698
air gap	brick	3.8797
fiber board	cement plaster	3.5032
fiber board	brick	3.5280

As expected, the ratios in Table 12 approach 4, with the maximum ratios occurring for a combination of an air gap and either cement plaster or brick. Polystyrene is the second best insulating material according to this criterion. These material combinations match those from Table 11 with the lowest values of α_{ideal}, which suggests that checking values of α_{norm} is not really necessary. So, based on minimizing α_{ideal}, these top four materials (two insulating and two massive) will be considered, for practical implications, in the next steps: determining the optimal proportion of materials and material distribution.

6.3 PROPORTION OF MATERIALS

Based on the materials selected in Chapter 6.2, the optimal proportion (v_{opt}) is calculated using Equation (5.6) (or Equation (5.18)). For each combination, the proportion is close to one-half: 48.5% air gap to brick, 48.1% air gap to cement plaster, 50.1% polystyrene to brick, and 48.7% polystyrene to cement plaster. Where higher R-values are required, a greater proportion of insulation may be necessary. This is discussed more in Chapter 6.6.

6.4 MATERIAL DISTRIBUTION

Results have shown that the best distribution for minimizing decrement factor is one with insulation towards the inner- and outer-most surfaces, with thermal mass layered symmetrically throughout the wall. Layers are distributed evenly based on the required proportion of each material. A viable design must account for these recommended guidelines while balancing other considerations, such as feasibility of the actual installation. For instance, these guidelines are based on continuous layers of material in the wall, whereas in practice, if wood-frame construction is used, either on-center or staggered studs will interfere with the continuity of these layers. However, staggered studs and other advanced framing techniques are still useful for reducing thermal bridging effects that diminish the performance of an actual wall over the modeling prediction.

For practical reasons, siding and sheathing are included at the outermost layers and a thin layer of gypsum or plaster board is included at the innermost layer. The outermost layers are required to shield the building exterior from weather (air and moisture infiltration) and to provide a “finished” aesthetic appearance. The innermost layer is also required for aesthetic purposes, as well as to restrict infiltration.

It is expected that these layers are sufficiently thin as to allow the strategic distribution of insulating and thermally massive materials to be effective. Insulated sheathing may also be used with siding to increase the overall R-value of the wall, and its position towards the outermost surface is consistent with material distribution recommended here.

The use of air gaps (or any gas) for insulating layers must be employed cautiously, as thicker layers will allow greater natural convection and surfaces with high emissivity values will lead to large quantities of radiative heat transfer [47]. Moreover, the properties of air evaluated in

the material selection above corresponds to a 1/2 inch (12.7 mm) vertical air space and an effective emittance of 0.05, which represents a surface similar to bright aluminum foil [45]. Building materials more commonly have an average emittance of 0.90, which reduces the insulating effectiveness of an air gap significantly. For example, from Table 3 in Chapter 26 of ASHRAE Fundamentals, a 1/2 inch (12.7 mm) vertical air space with an effective emittance of 0.05 has an R-value of 2.56 $h \cdot ft^2 \cdot °F/Btu$ (0.45 $m^2 \cdot K/W$) while the same air space with an effective emittance of 0.82 has an R-value of 0.91 $h \cdot ft^2 \cdot °F/Btu$ (0.16 $m^2 \cdot K/W$). This is a 64% reduction in R-value. Practically speaking, air gaps also require bordering layers to eliminate (or restrict) horizontal airflow. For these reasons, the final design will rely on the polystyrene insulation rather than air gaps. The final distribution of materials will depend on the total number of layers, which is discussed next.

6.5 NUMBER OF LAYERS

Since the overall wall thickness is set, materials have been selected, material proportions determined, and the general distribution of these materials has been identified, the final step is to predict the optimal number of layers to use. Based on the primary ICI configuration, 3-layers may be used, or it may be beneficial to pursue a 5-layer design. For simplicity and ease of installation, and without the use of pre-fabricated panels, a 3-layer design is likely advantageous. It may be unlikely that a larger number of layers will be feasible to install without the use of pre-fabricated panels, which are available from a number of different manufacturers with some layering options. However, if a 5-layer design is feasible, the designer may compare the two

configurations using the transmission matrix method or other building design tools, such as a load calculation program or a whole building energy model.

Another type of construction that accommodates the ICI layered configuration is the insulated concrete form (ICF), which has commonly been used at the basement or foundation level, but whose use is expanding to above-grade levels to encompass the entire building envelope (excluding doors, windows, etc.) [52].

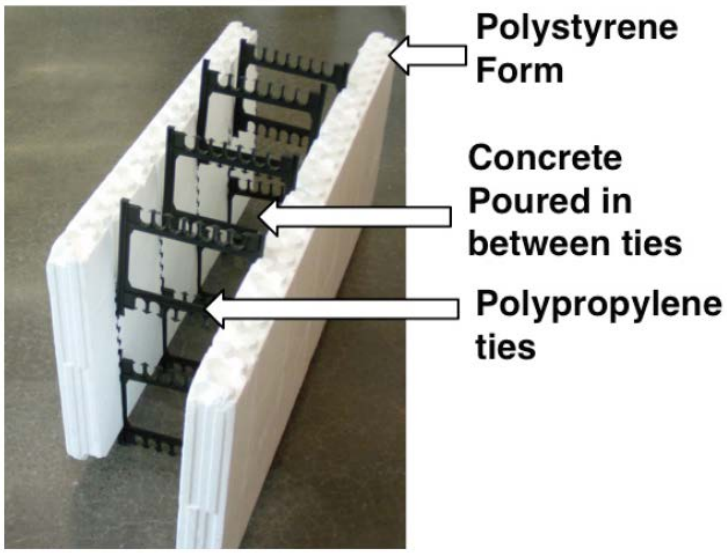

Figure 6.1 Insulated concrete form, as one section, without poured concrete. [53]

The costs and benefits of using an ICF construction method have been documented by the U.S. Department of Energy [54] and the U.S. Department of Housing and Urban Development [55]. The materials analysis conducted in Chapters 6.2 and 6.3 may be carried out for an ICF design in a similar manner by comparing different types of concrete and types of insulation that can double in purpose as concrete forms.

6.6 DESIGN SUMMARY

The overall design wall thickness is set to 5-1/2 inches (139.7 mm) between studs and 6 inches (152.7 mm) overall when an outer layer of siding with sheathing underneath and an inner layer of gypsum or plaster board are included. Brick, cement plaster, or materials with similar thermal properties are selected to pair with polystyrene insulation. Based on the optimal volumetric proportion of materials, the design should include roughly 50% insulation compared to other materials. With these design features in mind, three hypothetical walls are configured with 3, 5, and 7 layers, as shown in Table 13, Table 14, and Table 15, respectively.

Table 13. Wall design based on 3-layer ICI configuration.

	Material	**Thickness *(in)***
Outermost	*Aluminum, steel, or vinyl siding, over sheathing*	*0.25*
Insulation (I)	Polystyrene insulation	1.5
Thermal Mass (C)	Brick, cement plaster, or similar	2.5
Insulation (I)	Polystyrene insulation	1.5
Innermost	*Gypsum or plaster board*	*0.25*

Table 14. Wall design based on 5-layer ICI configuration.

	Material	**Thickness *(in)***
Outermost	*Aluminum, steel, or vinyl siding, over sheathing*	*0.25*
Insulation (I)	Polystyrene insulation	1
Thermal Mass (C)	Brick, cement plaster, or similar	1.25
Insulation (I)	Polystyrene insulation	1
Thermal Mass (C)	Brick, cement plaster, or similar	1.25
Insulation (I)	Polystyrene insulation	1
Innermost	*Gypsum or plaster board*	*0.25*

Table 15. Wall design based on 7-layer ICI configuration.

	Material	**Thickness *(in)***
Outermost	*Aluminum, steel, or vinyl siding, over sheathing*	*0.25*
Insulation (I)	Polystyrene insulation	0.75
Thermal Mass (C)	Brick, cement plaster, or similar	0.833
Insulation (I)	Polystyrene insulation	0.75
Thermal Mass (C)	Brick, cement plaster, or similar	0.833
Insulation (I)	Polystyrene insulation	0.75
Thermal Mass (C)	Brick, cement plaster, or similar	0.833
Insulation (I)	Polystyrene insulation	0.75
Innermost	*Gypsum or plaster board*	*0.25*

Each wall has 49.9% insulation compared to other materials and an overall R-value of 18.4 $h \cdot ft^2 \cdot °F/Btu$ (3.25 $m^2 \cdot K/W$). The resulting magnitude ratio for each wall (assuming h_{in} = 20 $W/m^2 \cdot K$) is M(3-layers) = 2.75e-03, M(5-layers) = 2.47e-03, and M(7-layers) = 2.85e-03, which shows a reduction between the 3- and 5-layer configurations and an increase with the 7-layer configuration.

According to the International Energy Conservation Code (IECC), Pittsburgh, PA is in climate zone 4-5 [56]. As a result, the recommended design for a mass wall is R-13, or R-17, when more than 50% of the insulation in the wall is located towards the inside surface. For a wood frame wall, the recommended R-value is 20, or alternatively, R-13 in the wall cavity with an additional R-5 in insulated sheathing.

Insulated sheathing can easily be added to any of these configurations to reach R-20. It is also possible to increase the overall R-value of the wall by using more insulation in the wall cavity than brick, cement plaster, or other thermally massive material. Roughly 60% insulation will increase the overall resistance to R-20, to satisfy the IECC recommendation.

While the analysis in Chapter 5 originally suggests that going above 60% insulation will hamper the transient response of the wall system, it is important to recognize that that analysis was based on a 278 mm thick wall. According to Figure 5.19 (c), for thinner walls, a higher percentage insulation is actually optimal. For a 140 mm wall, the optimal percentage insulation is about 65 or 66%. To fully understand the implications of reducing thermal mass for insulation, the wall designs should be evaluated further using the transmission matrix method, a load calculation, or a full building simulation.

The transmission matrix method is used here to obtain magnitude ratios for various iterations of the 140 mm design walls using the materials and configurations in Table 13, Table 14, and Table 15 and explore this trade-off further.

Table 16. Magnitude ratio of 3, 5, and 7 layer design walls at five different proportions of insulation.

Magnitude Ratio	Percentage Insulation (%)				
	30	40	50	60	70
3-Layer ICI	5.14×10^{-3}	3.65×10^{-3}	2.93×10^{-3}	2.61×10^{-3}	2.58×10^{-3}
5-Layer ICI	4.89×10^{-3}	3.30×10^{-3}	2.61×10^{-3}	2.40×10^{-3}	2.53×10^{-3}
7-Layer ICI	5.61×10^{-3}	3.79×10^{-3}	3.02×10^{-3}	2.78×10^{-3}	7.92×10^{-4}
R-value	9.9	12.9	15.8	18.7	21.7

Table 17. Difference in magnitude ratio of 3, 5, and 7 layer design walls deviating from 50% insulation.

Difference in Magnitude Ratio	Percentage Insulation (%)				
	30	40	50	60	70
3-Layer ICI	75%	24%	-	-11%	-12%
5-Layer ICI	87%	26%	-	-8%	-3%
7-Layer ICI	86%	26%	-	-8%	-74%
R-value	-37%	-19%	-	19%	37%

In Table 16, the magnitude ratio and R-value for each wall is shown for five different proportions of insulation ranging from 30 to 70% insulation. The differences between 50% insulation and either increasing or decreasing proportions are shown in Table 17 for magnitude ratio and R-value. For example, the magnitude ratio of the 5-layer wall is reduced by 8% going from 50 to 60% insulation, representing an improvement in both transient (M) and static (R-value) performance. In this case, the design trade-off with increasing the percentage of insulation in a multi-layer wall occurs between 60 and 70% insulation, and the best design using the selected materials is the 5-layer configuration with about 60-66% insulation. This demonstrates the limitations of using the simplified, albeit expedited, surrogate methods developed in Chapter 5.2 and the benefits of using the transmission matrix method to evaluate multiple variations.

Ultimately, if a conflict exists between minimizing magnitude ratio and satisfying R-value requirements, then the decision will depend on the location of the building and the corresponding climate. In particular, if the average annual temperature is close to the interior temperature setpoint, the magnitude ratio is the more important design criterion. As the average annual temperature deviates more from the interior temperature setpoint, the R-value becomes the more important design criterion. This is likely the case where R-value requirements are strict and recommended values are widely accepted. Then, if the overall wall thickness is restricted, it will be necessary to increase insulation in the wall regardless of how it affects the wall system's transient response. This concept will be explored further in Chapter 7.

In general, designing for both magnitude ratio and R-value are not mutually exclusive. This simple case study demonstrates the ease and quickness of employing the tools and guidelines from Chapter 5 to implement a multi-layer wall design for improved transient performance over the typical wood frame construction that relies on insulation alone. This design

process is easily reproducible for other climate regions and any set of materials or overall wall thickness. Trade-offs between cost and performance can supplement the design guide presented here. In Chapter 7, an energy modeling procedure will attempt to compare different wall configurations, such as those discussed here and described in previous chapters, and to quantify the energy saving potential of a multi-layer design.

7.0 ESTIMATING ENERGY SAVINGS OF OPTIMIZED MULTI-LAYER WALLS

The primary objective of this chapter is to evaluate the relative performance of optimal and conventional multi-layer wall configurations in a building application. To assess energy saving potential, a time-domain analysis is carried out to determine the inside surface temperature variation due to ambient temperature fluctuations and one-dimensional conduction through multiple layers. This temperature difference is used to calculate heat flux for each hour of a year. Then, heat flux is converted to an energy per unit area measure/metric and summed over each hour to estimate annual performance. This method, described in more detail in Chapter 7.1.3, is not meant to be a highly accurate prediction of actual energy transfer or heating and cooling loads. Rather, it will help quantify how much better an optimized multi-layer wall might perform over non-optimized and traditional designs.

7.1 METHODOLOGY

This analysis begins with the selection of input signals for testing the various designs. Through Chapter 6, analysis has been based on using sinusoidal or harmonic inputs to a multi-layer wall system where each system is modeled as a high-order low-pass filter. For this analysis, real sampled temperature data is selected from representative climate locations. Ambient dry-bulb temperature data is available as .tmy3 weather data from the National Renewable Energy

Laboratory (NREL) for numerous locations [57]. It is shown in Appendix B that these data sets exhibit two dominant frequencies, those corresponding to one day (ω_{day}) and to one year (ω_{year}). This work has been based on optimizing multi-layer walls at a frequency corresponding to one day (ω_{day}).

Class I weather data (that with the lowest uncertainty) is used when available for each location. A map of the continental United States that is color-coded and labeled by climate zone is shown in Figure 7.1. Locations from each climate zone are selected as representative data sets for analysis in this chapter.

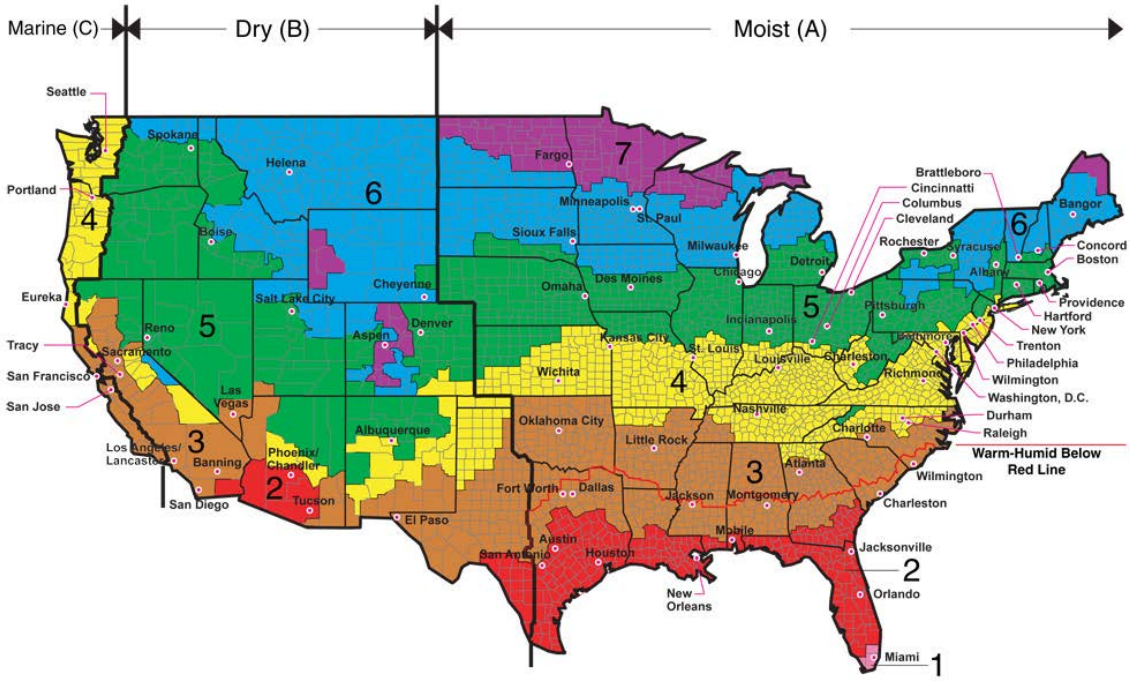

Figure 7.1 Climate zone map of the continental United States [58].

The various designs to be tested include those from Chapter 6 as well as four other insulation-concrete configurations, a standard wood frame wall, and an idealized wall

represented by a digital filter. In total, eight wall configurations, plus the "best case" digital filter will be compared.

7.1.1 Digital Filter

The "best case" is that in which the magnitude ratio (decrement factor) is minimized for a sinusoidal input with a 24 hour period. In this case, based on dry-bulb temperature data, the 24 hour frequency and other non-dominant frequencies are completely filtered out, so that only the annual (8760 hour) frequency remains. This is accomplished by implementing a digital low-pass filter and illustrated in Figure 7.2 and Figure 7.3, where the input and output to the digital filter are shown for two data sets.

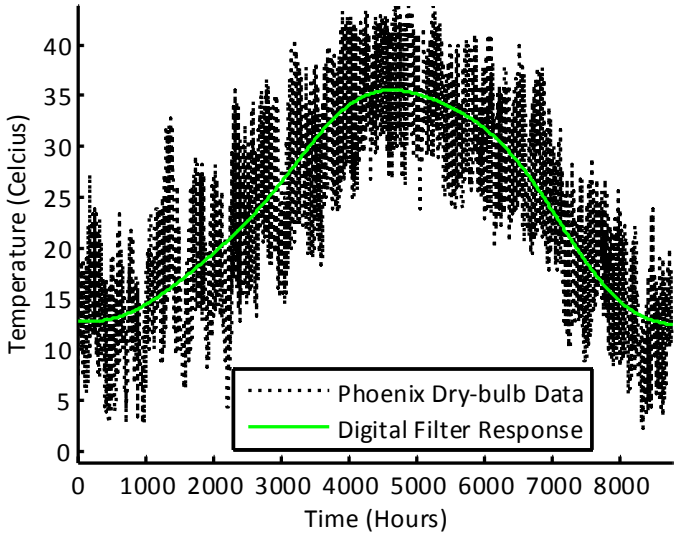

Figure 7.2 Digital filter response to dry-bulb temperature data from Phoenix, AZ (climate zone 2).

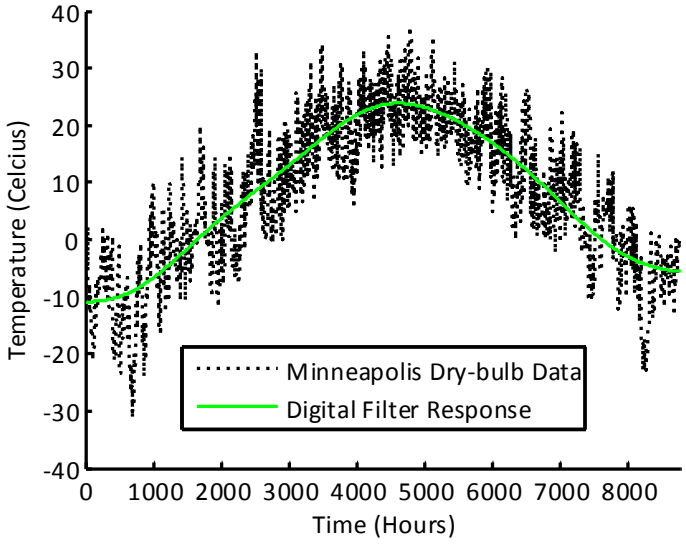

Figure 7.3 Digital filter response to dry-bulb temperature data from Minneapolis, MN (climate zone 6).

The digital implementation is created in Matlab as a ninth-order lowpass Chebyshev Type II filter. It has a stopband attenuation of 40 dB and a stopband edge frequency of 1.39×10^{-7} Hz with a normalized value of 0.001 to accomplish complete filtering of all non-annual temperature variations. This ultimately provides a benchmark against which other configurations may be evaluated.

7.1.2 Test Walls

In total, eight wall configurations are tested. The 3-, 5-, and 7-layer ICI walls described in Chapter 6 are tested here along with five others, shown in the tables that follow. Each wall includes a $^1/_4$ inch wood siding layer at the outermost layer and $^1/_4$ inch layer of gypsum or plasterboard at the innermost layer. Thermal properties from Table 10 are used with the addition of plywood siding (k = 0.10 W/m·K, ρ = 450 kg/m^3, and C_p = 1.88 kJ/kg·K). The average of the

brick and cement plaster properties are used to represent the thermally massive layers (k = 0.81 W/m·K, ρ = 1890 kg/m^3, and C_p = 0.82 kJ/kg·K).

Table 18. Standard wood frame wall with outer layers of siding and gypsum or plasterboard.

	Material	**Thickness *(in)***
Outermost	*Aluminum, steel, or vinyl siding, over sheathing*	*0.25*
Insulation (I)	Polystyrene insulation	3.0625
Innermost	*Gypsum or plasterboard*	*0.25*

Table 19. CI wall configuration with outer layers of siding and gypsum or plasterboard.

	Material	**Thickness *(in)***
Outermost	*Aluminum, steel, or vinyl siding, over sheathing*	*0.25*
Thermal Mass (C)	Brick, cement plaster, or similar	2.5
Insulation (I)	Polystyrene insulation	3.0
Innermost	*Gypsum or plaster board*	*0.25*

Table 20. IC wall configuration with outer layers of siding and gypsum or plasterboard.

	Material	**Thickness *(in)***
Outermost	*Aluminum, steel, or vinyl siding, over sheathing*	*0.25*
Insulation (I)	Polystyrene insulation	3.0
Thermal Mass (C)	Brick, cement plaster, or similar	2.5
Innermost	*Gypsum or plaster board*	*0.25*

Table 21. CIC wall configuration with outer layers of siding and gypsum or plasterboard.

	Material	**Thickness *(in)***
Outermost	*Aluminum, steel, or vinyl siding, over sheathing*	*0.25*
Thermal Mass (C)	Brick, cement plaster, or similar	1.25
Insulation (I)	Polystyrene insulation	3.0
Thermal Mass (C)	Brick, cement plaster, or similar	1.25

Table 21 (continued).

Innermost	*Gypsum or plaster board*	*0.25*

The standard wood frame wall in Table 18 is approximately 3.6 inches wide with 85.7% insulation and an R-value of 18.4 $h \cdot ft^2 \cdot °F/$ Btu (3.25 $m^2 \cdot K/W$). All other walls have the same R-value except the air-copper combination, whose basic configuration is illustrated in Table 22.

Table 22. Basic AUA wall configuration, 25 total layers not shown.

	Material	**Thickness *(in)***
Outermost	*Aluminum, steel, or vinyl siding, over sheathing*	*0.25*
Air gap (A)	Air	0.25
Copper (U)	Copper	0.25
Air gap (A)	Air	0.25
…	…	…
Innermost	*Gypsum or plaster board*	*0.25*

The R-value of this wall is approximately 18.2 $h \cdot ft^2 \cdot °F/$ Btu (3.21 $m^2 \cdot K/W$) with 48% air compared to copper. All of the insulation-concrete walls have 49.9% insulation, as in Chapter 6.

Given that each of the eight walls has the same overall thermal resistance, any differences in energy transfer for the same input can be attributed to the material combination and distribution, including number of layers. By simulating real temperature data, a link may be established between magnitude ratio performance (the focus of the optimization procedure in Chapter 5 and the design guidelines in Chapter 6) and energy saving potential. The method used to simulate each wall is the same.

7.1.3 Simulation Method

The transmission matrix method is used to model each wall and obtain its corresponding transfer function. The linear simulation function (*lsim*), part of Matlab's Control System Toolbox, is used to simulate the time domain response of each multi-layer wall to the dry-bulb temperature data for each climate location. The temperature data set includes hourly samples for one year (8760 hours), so the system transfer function is modeled in hourly units.

While an inside convection coefficient value of h_{in} = 20 W/m^2·K has been used to analyze frequency response at ω_{day} in Chapters 5 and 6, the non-zero coefficient results in an unrealistic response at the frequency corresponding to one year (ω_{year}). Since the annual temperature swing occurs over days and months, and the time constant of any of these roughly 6-inch walls is on the order of hours, the magnitude ratio of each wall should approach 1 for ω_{year} or other low frequencies. However, this only occurs for very small (on the order of 1x10^{-2} W/m^2·K) values of h_{in} with the transmission matrix methodology used. As a result, it was necessary to approximate h_{in} as zero in order to simulate the response to annual temperature variations on a realistic scale. By assuming no inside convection, or a perfectly insulated inside boundary condition, the inside surface temperature is allowed to float as a result of the outside temperature input.

When a non-zero inside convection coefficient is included, the representative circuit was shown in Figure 3.1 where the resistance $R_{h,rm}$ connects the inner-most surface temperature node to ground. This representation makes the room equivalent to the circuit reference temperature. So, in effect, the room air temperature is isothermally fixed at 0 °C. The room is then essentially an infinite sink to which heat energy may be transferred without limit.

In this case, the larger h_{in} becomes, the more heat transfer occurs from the inside wall surface to this infinite sink. As a result, the inside surface temperature is constantly being "cooled", shedding energy into the room, and approaching the lower thermal potential (e.g. 0 °C). That is, the inside surface temperature approaches that of the infinite sink, namely zero. In turn, the ratio between inside and outside fluctuations approaches zero (e.g. $T_{s,rm}/T_{s,amb} \rightarrow 0$ as $T_{s,rm} \rightarrow 0$).

This is illustrated in Figure 7.4 to show the difference in frequency response with variations of inside convection coefficient (h_{in}) values. Specifically, Figure 7.4 shows four Bode diagrams (magnitude ratio versus frequency) for the ICI wall described in Table 13. Three vertical lines demarcate the frequencies corresponding to 2 hours, 24 hours, and 1 year (8760 hours).

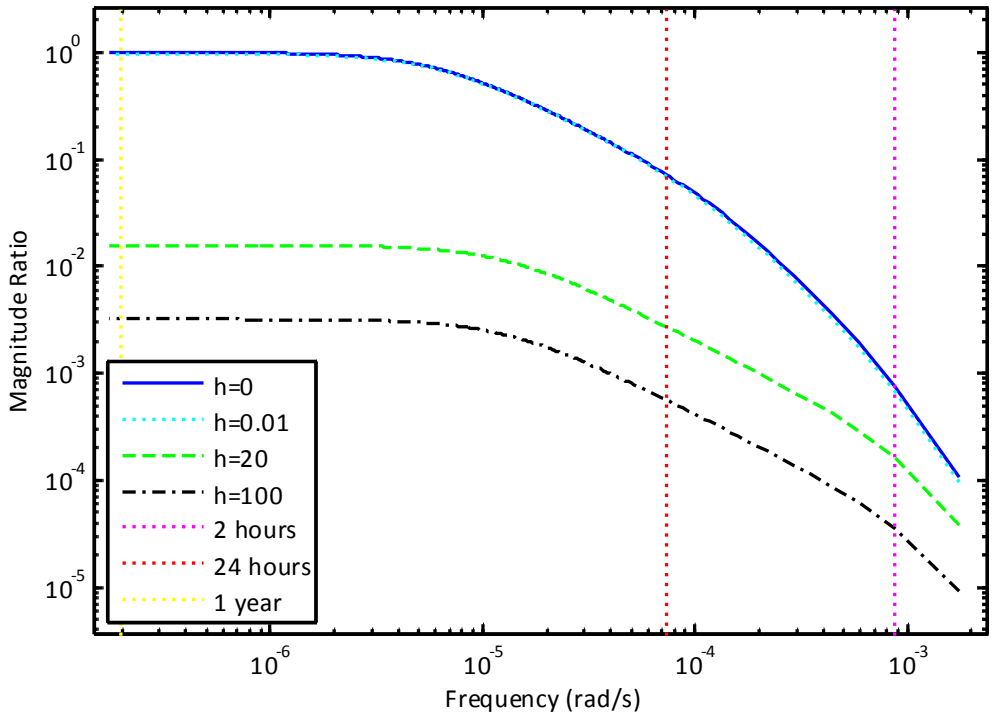

Figure 7.4 Bode diagrams for ICI wall including outer layers of siding and gypsum/plasterboard.

One curve is shown for each of four h_{in} values ranging from 0 to 100. The magnitude ratio decreases as h_{in} values increase. Using a non-zero inside convection coefficient creates an offset in the frequency response. The offset increases with increasing h_{in} values, so the magnitude ratio at very low frequencies is not unity. However, regardless of the h_{in} value, the magnitude ratio is lower for higher frequencies (such as that corresponding to 2 hours) than lower frequencies (such as ω_{day} and ω_{year}).

Mathematically, the transfer function relating $T_{s,rm}$ to $T_{s,amb}$ and including R_h was presented in Equation (3.20), where $R_h = 1/h_{in}$. When h_{in} is zero, the transfer function reduces to one over the fourth element of the transmission matrix, which directly relates $T_{s,rm}$ to $T_{s,amb}$. This case also assumes no heat flux at the inner-most temperature node, which represents a perfectly insulated inside boundary condition. When h_{in} is non-zero, the transfer function includes terms for both temperature ($T_{s,rm}$ due to $T_{s,amb}$) and heat flux ($q"_{s,rm}$ due to $T_{s,amb}$). At low frequencies, such as ω_{year}, the circuit becomes purely resistive, because the impedances of the capacitive elements become zero at low frequencies, or long time scales. Then, temperatures in the wall are at steady state (or quasi steady state), and heat flux at the inner-most surface due to temperature changes at the outermost surface dominates. Thus, the assumption that the room air temperature is isothermally 0 °C is only valid at a shorter time scale, where the transient solution is relevant. Since the simulation evaluates both short and long time scales, it was necessary to assume $h_{in} = 0$ for all time steps. To reiterate, this represents a perfectly insulated inside boundary condition and allows the inside surface temperature to change as a result of the outside temperature input alone.

Two full years are simulated and the outputs from the second year are analyzed (the response to initial conditions is no longer apparent after fewer than 36 hours in some cases, but

the simulation is fast enough that it is just as easy to simulate two full years). After the interior surface temperature is determined for each hour, it is compared to a fixed setpoint temperature to determine hourly temperature differences. The temperature difference across the wall ultimately leads to heating and cooling loads, so the calculation distinguishes between heating and cooling loads by using two setpoint temperatures. The latest thermostat recommendations from the U.S. Energy Department suggest using a heating setpoint of 68 °F (20 °C) and a cooling setpoint of 78 °F (25.6 °C), which leaves a 10 °F range in which no conditioning would be required [59].

Once hourly temperature differences are calculated, they are used to develop a measure of energy transfer and a representation of potential air conditioning loads. Although it was necessary to assume h_{in} as zero for the simulation procedure, the assumption about inside convection is modified in order to form an energy-based metric. The total annual heating, cooling, and combined heat flux is calculated for each wall, by summing over each hour of the year and assuming that h_{in} = 1 W/m^2·K for $q'' = h_{in} \cdot \Delta T$ (W/m^2). Then, the total is converted to energy flux (kWh/m^2). The heat or energy flux ultimately determines energy performance based on specific building dimensions. Therefore, it is used here to compare the energy performance of the different wall configurations, without loss of generality.

Since this model is somewhat restricted in scope, it cannot accurately predict actual energy consumption for a building, but comparing energy flux values does provide an indication of relative performance. As in even the most sophisticated whole building simulation programs, the results here are an indication of which designs are expected to perform better than others, rather than to provide an accurate prediction of complex heat transfer phenomena. That being said, a sophisticated whole building simulation will be much closer to the actual building

performance than more simplified simulations (those that use more simplifying assumptions, in number and/or in scope).

7.2 INITIAL SIMULATION RESULTS

The initial simulation shows that the climate zone has a significant impact on performance. This is shown in Table 23 for six locations representing the six different climate zones in the United States. The rows in this table are shaded from highest energy flux with darkest shading to the lowest with no shading at all.

Table 23. Combined heating and cooling energy flux (kWh/m^2) for simulated walls including extra outer layers (siding and gypsum or plasterboard) and assuming the inside convection coefficient (h_{in}) is zero.

Climate Location (Zone)	Standard Wood Frame	CI	CIC	IC	3-ICI	5-ICI	7-ICI	AUA	Digital Filter
Miami, FL (1)	12.9	12.5	10.0	9.3	10.1	10.1	10.2	9.2	8.1
Phoenix, AZ (2)	47.4	46.8	44.6	43.9	44.6	44.7	44.7	43.8	42.7
Bakersfield, CA (3)	44.2	43.2	39.5	38.6	39.5	39.5	39.6	38.5	37.0
Sterling, VA (4)	76.3	75.8	72.9	72.4	72.9	73.0	73.0	72.4	71.6
Pittsburgh, PA (5)	90.0	89.7	88.0	87.5	88.0	88.1	88.1	87.5	86.5
Minneapolis, MN (6)	115.6	115.2	113.1	112.6	113.1	113.2	113.2	112.5	111.1

The location with the mean ambient dry-bulb temperature (°C) closest to the setpoint band (between heating and cooling temperatures) results in the lowest heat flux. This is Miami, FL (climate zone 1) with T_{mean} = 24.5 °C, whereas the opposite is true for Minneapolis, MN

(climate zone 6) with T_{mean} = 7.73 °C. This is expected, since the outside temperature is driving the inside surface temperature, and a smaller difference between the inside surface temperature and the setpoint temperatures results in lower heat flux. This is illustrated in Figure 7.5 for four climate locations.

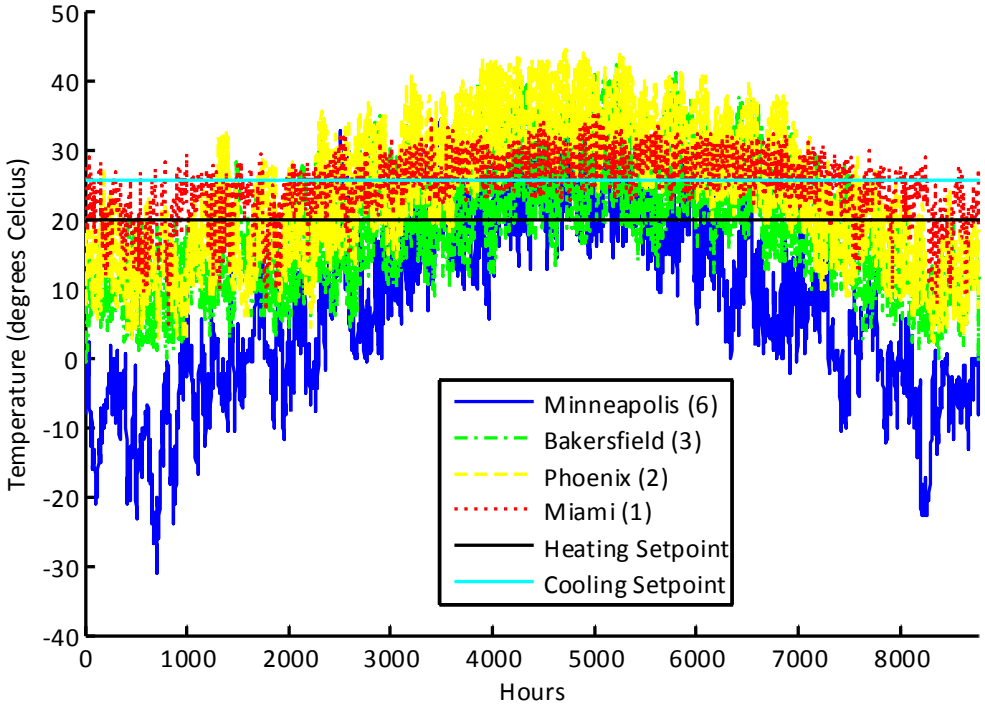

Figure 7.5 Annual dry-bulb temperature data for four climates shown with interior setpoints (°C).

From Table 23, there are three key results. First, there is a decrease in energy flux between the Standard Wood Frame wall and all other walls, with the Digital Filter producing the lowest energy flux values for all climate zones. So, even the non-optimized multilayer walls, such as the two-layer CI configuration, yield lower annual energy flux than the traditional design.

Second, the percent difference between the simulated wall responses and the digital filter response depends on climate zone. The difference in predicted energy flux between each of the eight simulated walls and the digital filter is calculated for each of the six climate zones. The average of the differences between each wall and the digital filter is reported in Table 24 as a percentage for each representative climate.

Table 24. Average, for six representative climates, of the differences in predicted energy flux between each wall and the digital filter.

Climate Location (Zone)	Average Difference between Wall and Filter Responses
Miami, FL (1)	22.6%
Phoenix, AZ (2)	5.2%
Bakersfield, CA (3)	8.0%
Sterling, VA (4)	2.7%
Pittsburgh, PA (5)	2.1%
Minneapolis, MN (6)	2.2%

Because energy flux is an indication of energy consumption, the greatest energy saving potential occurs in climate zones 1 and 3. Climate zones 5 and 6 show the lowest predicted energy saving potential from replacing a Standard Wood Frame wall with an ideal filter.

Finally, both the IC and AUA walls (highlighted in red text in Table 23) outperform all others in every climate zone with the AUA configuration resulting in the lowest energy flux in climate zones 1, 2, 3 and 6. Based on Chapters 5 and 6, it is unexpected that the IC wall results in lower energy flux than the ICI walls, which have been shown to have lower magnitude ratios at the 24-hour frequency (ω_{day}).

Specifically, analysis from Chapter 5 indicated that ICI would be the best configuration based on it having the lowest magnitude ratio for the same thermal resistance and capacitance.

However, this analysis was based on the frequency response to a harmonic input at a specific frequency (ω_{day}) rather than actual temperature data. It also used only insulating and massive materials without any extra surface layers and a non-zero inside convection coefficient (h_{in}). These three differences are explored for their effects on the multi-layer wall energy flux simulation results.

7.3 ADDITIONAL ANALYSIS

First, the same eight walls (with outer layers of siding and gypsum/plasterboard) are simulated with pure harmonic inputs rather than actual temperature data. Actual temperature data resulted in minimums for IC and AUA walls; whereas, previous analysis based on frequency response to a harmonic input resulted in minimum values for ICI walls. If the simulation results in minimum values for ICI walls when a harmonic input is used, then the indication is that the non-harmonic nature of the temperature data input accounts for the unexpected IC and AUA results. The key difference would be in the harmonic or non-harmonic nature of the input signal and the configuration(s) yielding minimum energy flux. The harmonic inputs are estimated from each temperature data set, so the actual energy flux results are not necessarily comparable between the harmonic estimate and actual temperature inputs.

Each harmonic input corresponds to the six representative climate locations listed in Table 23. The input for each location is a two component sine wave with a one day (24 hour) and a one year (8760 hour) period. The mean annual temperature is determined from the dry-bulb temperature data, which is also used to estimate the daily and annual temperature swings. Results

from simulating the eight walls with the two-component sine waves are shown in Table 25 in terms of combined energy flux (kWh/m^2).

Table 25. Combined heating and cooling energy flux (kWh/m^2) from walls simulated with two-component sine wave inputs. Walls include extra outer layers (siding and gypsum or plasterboard), and the simulation assumes inside convection coefficient (h_{in}) is zero.

Climate Location (Zone)	Standard Wood Frame	CI	CIC	IC	3-ICI	5-ICI	7-ICI	AUA
Miami, FL (1)	100.4	98.8	95.8	95.9	95.8	95.8	95.8	96.3
Phoenix, AZ (2)	180.5	179.2	177.0	177.0	177.0	177.1	177.1	177.4
Bakersfield, CA (3)	402.4	401.9	401.3	401.1	401.3	401.3	401.4	401.3
Sterling, VA (4)	274.2	272.9	270.6	270.6	270.6	270.6	270.6	270.8
Pittsburgh, PA (5)	278.3	277.4	275.9	275.8	275.9	275.9	275.9	275.9
Minneapolis, MN (6)	352.0	351.3	349.9	349.7	349.9	350.0	350.0	349.7

The difference in values between Table 23 and Table 25 is due to the fact that the two-component sine wave is a poor representation of the actual temperature data. However, the point of this analysis in not to compare actual energy flux values. Instead, the objective is to consider the overall trends among the different walls and climates. Among climates, the lowest energy flux occurs for walls in climate zone 1 and the highest energy flux results from simulations in climate zone 6.

The lowest energy flux for each location in Table 25 is highlighted in red text, which shows mixed results in climate zones 1, 2, and 4. The IC configuration is best in three out of six locations. Minneapolis, MN has energy flux results minimized by the IC and AUA configurations, the same as in Table 23. In general, the response to harmonic inputs shown in Table 25 do not show lower energy flux for ICI wall configurations, which would have been expected based on the analysis in Chapter 5. Rather, IC as well as ICI, CIC, and AUA

configurations appear to do best depending on climate zone. While there are differences between the response to real, non-harmonic data (Table 23) and harmonic inputs (Table 25), those differences do not offer a clear explanation for the discrepancy between the analysis in Chapter 5 favoring ICI configurations and the results in Table 23 for which IC and AUA are best.

Next, the eight walls are re-evaluated using only the primary insulating and massive materials without any extra surface layers. Specifically, the siding and gypsum/plasterboard are removed from the inner and outermost surfaces, so the remaining insulation/thermal mass configuration is the same, but the overall R-value is reduced slightly. These revised configurations are simulated, and the combined energy flux results are shown in Table 26.

Table 26. Combined heating and cooling energy flux (kWh/m^2) for simulated walls *without* extra outer layers (siding and gypsum or plasterboard) and assuming the inside convection coefficient (h_{in}) is zero.

Climate Location (Zone)	Standard Wood Frame	CI	CIC	IC	3-ICI	5-ICI	7-ICI	AUA
Miami, FL (1)	14.6	14.4	10.2	9.4	10.2	10.3	10.3	9.3
Phoenix, AZ (2)	50.3	50.0	44.7	44.0	44.7	44.8	44.8	43.9
Bakersfield, CA (3)	48.8	48.4	39.6	38.7	39.6	39.7	39.7	38.6
Sterling, VA (4)	79.1	78.8	73.1	72.5	73.1	73.1	73.2	72.4
Pittsburgh, PA (5)	91.9	91.7	88.1	87.6	88.1	88.2	88.2	87.5
Minneapolis, MN (6)	117.2	117.0	113.2	112.6	113.2	113.3	113.3	112.6

Again, the walls resulting in the lowest energy flux for a given climate are highlighted in red text. For every climate, as in Table 23, the IC and AUA configurations are the best, with AUA slightly better in every climate except Minneapolis. These results favor the IC over the ICI

configurations. This indicates that the inclusion of the extra outer layers does not account for the difference between predictions in Chapter 5, based on magnitude ratio, and the simulated energy flux results.

The third consideration to explore is the difference in the inside convection coefficient (h_{in}) values used. In Chapter 5, the inside convection coefficient was selected to be within a realistic range of expected values. So, h_{in} = 20 W/m^2·K was used when validating the transmission matrix method against a finite volume solution and then in subsequent calculations and analysis. Assuming an inside convection coefficient of zero for simulations was necessary to achieve realistic performance at a frequency of one year (described in Chapter 7.1.3). This is illustrated as values of h_{in} from 0 to 1000 W/m^2·K are now considered.

The magnitude ratio is calculated for each of the eight walls, first including the extra outer layers of siding and gypsum/plasterboard and displayed in Table 27 and Table 28 and then without these extra layers and displayed in Table 29 and Table 30. The first of each of the two sets of tables corresponds to a frequency of one day and the second to a frequency of one year. In Table 27 and Table 29, the two lowest values for each row are highlighted in red text. There is little difference among the different walls at the time scale of one year, as shown in Table 28 and Table 30.

Table 27. Magnitude ratio at ω_{day} for seven walls including outer layers of siding and gypsum or plasterboard for a range of inside convection coefficient values.

h_{in}	Standard Wood Frame	CI	CIC	IC	3-ICI	5-ICI	7-ICI	AUA
0	5.90×10^{-1}	4.84×10^{-1}	7.77×10^{-2}	4.32×10^{-2}	7.23×10^{-2}	4.92×10^{-2}	4.88×10^{-2}	8.44×10^{-3}
0.001	5.50×10^{-1}	4.33×10^{-2}	7.89×10^{-2}	4.87×10^{-1}	7.06×10^{-2}	4.88×10^{-2}	4.87×10^{-2}	8.64×10^{-3}
0.01	5.45×10^{-1}	4.32×10^{-2}	7.89×10^{-2}	4.83×10^{-1}	7.00×10^{-2}	4.85×10^{-2}	4.84×10^{-2}	8.61×10^{-3}
0.1	4.97×10^{-1}	4.29×10^{-2}	7.82×10^{-2}	4.41×10^{-1}	6.41×10^{-2}	4.52×10^{-2}	4.57×10^{-2}	8.32×10^{-3}

Table 27 (continued).

1	2.27×10^{-1}	3.93×10^{-2}	7.05×10^{-2}	2.01×10^{-1}	3.31×10^{-2}	2.63×10^{-2}	2.83×10^{-2}	6.10×10^{-3}
5	6.00×10^{-2}	2.70×10^{-2}	4.14×10^{-2}	5.34×10^{-2}	1.00×10^{-2}	8.74×10^{-3}	9.93×10^{-3}	2.63×10^{-3}
10	3.10×10^{-2}	1.85×10^{-2}	2.53×10^{-2}	2.76×10^{-2}	5.33×10^{-3}	4.73×10^{-3}	5.44×10^{-3}	1.52×10^{-3}
20	1.58×10^{-2}	1.11×10^{-2}	1.39×10^{-2}	1.41×10^{-2}	2.75×10^{-3}	2.47×10^{-3}	2.85×10^{-3}	8.20×10^{-4}
100	3.20×10^{-3}	2.57×10^{-3}	2.96×10^{-3}	2.85×10^{-3}	5.64×10^{-4}	5.11×10^{-4}	5.93×10^{-4}	1.75×10^{-4}
1000	3.21×10^{-4}	2.65×10^{-4}	3.00×10^{-4}	2.85×10^{-4}	5.67×10^{-5}	5.15×10^{-5}	5.99×10^{-5}	1.77×10^{-5}

Table 28. Magnitude ratio at ω_{year} for seven walls including outer layers of siding and gypsum or plasterboard for a range of inside convection coefficient values.

h_{in}	Standard Wood Frame	CI	CIC	IC	3-ICI	5-ICI	7-ICI	AUA
0	1.00	1.00	9.99×10^{-1}	9.98×10^{-1}	9.99×10^{-1}	1.00	1.00	9.98×10^{-1}
0.001	9.97×10^{-1}	9.95×10^{-1}	9.96×10^{-1}	9.97×10^{-1}	9.96×10^{-1}	9.96×10^{-1}	9.96×10^{-1}	9.95×10^{-1}
0.01	9.70×10^{-1}	9.68×10^{-1}	9.69×10^{-1}	9.70×10^{-1}	9.69×10^{-1}	9.69×10^{-1}	9.69×10^{-1}	9.68×10^{-1}
0.1	7.63×10^{-1}	7.62×10^{-1}	7.62×10^{-1}	7.62×10^{-1}	7.62×10^{-1}	7.62×10^{-1}	7.62×10^{-1}	7.64×10^{-1}
1	2.44×10^{-1}	2.43×10^{-1}	2.43×10^{-1}	2.43×10^{-1}	2.43×10^{-1}	2.43×10^{-1}	2.43×10^{-1}	2.46×10^{-1}
5	6.06×10^{-2}	6.03×10^{-2}	6.03×10^{-2}	6.03×10^{-2}	6.03×10^{-2}	6.03×10^{-2}	6.03×10^{-2}	6.11×10^{-2}
10	3.13×10^{-2}	3.11×10^{-2}	3.11×10^{-2}	3.11×10^{-2}	3.11×10^{-2}	3.11×10^{-2}	3.11×10^{-2}	3.15×10^{-2}
20	1.59×10^{-2}	1.58×10^{-2}	1.58×10^{-2}	1.58×10^{-2}	1.58×10^{-2}	1.58×10^{-2}	1.58×10^{-2}	1.60×10^{-2}
100	3.22×10^{-3}	3.20×10^{-3}	3.20×10^{-3}	3.20×10^{-3}	3.20×10^{-3}	3.20×10^{-3}	3.20×10^{-3}	3.24×10^{-3}
1000	3.23×10^{-4}	3.21×10^{-4}	3.21×10^{-4}	3.21×10^{-4}	3.21×10^{-4}	3.21×10^{-4}	3.21×10^{-4}	3.25×10^{-4}

Table 29. Magnitude ratio at ω_{day} for seven walls ***without*** extra outer layers for a range of inside convection coefficient values.

h_{in}	Standard Wood Frame	CI	CIC	IC	3-ICI	5-ICI	7-ICI	AUA
0	9.49×10^{-1}	9.20×10^{-1}	9.04×10^{-2}	4.64×10^{-2}	9.05×10^{-2}	6.01×10^{-2}	6.01×10^{-2}	1.04×10^{-2}
0.001	9.46×10^{-1}	4.64×10^{-2}	9.04×10^{-2}	9.17×10^{-1}	9.03×10^{-2}	6.01×10^{-2}	6.00×10^{-2}	1.04×10^{-2}
0.01	9.23×10^{-1}	4.63×10^{-2}	9.04×10^{-2}	8.95×10^{-1}	8.91×10^{-2}	5.95×10^{-2}	5.96×10^{-2}	1.03×10^{-2}
0.1	7.43×10^{-1}	4.62×10^{-2}	9.01×10^{-2}	7.20×10^{-1}	7.88×10^{-2}	5.45×10^{-2}	5.54×10^{-2}	9.95×10^{-3}
1	2.48×10^{-1}	4.44×10^{-2}	8.41×10^{-2}	2.40×10^{-1}	3.65×10^{-2}	2.94×10^{-2}	3.22×10^{-2}	7.21×10^{-3}
5	6.23×10^{-2}	3.40×10^{-2}	4.99×10^{-2}	6.03×10^{-2}	1.07×10^{-2}	9.58×10^{-3}	1.10×10^{-2}	3.11×10^{-3}
10	3.22×10^{-2}	2.40×10^{-2}	2.96×10^{-2}	3.12×10^{-2}	5.70×10^{-3}	5.19×10^{-3}	6.04×10^{-3}	1.80×10^{-3}
20	1.64×10^{-2}	1.42×10^{-2}	1.58×10^{-2}	1.58×10^{-2}	2.94×10^{-3}	2.71×10^{-3}	3.17×10^{-3}	9.76×10^{-4}
100	3.32×10^{-3}	3.16×10^{-3}	3.28×10^{-3}	3.21×10^{-3}	6.04×10^{-4}	5.61×10^{-4}	6.60×10^{-4}	2.09×10^{-4}

Table 29 (continued).

1000	3.33×10^{-4}	3.21×10^{-4}	3.29×10^{-4}	3.22×10^{-4}	6.07×10^{-5}	5.66×10^{-5}	6.66×10^{-5}	2.12×10^{-5}

Table 30. Magnitude ratio at ω_{year} for seven walls *without* extra outer layers for a range of inside convection coefficient values.

h_{in}	Standard Wood Frame	CI	CIC	IC	3-ICI	5-ICI	7-ICI	AUA
0	1.00	1.00	1.00	9.98×10^{-1}	1.00	1.00	1.00	9.98×10^{-1}
0.001	9.97×10^{-1}	9.95×10^{-1}	9.97×10^{-1}	9.97×10^{-1}	9.97×10^{-1}	9.97×10^{-1}	9.97×10^{-1}	9.95×10^{-1}
0.01	9.71×10^{-1}	9.69×10^{-1}	9.70×10^{-1}	9.71×10^{-1}	9.70×10^{-1}	9.70×10^{-1}	9.70×10^{-1}	9.70×10^{-1}
0.1	7.70×10^{-1}	7.68×10^{-1}	7.68×10^{-1}	7.69×10^{-1}	7.68×10^{-1}	7.68×10^{-1}	7.68×10^{-1}	7.70×10^{-1}
1	2.50×10^{-1}	2.49×10^{-1}	2.49×10^{-1}	2.49×10^{-1}	2.49×10^{-1}	2.49×10^{-1}	2.49×10^{-1}	2.52×10^{-1}
5	6.26×10^{-2}	6.23×10^{-2}	6.23×10^{-2}	6.23×10^{-2}	6.23×10^{-2}	6.23×10^{-2}	6.23×10^{-2}	6.32×10^{-2}
10	3.23×10^{-2}	3.22×10^{-2}	3.22×10^{-2}	3.22×10^{-2}	3.22×10^{-2}	3.22×10^{-2}	3.22×10^{-2}	3.26×10^{-2}
20	1.64×10^{-2}	1.63×10^{-2}	1.63×10^{-2}	1.63×10^{-2}	1.63×10^{-2}	1.63×10^{-2}	1.63×10^{-2}	1.66×10^{-2}
100	3.33×10^{-3}	3.31×10^{-3}	3.31×10^{-3}	3.31×10^{-3}	3.31×10^{-3}	3.31×10^{-3}	3.31×10^{-3}	3.36×10^{-3}
1000	3.34×10^{-4}	3.32×10^{-4}	3.32×10^{-4}	3.32×10^{-4}	3.32×10^{-4}	3.32×10^{-4}	3.32×10^{-4}	3.37×10^{-4}

It is seen in Table 28 and Table 30 that the magnitude ratio of any of the eight walls only approaches 1 as the inside convection coefficient approaches 0 (on the order of 1×10^{-2} W/m^2·K). Recall that the annual temperature swing occurs over days and months, and the time constant of any of the roughly 6-inch simulated walls is on the order of hours, so the magnitude ratio of each wall should approach 1 for ω_{year} or other low frequencies. Thus to reiterate, it was necessary to assume h_{in} was zero to simulate the response to annual temperature variations on a realistic scale. Table 28 and Table 30 also show that the magnitude ratio at ω_{year} exhibits the same trends whether or not extra outer layers are included, which makes sense given the long time scale of the annual temperature variations. Similarly, Table 27 and Table 29 show the same trends in magnitude ratio, which indicates that the extra outer layers do not affect the overall performance of the eight walls under consideration.

Values from 1 to 100 W/m^2·K are considered more realistic values of h_{in} given that natural convection is typically estimated at 5 or 6 W/m^2·K [60] and values of h_{in} less than 1 W/m^2·K are unlikely to occur in a building application. When these more realistic values are reviewed, the corresponding magnitude ratios consistently favor the multi-layer configurations presented in Chapter 5, such as the ICI and AUA configurations (number of layers depends on overall wall thickness, which is about 140 mm here but 278 mm in most of Chapter 5 analysis).

For h_{in} = 0 W/m^2·K, the lowest magnitude ratio at ω_{day} occurs for the AUA configuration followed by the IC configuration, which coincides with the trends observed from simulating the walls with real temperature data, as shown in Table 23. This suggests that magnitude ratio is in fact indicative of energy flux (in terms of relative performance) for these eight simulated walls. It also makes sense that if the inside surface is perfectly insulated (h_{in} = 0 W/m^2·K), then the lowest magnitude ratio would result from stacking all the insulation towards the outermost layer, as in the IC configuration. This is essentially the equivalent of forming an ICI configuration. The air-copper combination produces a lower magnitude ratio than the insulation-concrete walls as a primary result of the material combination and thermal properties, as opposed to the material distribution. So, for the dry-bulb data simulations, the AUA and IC configurations have the lowest energy per unit area whereas previous analysis indicated that the ICI configurations would be best because of their lower magnitude ratios. Using different inside convection coefficient (h_{in}) values has been shown to account for this discrepancy.

In general, all the multi-layer walls have lower magnitude ratios than the Standard Wood Frame wall as well as lower annual energy flux. Based on the simulated results using h_{in} = 0 W/m^2·K, each multi-layer wall demonstrates a reduction in energy flux over the Standard Wood Frame wall. With outer layers of siding and gypsum/plasterboard, the potential reduction in

energy per unit area between each multi-layer wall and the Standard Wood Frame wall ranges from less than 1% to 28.4% depending on the climate zone. The greatest predicted improvement is in climate zone 1, represented by Miami, FL. The range increases to 36.4% when the extra outer layers are removed, even for a lower overall R-value. To provide additional data on potential energy savings from these multi-layer walls, the energy flux resulting from the "best case" digital filter is now considered.

7.4 DIGITAL FILTER AND RELATIVE ENERGY FLUX RESULTS

The difference in predicted energy flux between each wall and the digital filter is calculated for 15 climate locations and shown as percentages in Table 31.

Table 31. Percent difference in annual combined energy flux between each of the eight walls and the "best case" digital filter results for 15 climates.

Climate Location (Zone)	Stnd Wood Frame	CI	CIC	IC	3-ICI	5-ICI	7-ICI	AUA
Atlanta, GA (3)	10.6%	9.5%	4.5%	3.5%	4.6%	4.7%	4.7%	3.4%
Bakersfield, CA (3)	16.3%	14.3%	6.2%	4.2%	6.3%	6.4%	6.5%	4.0%
Chicago, IL (5)	5.0%	4.6%	1.9%	1.2%	1.9%	2.0%	2.0%	1.1%
Denver, CO (5)	5.2%	4.4%	1.4%	0.9%	1.4%	1.4%	1.4%	0.9%
Fort Worth, TX (3)	13.4%	12.4%	6.6%	4.5%	6.6%	6.8%	6.9%	4.3%
Lexington, KY (4)	5.4%	4.9%	2.9%	2.4%	2.9%	3.0%	3.0%	2.3%
Miami, FL (1)	37.5%	35.7%	19.9%	13.5%	20.0%	20.7%	20.9%	12.7%
Minneapolis, MN (6)	3.9%	3.6%	1.8%	1.3%	1.8%	1.9%	1.9%	1.3%
Norfolk, VA (4)	9.0%	8.4%	3.8%	2.7%	3.9%	4.0%	4.0%	2.6%
Phoenix, AZ (2)	9.9%	8.7%	4.2%	2.7%	4.3%	4.4%	4.5%	2.5%
Pittsburgh, PA (5)	4.0%	3.6%	1.8%	1.2%	1.8%	1.9%	1.9%	1.2%
Seattle, WA (5)	2.0%	1.7%	0.8%	0.5%	0.8%	0.8%	0.8%	0.5%
Springfield, MO (4)	7.5%	6.8%	3.4%	2.7%	3.4%	3.5%	3.5%	2.6%
Sterling, VA (4)	6.2%	5.5%	1.8%	1.1%	1.9%	1.9%	2.0%	1.1%

Table 31 (continued).

Wilmington, DE (4)	5.1%	4.6%	1.9%	1.4%	2.0%	2.0%	2.0%	1.3%
Wall Average	9.4%	8.6%	4.2%	2.9%	4.2%	4.4%	4.4%	2.8%

For example, the predicted energy flux in Miami, FL using a Standard Wood Frame wall is 37.5% more than the energy flux using the digital filter on the same temperature data. Based on the difference in annual energy flux between the digital filter and the Standard Wood Frame wall, climate zone 1 has the highest energy savings potential followed by climate zone 3 and then zones 2 and 4. These cells are shaded in grey, where darker shading indicates a larger difference in predicted energy flux between the wall and the digital filter for the given climate location simulated.

The average, across climate, of the difference between each wall and the digital filter is also reported. The smallest difference occurs between the AUA configuration and the digital filter. The configurations with the smallest differences compared to the "best case" digital filter are highlighted in red text. These correspond to the IC and AUA configurations, which are also highlighted in Table 23 and minimize magnitude ratios in Table 27 and Table 29 when h_{in} = 0 W/m^2·K.

Some cases in Table 31 show a very small difference in energy flux (0.5%) when compared to the digital filter. In particular, there is lower energy saving potential predicted in climate zones 5 and 6 and more in climate zones 1, 2, and 3. This indicates that reducing the magnitude ratio in these climates (5 and 6) will not result in heat flux or energy savings, because temperatures are consistently below the setpoint band. This is illustrated in Figure 7.6, Figure 7.7, and Figure 7.8 each of which shows the dry-bulb temperature data, digital filter response,

and AUA configuration response (with outer layers of siding and gypsum/plasterboard) for a given climate.

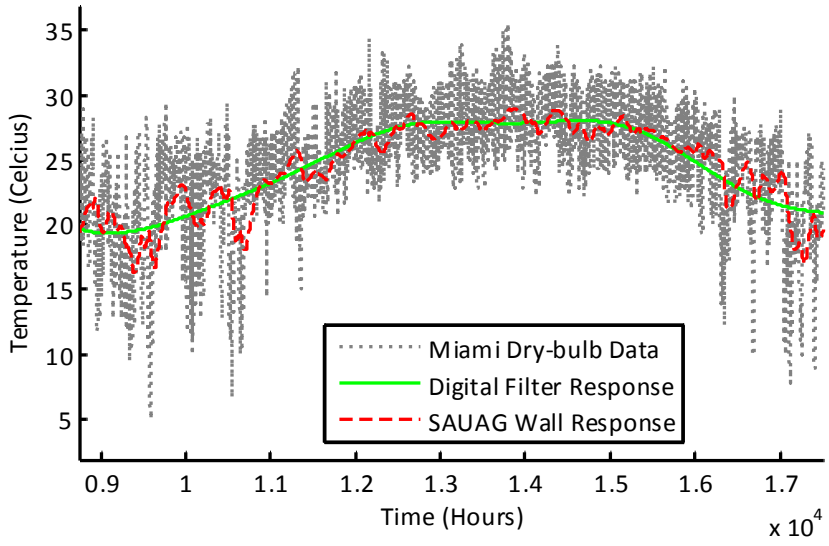

Figure 7.6 Dry-bulb temperature data from Miami, FL (climate zone 1) with digital filtered response and simulated wall response for AUA configuration including outer layers of siding and gypsum/plasterboard.

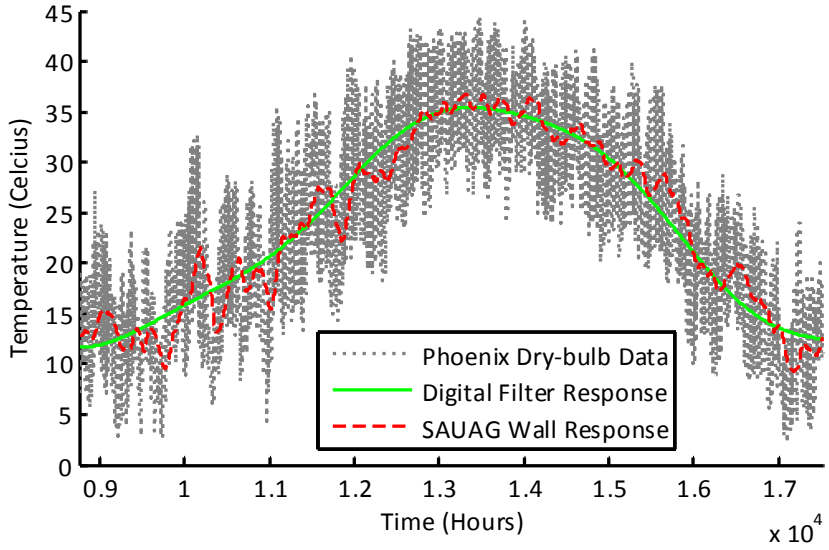

Figure 7.7 Dry-bulb temperature data from Phoenix, AZ (climate zone 2) with digital filtered response and simulated wall response for AUA configuration including outer layers of siding and gypsum/plasterboard.

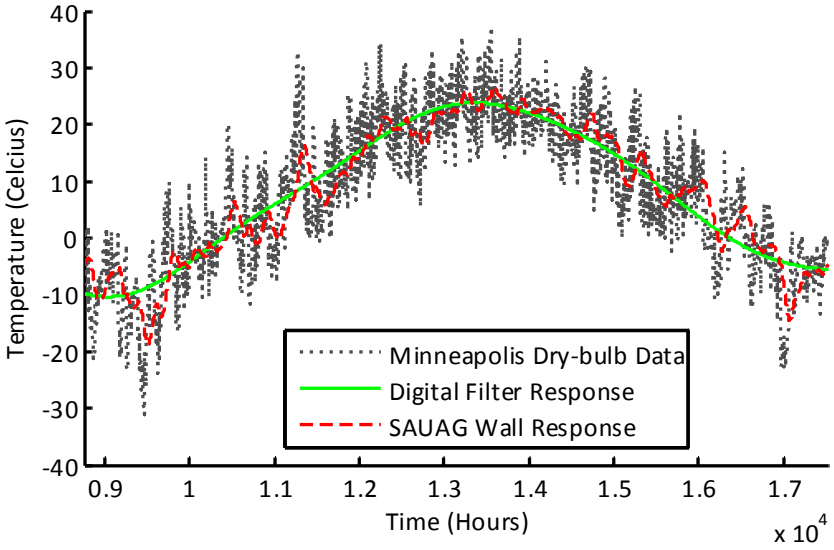

Figure 7.8 Dry-bulb temperature data from Minneapolis, MN (climate zone 6) with digital filtered response and simulated wall response for AUA configuration including outer layers of siding and gypsum/plasterboard.

The AUA wall response appears roughly the same compared to the digital filter in each of the three climates, but the temperatures in climate zones 1 and 2 are closer to the setpoint temperatures for more hours out of the year. Thus, the potential energy savings from optimized multi-layer walls depends largely on climate, as described previously in Chapter 7.2.

It is also apparent that there is a greater difference in energy saving potential between optimizing the total number of layers and using a more favorable material combination (e.g. air and copper) or a more evenly distributed configuration. It was suggested in Chapter 5 that further reductions in magnitude ratio may not be worthwhile if the energy savings do not outweigh potential increases in manufacturing and installation costs. According to the simulation results presented in Table 31, the difference in energy flux from layering depends on climate and ranges from 0 to 0.9%. Ultimately, the difference in energy consumption resulting from a reduced or minimized magnitude ratio will also be a factor of building size and exterior surface area when comparing different wall designs.

On average, from Table 31, an optimized multi-layer wall comes within 2-5% of the "best case" digital filter. This demonstrates that the optimized multi-layer walls can approach the performance of an idealized digital filter. In almost all cases, even the extreme climates, the optimal configurations improve 50% or more over the Standard Wood Frame when compared to the "best case" digital filter. For example, in Pittsburgh, PA, the digital filter results in 4.0% lower energy flux per year when compared to the Standard Wood Frame wall. In the same climate, the digital filter yields only 1.2% improvement over the AUA configuration, which represents an improvement greater than 50% between the Standard Wood Frame wall and the optimal (AUA configuration) multi-layer wall.

By comparing Table 27 and Table 31, magnitude ratio reductions and energy saving potential can be related. In Table 27 for h_{in} = 0 W/m^2·K, the magnitude ratio is reduced by one order of magnitude (1×10^{-1} to 1×10^{-2}) between the CI and other multi-layer configurations comprised of insulation and concrete (CIC, IC, ICI). Between these configurations (CIC, IC, ICI) and the AUA configuration, the magnitude ratio is reduced by another order of magnitude (1×10^{-2} to 1×10^{-3}). The corresponding columns in Table 31 show, on average, a 50% reduction in annual energy flux from the first order of magnitude change and 30% from the second, or 66% overall (between the CI and AUA configurations). The first order of magnitude change is related to layering or material distribution effects, while the second results primarily from using a different material combination.

Given that the walls with the lowest magnitude ratios under the conditions evaluated also result in the lowest combined annual heat or energy flux, it has been shown that magnitude ratio is a good prediction of relative energy performance. In other words, simulation results indicate that the tools developed in Chapter 5 are valid methods of designing multi-layer walls for reduced energy consumption. However, a relatively limited number of cases have been evaluated. To show conclusively that relative magnitude ratio is a reliable predictor of relative energy consumption, more simulations or additional studies ought to be conducted. Considerations for future work are discussed more in Chapter 8.

The work in Chapter 7 has demonstrated other important results. For example, simulation results indicate that the optimal and non-optimized multi-layer walls may realize significant reductions in annual combined energy flux. This supports the simplified design guidelines presented in Chapter 6, which may not always produce truly optimal configurations, but still result in significant improvements over standard wood frame construction. Actual energy savings

will depend largely on the climate location and inside convection coefficient values. As in other building energy modeling methods, differences in energy are relative and meant to be used for comparing design variations, rather than for predicting actual energy performance. With this in mind, it is also worth recognizing that all of the multi-layer configurations resulted in lower energy transfer than the Standard Wood Frame wall, which indicates that the transient response (magnitude ratio) is an important consideration, in addition to the standard static design metric (R-value). The results presented in Chapter 7 and in previous chapters are reviewed in Chapter 8 along with areas of future work.

8.0 CONCLUSIONS AND FUTURE WORK

8.1 CONCLUSIONS

The goal of this work was to provide generalized analysis of multi-layer walls for building envelopes to help mitigate energy consumption for heating and cooling. The initial work described in Chapter 4 identified the existence of optimal multi-layer configurations based on a frequency response methodology. This methodology was refined in Chapter 5 and the search for optimal configurations expanded. Both heuristic and formalized approaches were used to identify materials, layers, and distributions that minimize magnitude ratio (decrement factor) or maximize phase lag (time delay). Chapters 6 and 7 explored the practical limitations and implications of implementing the configurations developed in Chapter 5, while Chapter 7 focused specifically on placing the optimized magnitude ratio results in the context of real energy savings potential. The analysis in Chapter 7 also highlighted the importance of the inside convection coefficient on magnitude ratio and heat, or energy, flux. Key findings and contributions for multi-layer wall design are listed below.

- Demonstrating that:
    - an optimal number of layers and material combinations, proportions and distributions exist
    - an ICI configuration is better than IC, CI, and CIC

    - material combinations exist that outperform insulation-concrete (e.g. air-copper)
    - magnitude ratio can predict relative energy performance
    - some climate zones are expected to benefit more than others
- Developing tools for optimal multi-layer wall design, including:
    - Transmission Matrix Method (TMM)
    - Analytical Methods
- Producing generalized design guidelines, such as:
    - Use thermal mass
    - Pair low conductivity material with high heat capacity material
    - Locate insulation at outermost layers
    - Use even, symmetric layers throughout
    - Minimize extra outer layers (e.g. siding) to about 1 cm (3/8” ~ 0.4 inches) or less

The primary contributions of this work are the tools and guidelines for optimal multi-layer wall design. The Transmission Matrix Method was developed beyond the scope previously presented in existing literature. Specifically, it was developed with the use of Matlab to generate a mesh-independent model of one-dimensional conduction for frequency response analysis. This is used to predict time lag and decrement for evaluating building envelope performance. As in other building modeling tools, results indicate relative performance rather than actual predictions.

A method for including convection at the inside wall surface was also presented. The Transmission Matrix Method (TMM) with a realistic non-zero inside convection coefficient

(between 5 and 20 $W/m^2 \cdot K$, based on values seen in existing literature) is valid for comparing performance at the frequency corresponding to one day (24 hours). This was validated via a finite volume solution for accuracy, but the advantage of the TMM is evident in its relatively quick computation time. In addition to the TMM, an analytical method was presented for determining optimal material combinations and proportions of each material. The analytical method is also very quick compared to setting up and solving a finite difference or finite volume model.

The speed of the TMM enabled the evaluation of an expansive search space, including varying multi-layer wall design parameters far beyond the scope considered in existing literature. In turn, the results presented herein offer comprehensive guidelines that previous analysis was unable to provide. This work showed that optimal material combinations, proportions and distributions exist and that an optimal number of layers exists for a multi-layer wall. In terms of materials, certain combinations out-perform others based on the pairing of insulating and thermally massive properties. The optimal proportion lies around 50% within a range of 45-65% of the insulating material. And, distributing insulating materials at the inner- and outer-most layers yields better performance in terms of time lag, decrement factor, and energy saving potential.

The energy simulation results showed that magnitude ratio, or decrement factor, may be a reliable predictor of relative energy performance. Although this result requires further exploration, it is promising, because it may eliminate the need for time consuming whole-building energy simulations or at least expedite those solutions. Additionally, the simulation results from Chapter 7 illustrated the real benefit of optimizing multi-layer wall designs in terms of energy saving potential. Some climate zones will benefit more than others, and some design

features will yield larger improvements than others, but overall, the reductions in magnitude ratio from optimizing multi-layer wall design features are expected to have a beneficial impact on building energy consumption.

While this work has been successful in identifying optimal multi-layer wall designs and producing generalized design guidelines and analysis tools, additional work may be useful to support and enhance the findings presented in this thesis. In particular, the addition of whole building energy simulations, physical testing, and refined modeling are described in Chapter 8.2. The relevance of this work to the development of smart insulation, whose variable thermal response is able to capitalize when conditions exist for energy savings, is also discussed in the following chapter.

8.2 FUTURE WORK

8.2.1 Whole Building Energy Simulations

Whole building energy simulations have become more sophisticated and reliable, and program development continues to improve the functionality and accuracy of these models. While they are not expected to represent actual building operation and energy consumption perfectly, the design community relies on these models to predict how design changes will affect the overall operation of a building, including changes in annual energy usage. Programs such as EnergyPlus incorporate full climate data, including dry-bulb temperature data as well as wind, solar, shading, etc. It also assumes one-dimensional conduction through walls, but there are additional models within the program to account for edge effects and other building-environment interactions that

were not addressed in the simple energy estimate presented in Chapter 7 of this thesis. Therefore, a whole building energy simulation from a reliable, validated, and respected software package like EnergyPlus, even with its own limitations, would provide greater insight into the energy saving potential of the optimized multi-layer wall configurations. It would also provide support for continuing to develop and implement the concept.

8.2.2 Physical Testing

The testing and analysis in this thesis has been carried out by modeling one-dimensional conduction. Nearly all of the literature that motivated this work was also conducted using numerical modeling or simulation methods. Physical testing would illuminate the limitations of the model as well as provide physical evidence to support the development of improved multi-layer walls for building applications.

8.2.3 Model Variable Thermal Properties

It has been assumed that the change in material thermal properties due to changes in temperature is negligible for the temperature range considered (approximately -40 to 45 °C). Moreover, the thermal properties of materials taken from ASHRAE Fundamentals Chapter 26 are based on a mean temperature of 24 °C. Although insulating materials that do not perform as well as predicted in design often result from poor installation, settling, shrinkage, or moisture content, most insulating materials do actually exhibit a temperature dependency.

Insulating materials that are porous and not truly homogeneous are described by an apparent thermal conductivity, which emphasizes the fact that the thermal properties are valid for

a given set of operating conditions, which may not be valid at other conditions. A figure from the ASHRAE text is reproduced below to show the variability in thermal conductivity for several insulating materials with changes in mean temperature.

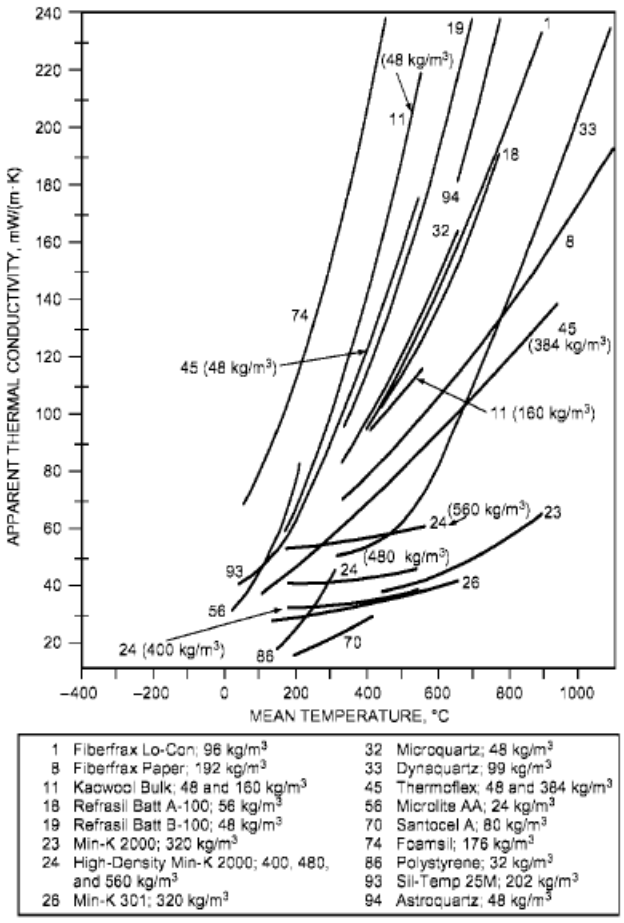

Figure 8.1 Variability of thermal conductivity with changes in mean temperature for various insulating materials. Taken from ASHRAE Fundamentals, Chapter 26 [45].

The transmission matrix method could be improved by incorporating a means of accounting for the temperature dependence of material thermal properties, especially the apparent thermal conductivity of porous materials. This would also enable modeling of phase change materials (PCM), which was the motivation for incorporating this modeling capability (temperature dependent thermal properties) in the EnergyPlus simulation program. This would

help further optimize material selection based on the mean temperature of a specific climate. It will also be useful for improving the accuracy of the model for air gaps, whose insulating performance depends on temperature as well as gap thickness, emittance, and other factors. Recall that air was selected for its use with the smart insulation concept.

8.2.4 Towards the Development of Smart Insulation

Smart insulation was described briefly in Chapter 5 as a type of variable insulation that can change between an insulating and conducting state. For this reason, it can be described as a thermal semiconductor. In essence, it provides the ability to turn insulation on and off, either to impede or facilitate heat transfer. In Chapter 5 design parameters were evaluated based on minimizing the magnitude ratio (decrement factor) and maximizing the phase lag (time delay). This informs the insulating state design and performance.

Air was introduced as an insulating material for its low thermal conductivity and because it is easier to transport (air is already funneled around buildings as part of traditional HVAC applications) and more practical than other materials (e.g. other gases, vacuumed cavities, liquids, or PCMs), including the fact that it is free and abundantly available. This is thought to enable the movement of layers from one position to another for the different states of the smart insulation concept. The design and analysis methods developed herein to minimize magnitude ratio or maximize phase lag can be repeated inversely to inform the form and material composition of a conducting state, rather than an insulating state.

The work from Kimber et al. [47] has shown how this multi-layer concept would work at the two extreme states based on a static analysis. It was shown that reducing heat transfer via radiation is critical to its effectiveness. Assuming proper coatings can achieve sufficiently low

emittance, then the results from Chapter 5 and 7 show the potential for a multi-layer air-copper combination to be an effective insulator against one-dimensional conduction based on its static and transient thermal response. Additional analysis will support further development.

APPENDIX A

WALL CONFIGURATIONS

The wall configurations from Al-Sanea [20] used to validate the RC model described in Chapter 4 are shown in Figure A. 1.

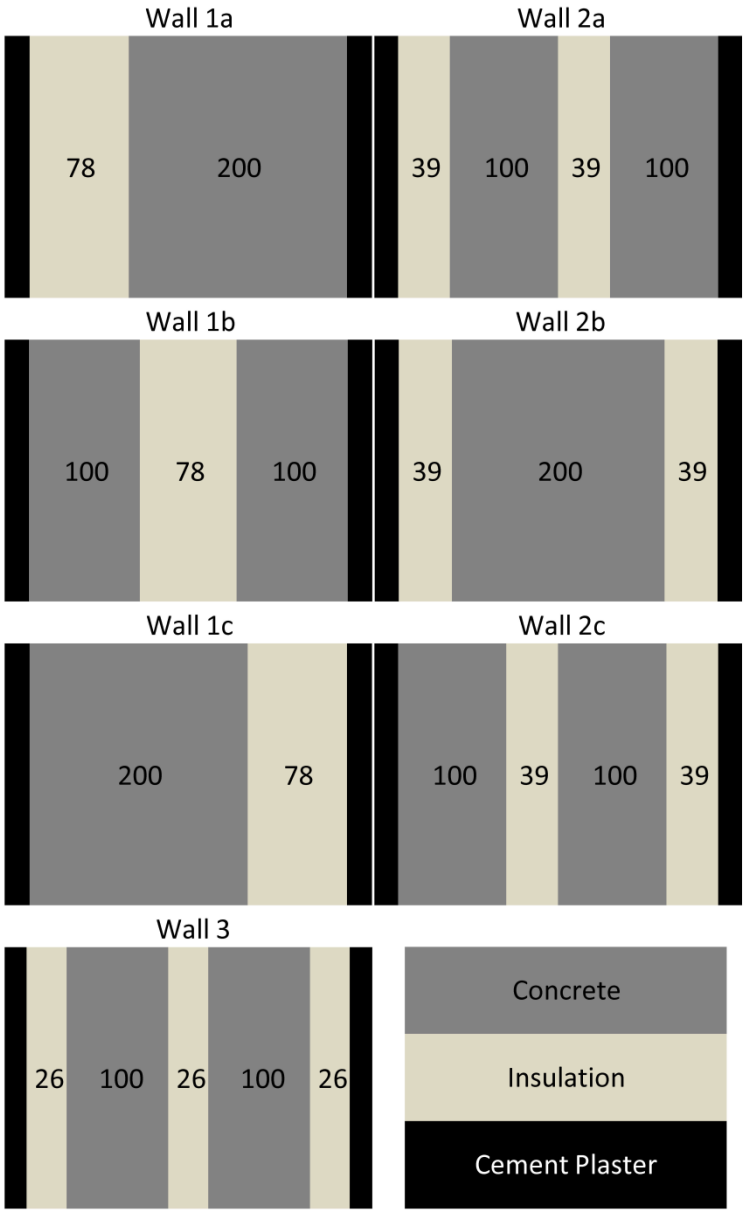

Figure A. 1. Wall configurations from Al-Sanea [20].

APPENDIX B

DOMINANT FREQUENCIES

The annual hourly ambient dry-bulb temperature is obtained from the National Renewable Energy Laboratory (NREL) weather database (.tmy3) for three U.S. cities: Pittsburgh, PA; Fargo, ND; and Las Vegas, NV. These represent, respectively, a mild climate, a cold climate, and a desert climate. Time domain plots of the dry-bulb temperature show that the 24-hour and 365-day frequencies dominate. This observation is confirmed using Matlab Fourier analysis (FFT) and plotting the power of the discrete Fourier transform (DFT). The annual hourly dry-bulb temperature is shown in Figure B. 1 for the whole year, where the 365 day period is visible. In Figure B. 2, the hourly dry-bulb temperature is shown for one week, so the 24 hour period is observed.

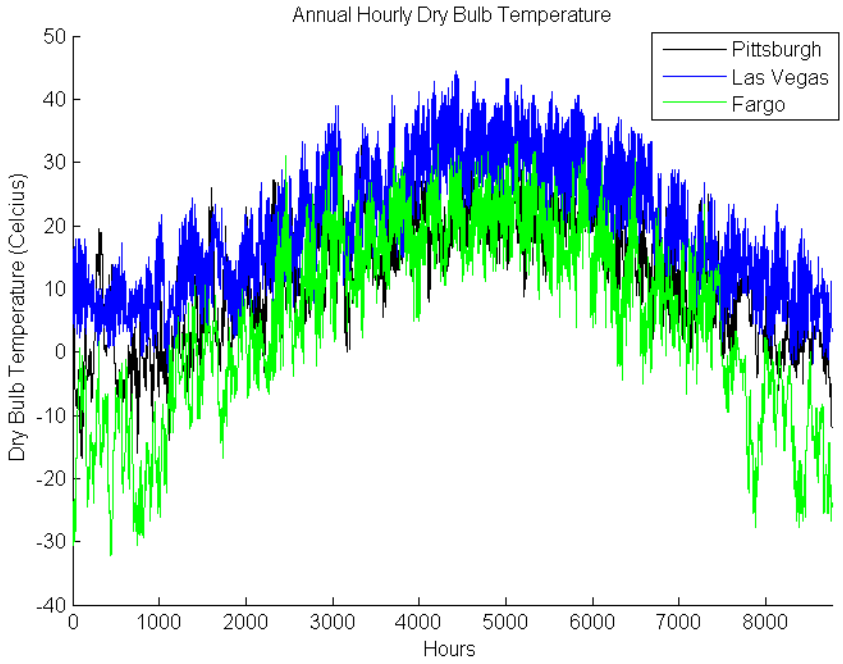

Figure B. 1. Annual hourly dry-bulb temperature for three representative U.S. climates.

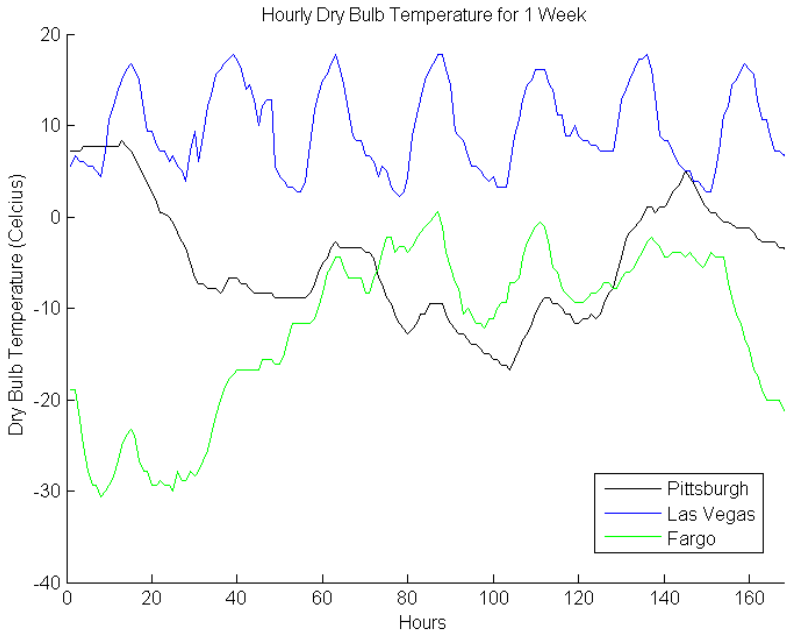

Figure B. 2. Hourly dry-bulb temperature for one week (168 hours).

APPENDIX C

TRANSMISSION MATRIX METHOD IMPLEMENTATION

There are numerous ways to actually implement the transmission matrix method. The method used in this work is described in more detail here. The folding method, also called the voltage divider method, is used to determine the transfer function between two voltages, or temperatures, while including an inside convection coefficient resistance ($R_{h,rm}$). It is formulated based on the circuit shown in Figure C. 1.

Voltage Divider Method

① $\frac{T_{s,rm}}{T_1} = \frac{R_{h,rm}}{R_{h,rm} + Z_2}$

② $Z_{eq} = \left[\left(R_{h,rm} + Z_2\right)^{-1} + Y\right]^{-1}$

③ $\frac{T_1}{T_{s,amb}} = \frac{Z_{eq}}{Z_{eq} + Z_1}$

$$\frac{V_2}{V_1} = \frac{T_{s,rm}}{T_{s,amb}} = \frac{T_{s,rm}}{T_1} \cdot \frac{T_1}{T_{s,amb}}$$

$$= \frac{R_{h,rm}}{(YZ_1Z_2 + Z_1 + Z_2) + R_{h,rm}(1 + YZ_1)}$$

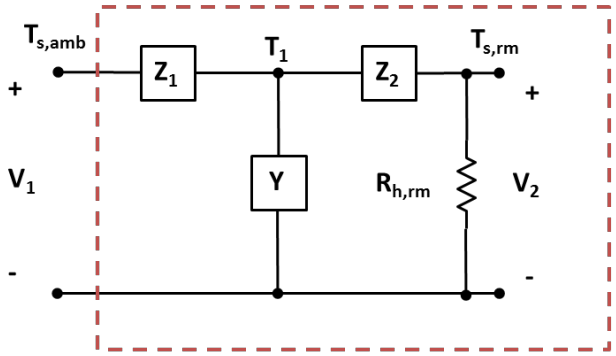

Figure C. 1. The folding method, or voltage divider method, relates V_2 and V_1 and includes resistance ($R_{h,rm}$) for the inside convection coefficient, as shown in the T-network circuit with impedences Z_1 and Z_2 and admittance Y.

The resulting transfer function for a single network is shown specifically in Equation (C 1) for comparison with elements of the transmission matrix, which were originally derived in Chapter 3.4.

$$\frac{V_2}{V_1} = \frac{R_{h,rm}}{\left(YZ_1Z_2 + Z_1 + Z_2\right) + R_{h,rm} \cdot \left(1 + YZ_1\right)} \qquad \text{(C 1)}$$

The T-network shown in Figure C. 1 (and previously shown in Figure 3.4) without the additional resistance ($R_{h,rm}$) represents each of the two networks shown in Figure C. 2, where V_1 is $V_{s,amb}$ and V_2 is $V_{s,rm}$, and V for voltage and T for temperature may be used interchangeably.

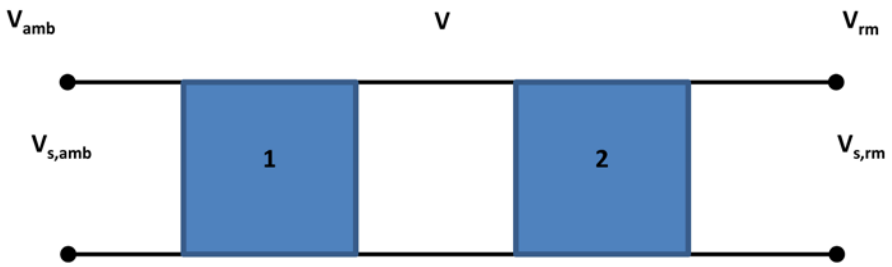

Figure C. 2. Transmission matrix line with two networks labeled 1 and 2 with voltages $V_{s,amb}$ and $V_{s,rm}$.

The transmission matrix representation for each network, relating the left end as inputs and the right end as outputs, was formulated in Chapter 3.4 and shown in Equation (3.13). It is shown with revised voltage notation in Equation (C 2), assuming only one T-network exists between ambient inputs and room outputs.

$$\begin{bmatrix} V_{s,rm} \\ I_{s,rm} \end{bmatrix} = \begin{bmatrix} (1+YZ_2) & -(YZ_1Z_2 + Z_1 + Z_2) \\ -Y & (1+YZ_1) \end{bmatrix} \begin{bmatrix} V_{s,amb} \\ I_{s,amb} \end{bmatrix} \tag{C 2}$$

The matrix elements are assigned representative letters A, B, C and D, as shown in Equation (C 3). By comparing Equations (C 1), (C 2), and (C 3), Equation (C 1) may be written in terms of the transmission matrix elements to form the transfer function in Equation (C 4). This was originally presented in Equation (3.20).

$$\begin{bmatrix} V_{s,rm} \\ I_{s,rm} \end{bmatrix} = \begin{bmatrix} A & B \\ C & D \end{bmatrix} \begin{bmatrix} V_{s,amb} \\ I_{s,amb} \end{bmatrix} \tag{C 3}$$

$$\frac{V_2}{V_1} = \frac{R_{h,rm}}{(-B) + R_{h,rm} \cdot (D)} \tag{C 4}$$

Determining the transfer function from Equation (C 4) is the final step of the transmission matrix calculation implemented in this work. Prior to this, intermediate matrices are multiplied, or convolved when individual elements are polynomials rather than integer values. For the example shown here, the first network has a transmission matrix (τ_1) and the second network has a transmission matrix (τ_2), which are combined as in Equation (C 5).

$$\begin{bmatrix} V_{s,rm} \\ I_{s,rm} \end{bmatrix} = \tau_2 \cdot \tau_1 \begin{bmatrix} V_{s,amb} \\ I_{s,amb} \end{bmatrix} \tag{C 5}$$

Equation (C 5) describes Figure C. 2, where the input $V_{s,amb}$ loads the first network (τ_1), which leads to some intermediate output V, between the two networks. This intermediate voltage then loads the second network (τ_2), which relates the intermediate voltage to the output voltage $V_{s,rm}$. The result is a single transmission matrix describing the overall transmission line and relating the primary input $V_{s,amb}$ to the final output $V_{s,rm}$. This method is valid for any number of networks along the transmission line, which represents one-dimensional heat conduction in this work. Finally, Equation (C 4) yields a transfer function between input and output voltages with an inside convection coefficient term, or if no inside convection coefficient is included, then the resulting transfer function is simply 1/D (the fourth element of the final transmission matrix) as shown in Equation (3.17).

BIBLIOGRAPHY

1. Better Buildings Challenge Reports First Year's Savings; Partners on Track to Meet 2020 Goal. 2013.

2. Chen, A. Closing in on Zero-Energy Buildings. Environmental Energy Technologies Division News, 2009. **8**.

3. Astm, Designation: C168-13 Standard Terminology Relating to Thermal Insulation. ASTM International.

4. Ciampi, M., et al., ON THE OPTIMIZATION OF BUILDING ENVELOPE THERMAL PERFORMANCE Multi-layered Wall Design to Minimize Heating and Cooling Plant Intervention in the Case of Time Varying External Temperature Fields. Civil Engineering and Environmental Systems, 2003. **20**(4): p. 231-254.

5. Zhu, L., et al., Detailed energy saving performance analyses on thermal mass walls demonstrated in a zero energy house. Energy and Buildings, 2009. **41**: p. 303-310.

6. Al-Sanea, S.a., M.F. Zedan, and S.N. Al-Hussain, Effect of thermal mass on performance of insulated building walls and the concept of energy savings potential. Applied Energy, 2012. **89**: p. 430-442.

7. Mishra, S., J.A. Usmani, and S. Varshney, Optimum Insulation Thickness of Building Walls for Energy Saving. International Journal of Engineering Science and Management, 2012. **2**(1): p. 88-95.

8. Kosny, J., et al. Energy Benefits of Application of Massive Walls in Residential Buildings. in RAE, ORNL Conference—Thermal Envelopes VIII. 2001.

9. Coffman, C., R. Duffin, and G. Knowles, Are adobe walls optimal phase-shift filters? Advances in Applied Mathematics, 1980. **1**(1): p. 50-66.

10. Al-Sanea, S.a. and M.F. Zedan, Effect of Insulation Location on Initial Transient Thermal Response of Building Walls. Journal of Thermal Envelope and Building Science, 2001. **24**: p. 275-300.

11. Al-Sanea, S.A., et al., Heat Transfer Characteristics and Optimum Insulation Thickness for Cavity Walls. Journal of Building Physics, 2003. **26**(3): p. 285-307.

12. Kossecka, E. and J. Kosny, Influence of insulation configuration on heating and cooling loads in a continuously used building. Energy and Buildings, 2002. **34**: p. 321-331.

13. Sonderegger, R.C., Harmonic analysis of building thermal response applied to the optimal location of insulation within the walls. Energy and Buildings, 1977. **1**: p. 131-140.

14. Bojić, M.L. and D.L. Loveday, The influence on building thermal behavior of the insulation/masonry distribution in a three-layered construction. Energy and Buildings, 1997. **26**(2): p. 153-157.

15. Bojic, M., F. Yik, and P. Sat, Influence of thermal insulation position in building envelope on the space cooling of high-rise residential buildings in Hong Kong. Energy and Buildings, 2001. **33**: p. 569-581.

16. Aste, N., A. Angelotti, and M. Buzzetti, The influence of the external walls thermal inertia on the energy performance of well insulated buildings. Energy and Buildings, 2009. **41**: p. 1181-1187.

17. Asan, H. and Y.S. Sancaktar, Effects of Wall's thermophysical properties on time lag abd decrement factor. Energy & Buildings, 1998. **28**: p. 159-166.

18. Asan, H., Numerical computation of time lags and decrement factors for different building materials. Building and Environment, 2006. **41**: p. 615-620.

19. Asan, H., Investigation of wall's optimum insulation position from maximum time lag and minimum decrement factor point of view. Energy and Buildings, 2000. **32**(2): p. 197-203.

20. Al-Sanea, S.A. and M.F. Zedan, Improving thermal performance of building walls by optimizing insulation layer distribution and thickness for same thermal mass. Applied Energy, 2011. **88**: p. 3113-3124.

21. Mavromatidis, L.E., et al., Numerical estimation of time lags and decrement factors for wall complexes including Multilayer Thermal Insulation, in two different climatic zones. Applied Energy, 2012. **92**: p. 480-491.

22. Tsilingiris, P.T., On the thermal time constant of structural walls. Applied Thermal Engineering, 2004. **24**: p. 743-757.

23. Al-Sanea, S.a., M.F. Zedan, and S.N. Al-Hussain, Effect of masonry material and surface absorptivity on critical thermal mass in insulated building walls. Applied Energy, 2013. **102**: p. 1063-1070.

24. Kaynakli, O., A review of the economical and optimum thermal insulation thickness for building applications. Renewable and Sustainable Energy Reviews, 2012. **16**: p. 415-425.

25. Masoso, O.T. and L.J. Grobler, A new and innovative look at anti-insulation behaviour in building energy consumption. Energy and Buildings, 2008. **40**: p. 1889-1894.

26. Ozel, M., The influence of exterior surface solar absorptivity on thermal characteristics and optimum insulation thickness. Renewable Energy, 2012. **39**: p. 347-355.

27. Ozel, M., Determination of optimum insulation thickness based on cooling transmission load for building walls in a hot climate. Energy Conversion and Management, 2013. **66**: p. 106-114.

28. Mikhailov, V.V., Optimization of multilayer thermal insulation. Journal of Engineering Physics, 1980. **39**(2): p. 880-884.

29. Ginestet, S., et al., Thermal identification of building multilayer walls using reflective Newton algorithm applied to quadrupole modelling. Energy and Buildings, 2013. **60**: p. 139-145.

30. Jiang, F., X. Wang, and Y. Zhang, Analytical optimization of specific heat of building internal envelope. Energy Conversion and Management, 2012. **63**: p. 239-244.

31. Sambou, V., et al., Thermal optimization of multilayered walls using genetic algorithms. Energy and Buildings, 2009. **41**(10): p. 1031-1036.

32. Duffin, R.J. and G. Knowles, Temperature control of buildings by adobe wall design. Solar Energy, 1981. **27**(3): p. 241-249.

33. Tsilingiris, P.T., Thermal flywheel effects on the time varying conduction heat transfer through structural walls. Energy and Buildings, 2003. **35**(10): p. 1037-1047.

34. Davies, M.G., Optimum design of resistance and capacitance elements in modelling a sinusoidally excited building wall. Building and Environment, 1983. **18**: p. 19-37.

35. Hui, P. and H.S. Tan, A transmission-line theory for heat conduction in multilayer thin films. IEEE Transactions on Components, Packaging, and Manufacturing Technology: Part B, 1994. **17**(3): p. 426-434.

36. Weber, T. and G. Jóhannesson, An optimized RC-network for thermally activated building components. Building and Environment, 2005. **40**: p. 1-14.

37. Parnis, G., Building Thermal Modelling Using Electric Circuit Simulation. 2012.

38. Davies, M.G., Building Heat Transfer. 2004: John Wiley & Sons Ltd.

39. Maillet, D., et al., Thermal quadrupoles: solving the heat equation through integral transforms. 2000: Wiley New York.

40. Carslaw, H., Introduction to the mathematical theory of the conduction of heat in solids. 2nd ed. 1921, London: Macmillan and co.

41. Carslaw, H. and J. Jaeger, Conduction of Heat in Solids. 1947, Oxford: Clarendon Press.

42. Fraisse, G., et al., Development of a simplified and accurate building model based on electrical analogy. Energy and Buildings, 2002. **34**: p. 1017-1031.

43. Peng, C. and Z. Wu, Thermoelectricity analogy method for computing the periodic heat transfer in external building envelopes. Applied Energy, 2008. **85**: p. 735-754.

44. Bond, D.E.M., W.W. Clark, and M. Kimber, Configuring wall layers for improved insulation performance. Applied Energy, 2013. **112**: p. 235-245.

45. ASHRAE Handbook: Fundamentals. 2009, Atlanta, GA: American Society of Heating, Refrigerating and Air-Conditioning Engineers, Inc.

46. Salazar, A., On Thermal Diffusivity. European Journal of Physics, 2003. **24**(4): p. 351.

47. Kimber, M., W.W. Clark, and L. Schaefer, Conceptual analysis and design of a partitioned multifunctional smart insulation. Applied Energy, 2014. **114**: p. 310-319.

48. Pipes, L.A. and L.R. Harvill, Applied mathematics for engineers and physicists. Vol. 28. 1970: McGraw-Hill New York.

49. Matlab Global Optimization Toolbox. 2014, The MathWorks Inc.

50. Council, A.W., Details for Conventional Wood Frame Construction. 2001, American Forest and Paper Association: Washington, DC. p. 55.

51. Incropera, F.P., A.S. Lavine, and D.P. DeWitt, Fundamentals of heat and mass transfer. 2011: John Wiley & Sons.

52. VanderWerf, P.A. and P.C. Association, Concrete Systems for Homes and Low-rise Construction: A Portland Cement Association Guide. 2006: McGraw-Hill.

53. Rajagopalan, N., M.M. Bilec, and A.E. Landis, Residential life cycle assessment modeling: comparative case study of insulating concrete forms and traditional building materials. Journal of Green Building, 2010. **5**(3): p. 95-106.

54. Building America Case Study Technology Solutions for New Homes: Insulating Concrete Forms (Fort Myers, Florida). 2012, Pacific Northwest National Laboratory; Greencastle, Inc.; Energy Smart Home Plans.

55. NAHB Research Center, I., COSTS AND BENEFITS OF INSULATING CONCRETE FORMS FOR RESIDENTIAL CONSTRUCTION. 2001: Upper Marlboro, MD.

56. Association, I.C.C.I.a.A.T.E.W., IECC Compliance Options for Wood-Frame Wall Assemblies. 2014, International Code Council Inc. and APA – The Engineered Wood Association. p. 20.

57. 1991- 2005 Update: Typical Meteorological Year 3, E.S.C. Solar Resource Characterization Project, Editor.

58. Lstiburek, J., Understanding Attic Ventilation. Building Science Digest 2006. **102**: p. 2.

59. Thermostats. 2013 November 26, 2013 [cited 2014 May 18]; Available from: http://energy.gov/energysaver/articles/thermostats.

60. Crabb, J., N. Murdoch, and J. Penman, A simplified thermal response model. Building Services Engineering Research and Technology, 1987. **8**(1): p. 13-19.